

Aus dem Bereich der Molekularen Zellbiologie
Theoretische Medizin und Biowissenschaften
der Medizinischen Fakultät
der Universität des Saarlandes, Homburg/Saar

Ion Currents, Action Potentials and Their Modulation by $G\alpha_{q/11}$ Signaling Pathways in The Mouse Heart

*Dissertation zur Erlangung des Grades eines Doktors der
Naturwissenschaften*

der Medizinischen Fakultät
der UNIVERSITÄT DES SAARLANDES
2012

Vorgelegt von: Sara Pahlavan
geb. am. 15.07.1981 in Damavand, Tehran, Iran

To my dearests:

My beloved parents

My siblings *Mahdi, Maryam* and *Mohaddese*

Erklärung gemäß § 7 Abs. 1 Nr. 4

Ich erkläre hiermit an Eides statt, dass ich die vorliegende Arbeit ohne unzulässige Hilfe Dritter und ohne Benutzung anderer als der angegebenen Hilfsmittel angefertigt habe. Die aus anderen Quellen direkt oder indirekt übernommenen Daten und Konzepte sind unter Angabe der Quelle gekennzeichnet.

Weitere Personen waren an der inhaltlich-materiellen Erstellung der vorliegenden Arbeit nicht beteiligt. Insbesondere habe ich nicht die entgeltliche Hilfe von Vermittlungs- bzw. Beratungsdiensten (Promotionsberater/innen oder anderer Personen) in Anspruch genommen. Außer den Angegebenen hat niemand von mir unmittelbar oder mittelbar geldwerte Leistungen für Arbeiten erhalten, die im Zusammenhang mit dem Inhalt der vorgelegten Dissertation stehen.

Die Arbeit wurde bisher weder im Inland noch im Ausland in gleicher oder ähnlicher Form in einem anderen Verfahren zur Erlangung des Doktorgrades einer anderen Prüfungsbehörde vorgelegt.

Ich versichere an Eides statt, dass ich nach bestem Wissen die Wahrheit gesagt und nichts verschwiegen habe.

Vor Aufnahme der vorstehenden Versicherung an Eides Statt wurde ich über die Bedeutung einer eidesstattlichen Versicherung und die strafrechtlichen Folgen einer unrichtigen oder unvollständigen eidesstattlichen Versicherung belehrt.

Homburg, 09.10.2012

PAHLAVAN

Table of Contents

| | |
|---|-------------|
| Zusammenfassung | iv |
| Summary | viii |
| List of Abbreviations | xi |
| List of Figures | xiii |
| List of Tables | xvi |
| 1. Introduction | 1 |
| 1.1. The heart anatomy | 1 |
| 1.2. The conduction system of the heart | 2 |
| 1.3. Structure of a working cardiomyocyte | 3 |
| 1.4. The electrophysiological properties of a cardiomyocyte | 6 |
| 1.4.1. Resting membrane potential (V_R)..... | 6 |
| 1.4.2. Action potential (AP) | 7 |
| 1.4.3. Na^+ current | 9 |
| 1.4.4. L-type Ca^{2+} current..... | 11 |
| 1.4.5. K^+ currents..... | 15 |
| 1.4.5.1. Transient outward K^+ current (I_{to})..... | 17 |
| 1.4.5.2. Delayed rectifier K^+ currents (I_{Kur} , I_{Kr} , I_{Ks})..... | 17 |
| 1.4.5.3. Inwardly rectifying K^+ currents (I_{K1} , $I_{K(Ach)}$, $I_{K(ATP)}$)..... | 18 |
| 1.5. Action potential propagation in cardiac tissue | 19 |
| 1.6. Excitation-Contraction (EC) Coupling | 20 |
| 1.6.1. SR Ca^{2+} release channels (RyR)..... | 21 |
| 1.6.2. Sarco/endoplasmic reticulum Ca^{2+} -ATPase | 21 |
| 1.6.3. Na^+/Ca^{2+} exchange | 22 |
| 1.7. Signal transduction in cardiomyocytes | 23 |
| 1.7.1. $G_{\alpha_q/11}$ signaling pathway | 24 |
| 1.7.2. Rac signaling pathway | 26 |
| 1.8. Cardiac diseases | 29 |
| 1.8.1. Aldosterone..... | 29 |
| 2. Materials & Methods | 31 |
| 2.1. Chemicals and solutions | 31 |
| 2.2. Preparation of rat ventricular myocytes | 32 |
| 2.3. Generation of transgenic mice | 34 |
| 2.3.1. Heart-specific inducible $G_{\alpha_q}/G_{\alpha_{11}}$ knockout..... | 34 |
| 2.3.2. Heart-specific inducible Cav1.2 <i>I1624E</i> mutation..... | 34 |
| 2.3.3. Heart-specific constitutively active Rac1 | 35 |
| 2.4. Aldosterone Pump implantation | 35 |
| 2.5. Preparation of mouse ventricular myocytes | 35 |
| 2.6. Patch-clamp setup | 36 |
| 2.7. Patch-clamp technique | 37 |

| | |
|---|------------|
| 2.7.1. Electrophysiological experiments..... | 38 |
| 2.7.2. Action potential recording in ventricular myocytes..... | 40 |
| 2.7.3. Transient outward current (I_{toc}) measurement..... | 41 |
| 2.7.4. L-type Ca^{2+} current ($I_{Ca,L}$) measurement..... | 42 |
| 2.8. Photometry system..... | 44 |
| 2.9. Excitation-contraction coupling gain measurements..... | 45 |
| 2.10. Data statistics..... | 46 |
| 3. Results..... | 47 |
| 3.1. The effects of $G\alpha_q/G\alpha_{11}$ knockout on the basic electrophysiological properties of ventricular myocytes..... | 47 |
| 3.1.1. $G\alpha_q$ knockout modulates the electrophysiological properties of ventricular myocytes..... | 47 |
| 3.1.2. Tamoxifen alters the electrophysiological properties of ventricular myocytes..... | 52 |
| 3.1.3. Cre recombinase expression causes only minor changes in myocyte properties..... | 58 |
| 3.1.4. Two sets of genotypes are sufficient to study the effects of $G\alpha_q/G\alpha_{11}$ knockout in ventricular myocytes..... | 60 |
| 3.1.5. $G\alpha_q$ knockout modifies the electrical properties of cardiomyocytes, but its effects depend on $G\alpha_{11}$ expression..... | 62 |
| 3.2. Hyperaldosteronism-induced electrical remodeling in ventricular myocytes of wildtype and $G\alpha_q/G\alpha_{11}$ KO mice..... | 65 |
| 3.2.1. Aldosterone effects on C_M and V_R is mediated by $G\alpha_q/G\alpha_{11}$ proteins..... | 65 |
| 3.2.2. Cardiac action potential is greatly altered by hyperaldosteronism..... | 68 |
| 3.2.3. I_{toc} is the target of aldosterone effects in ventricular myocytes..... | 71 |
| 3.3. <i>I1624E</i> mutation in the IQ motif of Cav1.2 and the effects on the $I_{Ca,L}$ and EC Coupling gain..... | 74 |
| 3.3.1. Mutation in IQ motif of Cav1.2 modifies the channel function..... | 74 |
| 3.3.2. The I/E mutation results in alterations of EC coupling gain..... | 76 |
| 3.4. $I_{Ca,L}$ and EC coupling gain in the ventricular myocytes expressing RacET..... | 79 |
| 3.5. The effect of CytoD supplement on AP characteristics of cultured cardiomyocytes..... | 82 |
| 4. Discussion..... | 88 |
| 4.1. Heart-specific inducible $G\alpha_q/G\alpha_{11}$ knockout..... | 88 |
| 4.1.1. The impact of tamoxifen treatment and Cre recombinase expression..... | 90 |
| 4.1.2. The optimized genetic combinations to study $G\alpha_q$ knockout..... | 92 |
| 4.1.3. Physiological relevance of $G\alpha_q$ in ventricular myocytes..... | 93 |
| 4.2. The relationship between aldosterone and $G\alpha_q/G\alpha_{11}$ signaling in cardiac pathology..... | 96 |
| 4.2.1. The effect of hyperaldosteronism on C_M and V_R | 97 |
| 4.2.2. The role of $G\alpha_q/G\alpha_{11}$ signaling in HA-induced AP alterations..... | 97 |
| 4.3. Mutation in the IQ motif of Cav1.2 and the impact on EC coupling gain..... | 100 |
| 4.3.1. Generation of the murine cardiac Cav1.2 ^{I1624E} | 100 |
| 4.3.2. The impact of I/E mutation on the $I_{Ca,L}$ | 101 |
| 4.3.3. The impact of the I/E mutation on global Ca^{2+} transients..... | 102 |

| | |
|---|------------|
| 4.4. EC coupling gain in cardiomyocytes expressing RacET | 105 |
| 4.5. Cytochalasin D as a culture supplement | 107 |
| 4.5.1. C_M was reduced in long-term culture..... | 107 |
| 4.5.2. Preservation of AP shape in long-term culture..... | 108 |
| 5. References | 110 |
| Curriculum Vitae | 131 |
| Publications | 133 |
| Attachments | 136 |

Zusammenfassung

Das Herz ist ein Muskel, der das Blut durch den Körper pumpt um die Zellen mit Sauerstoff und Nährstoffen zu versorgen. Diese Pumpfunktion wird durch zwei besondere Charakteristiken der Herzzellen ermöglicht: (i) elektrische Erregbarkeit und (ii) Kontraktilität. Das Aktionspotenzial (AP) der Kardiomyozyten wird durch eine Welle von koordiniertem Öffnen und Schließen verschiedener Ionenkanäle geformt. Das Öffnen kardialer Ca^{2+} -Kanäle induziert einen Ca^{2+} -Einstrom, der zu einer massiven Ca^{2+} Ausschüttung aus dem Sarkoplasmatischen Retikulum führt. Der weit verbreitete, sekundäre Botenstoff Kalzium stellt hierbei die Verbindung zwischen der elektrischen Erregung und der mechanischen Kontraktion her, im folgenden elektro-mechanische Kopplung (EMK) genannt. Eine große Vielfalt intrazellulärer Signalkaskaden regulieren die physiologischen Eigenschaften von Kardiomyozyten. In dieser Arbeit habe ich solche Signalkaskaden und deren regulatorischen Prozesse untersucht, um deren Einfluss auf die Physiologie und Pathophysiologie des Herzen zu quantifizieren. Dabei konzentrierte ich mich auf die folgenden Fragestellungen: (i) Modulieren $G_{\alpha_{q/11}}$ -gekoppelte Signalwege die elektrophysiologischen Eigenschaften von ventrikulären Myozyten aus dem Mäuseherz? (ii) Sind $G_{\alpha_{q/11}}$ -gekoppelte Signalwege an durch Hyperaldosteronismus (HA) induzierten Veränderungen der elektrophysiologischen Eigenschaften von Maus-Kardiomyozyten beteiligt? (iii) Welche Wirkung hat die Veränderung der Calmodulin-Bindung von Cav1.2 auf die EMK? iv) Hat die GTPase Rac1 einen Einfluss auf die EMK? v) Kann Cytochalasin D die elektrophysiologischen Eigenschaften von ventrikulären Myozyten aus der Ratte in Langzeitkulturen konservieren?

$G_{\alpha_{q/11}}$ gekoppelte Rezeptoren werden *in vivo* durch Hormone wie Endothelin-1, Angiotensin-II und Epinephrine stimuliert. Durch akute Stimulation kommt es unter anderem zu einem Anstieg der intrazellulären Ca^{2+} Konzentration und in Folge dessen zu einer Aktivierung Ca^{2+} -abhängiger Proteine wie z.B. die konventionelle Protein Kinase C oder Calmodulin. Beides, direkter Kalziumanstieg wie auch Aktivierung

Kalzium-abhängiger Prozesse, moduliert die kontraktile Antwort der Kardiomyozyten. Demgegenüber führt eine chronische Stimulation von $G_{\alpha_{q/11}}$ Signalkaskaden zu pathologischen Antworten, z.B. Herzrhythmusstörungen, Hypertrophie oder Herzversagen. Trotz zahlreicher Untersuchungen der pathologischen Rolle von $G_{\alpha_{q/11}}$ gekoppelten Signalwegen, ist über deren physiologische Funktion in Kardiomyozyten wenig bekannt. In dieser Arbeit habe ich die Effekte der Deaktivierung der Gene *gnaq* und/oder *gna11* auf die elektrophysiologischen Eigenschaften ventrikulärer Myozyten untersucht und dabei Veränderungen der Membrankapazität, dem Ruhemembranpotenzial und der Aktionspotenzial (AP) Amplitude gefunden. Die Dauer des AP blieb hierbei unverändert. Daraus schloss ich, dass eine niedrige (physiologische) Stimulation sowohl von G_{α_q} - wie auch $G_{\alpha_{11}}$ -gekoppelten Signalwegen von großer Bedeutung für die grundsätzlichen Eigenschaften der Kardiomyozyten wie z.B. deren elektrophysiologischen Eigenschaften sind.

Das natürliche Hormon Aldosteron beeinflusst das Blutvolumen und damit den Blutdruck. Neben diesen hämodynamischen Effekten führt ein Überschuss von Aldosteron (Hyperaldosteronismus, HA) beim Menschen zu Erkrankungen des gesamten Organismus wie z.B. Hypertronie. Chronische Hypertronie wiederum führt zu Herzerkrankungen. Vor kurzem wurde interessanterweise berichtet, dass HA auch unabhängig vom Blutdruck zu Hypertrophie und Herzversagen führen kann. Der genau Mechanismus hierbei und besonders dessen Signalkaskade in Kardiomyozyten ist jedoch weitestgehend unbekannt. Ich habe in dieser Arbeit die Effekte von HA auf die elektrophysiologischen Eigenschaften von Kardiomyozyten untersucht und dabei eine wesentliche Abnahme der Dauer des AP sowie eine Erhöhung des transienten Auswärtsstroms, I_{toc} , festgestellt. Weiterhin konnte ich durch Induzierung einer HA in $G_{\alpha_q}/G_{\alpha_{11}}$ Doppelknockout Mäusen eine mögliche Beteiligung der $G_{\alpha_{q/11}}$ -gekoppelten Signalwege bei den HA-induzierten Veränderungen der elektrophysiologischen Eigenschaften der Kardiomyozyten nachweisen. Daraus folgerte ich, dass HA zu einer zellulären elektrophysiologischen Remodellierung beiträgt, und dass dieser Effekt durch Zielproteine innerhalb von $G_{\alpha_{q/11}}$ -gekoppelten Signalwegen gesteuert wird.

Die Eigenschaften des kardialen Ca^{2+} Kanals Cav1.2 werden durch verschiedene Mechanismen reguliert, wie etwa der Ca^{2+} - und spannungsabhängigen Inaktivierung. Das Ca^{2+} bindende Protein Calmodulin (CaM) vermittelt hierbei die Ca^{2+} -abhängige Inaktivierung (CDI). Ca^{2+} gesättigtes CaM interagiert mit dem sogenannten IQ Motiv im C-Terminus des Cav1.2-Proteins, um die Kalzium-abhängige Inaktivierung zu induzieren. Zur weiteren Untersuchung der Effekte der IQ-CaM Interaktion in der Cav1.2 Regulation wurde eine I/E Mutation (Ile1624 zu Glu) in der IQ Sequenz generiert. In dieser Arbeit habe ich die Effekte einer I/E Mutation des IQ Motivs auf die (i) Cav1.2 Funktion (ii) und die EMK untersucht. Dabei zeigte sich interessanterweise, dass die I/E Mutation eine wesentliche Reduzierung der $I_{\text{Ca,L}}$ Dichte verursacht. Trotz dieser niedrigen Dichte war die Amplitude von globalen Ca^{2+} Transienten in den ventrikulären Zellen der I/E Mäuse gesteigert. Ich konnte aufzeigen, dass diesem Phänomen eine Zunahme der Verstärkungsfunktion in der EMK zugrund lag. Diese übersteigerte Verstärkung des Kalziumeinstroms in der EMK war letztendlich die Ursache für kardiale Dysfunktion in den Mäusen mit der I/E Mutation.

Rac1 ist ein monomeres G-Protein, das durch einen Integrin-gekoppelten Signalweg aktiviert werden kann. Es stimuliert verschiedene zelluläre Prozesse, wie z.B. die Organisation des Zytoskeletts und die Produktion von reaktiven Sauerstoffradikalen (ROS). Bei einer Vielzahl von kardialen Pathologien, wie Kardiomyopathien und Herzrhythmusstörungen, kommt es zu einer Aktivitäts- und Expressionssteigerung von Rac1. Dennoch sind die hierbei auftretenden zellulären Mechanismen weitestgehend unerforscht. In dieser Arbeit habe ich die Effekte der Expression eines konstitutiv aktiven Rac1 (V12Rac1), in sogenannten RacET Mäusen, auf die EMK in ventrikulären Myozyten untersucht. Trotz einer erheblichen Abnahme des $I_{\text{Ca,L}}$, war die Amplitude der global Ca^{2+} Transienten in den ventrikulären Zellen von RacET Mäuse erhöht. Ähnlich wie bei den I/E-Mäusen liegt dieser Amplitudensteigerung eine erhöhte Verstärkungsfunktion in der EMK zugrunde.

Die Möglichkeit der Kultivierung von Kardiomyozyten ist deswegen von so Bedeutung, weil isolierte adulte Kardiomyozyten innerhalb weniger Stunden einem Remodellierung Prozess unterliegen, der zu einer De-Differenzierung der Herzmuskelzellen führt. Für

viele experimentelle Ansätze, wie z.B. chronische Hormongaben *in vitro* oder heterologe Expression von Proteinen, wäre eine Kultivierungsmöglichkeit von mehreren Tagen ohne De-Differenzierung der Zellen von großem Vorteil. Deswegen haben sich in der Forschung verschiedene Methoden etabliert, die versucht haben die Zellkulturkonditionen verbessern. Cytochalasin D (CytoD), ein Pilzmetabolit, ist bekannt für seine positiven Effekte auf die Kardiomyozytenkultivierung, da es deren Morphologie konserviert. Ich habe in dieser Arbeit zudem untersucht, ob CytoD auch die Funktion der Kardiomyozyten erhalten kann. Bei den Untersuchungen des AP konnte ich feststellen, dass 0.5 μM CytoD die elektrophysiologischen Eigenschaften adulte ventrikulärer Myozyten der Ratte über eine Dauer von 3 Tagen in der Kultur konservieren kann. Der Einsatz von CytoD bei der routinemäßigen Kultivierung von Kardiomyozyten ist folglich dann empfehlenswert, wenn es darum geht sowohl die morphologischen als auch elektrophysiologischen Eigenschaften der Zellen zu erhalten.

Summary

The heart is a muscular organ that pumps the blood throughout the entire body, supplying the cells with O₂ and nutrients. The pumping property originates from two important inherent characteristics of cardiac cells: excitability and contractility. Cardiomyocyte's action potential (AP) comprises a wave of coordinated openings and closings of multiple ion channels. The opening of cardiac Ca²⁺ channels results in Ca²⁺ influx that triggers a much larger Ca²⁺ release from sarcoplasmic reticulum, which is required for contraction. Therefore, the ubiquitous second-messenger Ca²⁺ links the electrical excitation to the mechanical contraction, a process called excitation-contraction (EC) coupling. Various intracellular signaling cascades regulate the physiological properties of cardiomyocytes including excitability and contractility. In this thesis, I studied these signaling pathways and regulatory processes and their contribution into the physiology and pathophysiology of cardiac cells. In particular, I addressed the following questions: (i) do G $\alpha_{q/11}$ signaling pathways modulate the electrophysiological properties of mouse ventricular myocytes? (ii) are G $\alpha_{q/11}$ pathways involved in hyperaldosteronism (HA)-induced alterations of cardiomyocytes' electrophysiological properties? (iii) what is the effect of altering calmodulin-binding of Cav1.2 on EC coupling gain? (iv) does the small GTPase Rac1 influence the EC coupling gain? (v) can Cytochalasin D preserve the electrophysiological properties of rat ventricular myocytes in long-term culture?

G $\alpha_{q/11}$ signaling is activated following binding of hormones such as endothelin-1, angiotensin-II or epinephrine to G-protein coupled receptors. Acute activation of these signaling pathways lead to non-genomic responses such as an increase in intracellular Ca²⁺ levels and activation of various PKC isoforms which both modulate cardiomyocyte's contractility. In contrast, chronic stimulation of G $\alpha_{q/11}$ signaling pathways results in pathological responses such as hypertrophy and heart failure, so called genomic effects. In cardiomyocytes, despite the increasing number of investigations on the pathological effects of G $\alpha_{q/11}$ signaling, its physiological function is

not well understood. In this thesis I studied the effects of $G\alpha_q/G\alpha_{11}$ -protein knockout on the electrophysiological characteristics of mouse ventricular myocytes and found alterations of membrane capacitance, resting membrane potential and AP amplitude, but not AP duration. Therefore, I concluded that both $G\alpha_q$ and $G\alpha_{11}$ are instrumental to the electrophysiological properties of cardiomyocytes by mediating the continuance of a basic rate of gene expression.

Aldosterone is a hormone that causes water retention in the kidney and consequently increases the blood volume and thus helps to maintain the blood pressure. Besides its homeostatic effect, aldosterone excess leads to pathological responses; one of the best known is hypertension. Persistent hypertension in turn results in various cardiac diseases. Previously, aldosterone was proposed to induce cardiac pathological responses independent of its effects on blood pressure. However the mechanism of aldosterone function and especially the signaling cascades involved in the responses of the cells, have not been well understood. In this thesis, I investigated the effects of HA on the cardiomyocyte's electrophysiology and found a substantial reduction of AP duration and I_{toC} up-regulation. Moreover, by inducing HA in $G\alpha_q/G\alpha_{11}$ knockout mice I found a possible contribution of $G\alpha_q/G\alpha_{11}$ signaling in the aldosterone-induced alteration of cardiomyocyte's electrophysiology. Thus, I concluded that aldosterone induces remodeling of cellular electrophysiology and $G\alpha_q/G\alpha_{11}$ signaling cascades are essentially involved in these genomic responses.

Following voltage-dependent activation, Cav1.2-channels can undergo voltage and/or Ca^{2+} -dependent inactivation. The Ca^{2+} -binding protein calmodulin (CaM) mediates the latter inactivation (CDI). Ca^{2+} -saturated CaM interacts with the IQ motif in the C terminus of Cav1.2 to accomplish this. To further investigate the impact of IQ-CaM interaction in Cav1.2 regulation, I/E mutation (Ile1624 to Glu) was generated in IQ sequence. Here I studied the effects of I/E mutation of IQ motif on the (i) Cav1.2 function and (ii) EC coupling gain. Interestingly, I/E mutation caused a substantial decrease of $I_{Ca,L}$ density. Despite $I_{Ca,L}$ reduction, the amplitude of global Ca^{2+} transients were increased in the ventricular myocytes from I/E mice, as a result of an enhanced

EC coupling gain. This increase in intracellular Ca^{2+} levels due to higher EC coupling gain was ultimately the cause of cardiac dysfunction in mice with the I/E mutation.

Rac1 is a monomeric G-protein that is activated downstream to integrin signaling and stimulates various cellular processes including cytoskeletal reorganization and ROS production. Rac1 has been shown to contribute to the development of cardiac pathological responses such as cardiomyopathy and atrial fibrillations. However the underlying mechanisms are not well understood. In this thesis, I studied the effects of expression of a constitutively active Rac1 (V12Rac1) on the EC coupling gain in ventricular myocytes. Despite a substantial decrease in steady-state $I_{\text{Ca,L}}$, the amplitude of global Ca^{2+} transients were increased in ventricular myocytes expressing constitutively active Rac1, as a result of an enhanced EC coupling gain. The higher intracellular Ca^{2+} levels, similar to I/E mutation, were the primary cause of cardiac dysfunction.

The potential to culture cardiomyocytes is highly important due to the fact that isolated adult cardiomyocytes initiate the process of remodeling in a few hours which leads to de-differentiation of cardiac cells. However, some biological studies such as chronic hormone treatment *in vitro* or expression of exogenous proteins by adenoviral gene transfer needs culturing of cardiomyocytes for longer time periods even days. Therefore different approaches were employed to prevent this remodeling process. Cytochalasin D (CytoD), a fungi metabolite, has been reported to have beneficial effect in the culture of cardiac cells since it could preserve the cardiomyocyte's morphology. In this thesis I investigated whether CytoD can preserve the cardiomyocyte's function, too. Studying the action potential, I found that CytoD at 0.5 μM can preserve the electrophysiological properties of ventricular myocytes along with morphology over a culturing period of three days. Thus, CytoD (0.5 μM) can be used as a routine culture supplement in primary culture of cardiomyocytes to preserve both morphology and function.

List of Abbreviations

| | |
|-----------------|--|
| 4-AP | 4-aminopyridine |
| a.u. | Arbitrary unit |
| CCD | Charged-coupled device |
| CCS | Ca ²⁺ -containing solution |
| CFS | Ca ²⁺ -free solution |
| Cys | Cystein |
| DAG | Diacylglycerol |
| DIV | Day in vitro |
| EGTA | ethylene glycol tetraacetic acid |
| ERK | Extracellualr receptor kinase |
| FKBP | FK-506 binding protein |
| GDP | Guanosine-5'-diphosphate |
| Glu | Glutamate |
| GPCR | G-protein coupled receptor |
| GTP | Guanosine-5'-triphosphate |
| h | hour |
| HEPES | 4-(2-hydroxyethyl)-1-piperazineethanesulfonic acid |
| Ilu | Isoleucin |
| IP ₃ | Inositol triphosphate |
| JNK | Jun kinase |
| kg | kilogram |
| LCS | low Ca ²⁺ -solution |
| LP | Long pass |
| mAKAP | Muscle-specific A kinase anchoring protein |
| MAPK | Mitogen-activated protein kinase |
| MEK | MAP kinase/ERK kinase |
| µg | microgram |
| mg | milligram |

| | |
|------------------|---|
| ml | milliliter |
| MLC2 | Myosin light chain2 |
| ms | millisecond |
| NADPH | Nicotinamide adenine dinucleotide phosphate |
| PAK | P21-activated kinase |
| pC | picocoulomb |
| Phe | Phenylalanine |
| PIP ₂ | Phosphatidyl inositol bisphosphate |
| PKA | Protein kinase A |
| PKC | Protein kinase C |
| PLC | Phospholipase C |
| RGS | Regulators of G-protein signaling |
| ROS | Reactive oxygen species |
| Ser | Serine |
| T _{1/2} | Half-life of drugs |
| Tyr | Tyrosine |

List of Figures

- Figure 1.1:** The graphical illustration of the anatomy of the heart
- Figure 1.2:** The graphical illustration of the heart conduction system
- Figure 1.3:** Schematic representation of cardiomyocyte's subcellular architecture
- Figure 1.4:** APs in different regions of the heart
- Figure 1.5:** Cardiac AP and the major underlying ion currents
- Figure 1.6:** Guinea pig (A) and Mouse (B) ventricular AP
- Figure 1.7:** Structure of Nav1.5
- Figure 1.8:** Structure of Cav1.2
- Figure 1.9:** EC coupling in cardiomyocyte
- Figure 1.10:** A model illustrating some signaling cascades in cardiomyocytes
- Figure 1.11:** integrin signaling
- Figure 1.12:** The schematic illustration of the Renin-Angiotensin-Aldosterone system
- Figure 2.1:** Patch-clamp setup
- Figure 2.2:** Sequence of pipette potentials (V_p) and pipette currents (I_p) during establishment of the whole cell configuration
- Figure 2.3:** Schematic illustration of AP amplitude and AP durations
- Figure 2.4:** I_{toc} measurement
- Figure 2.5:** $I_{Ca,L}$ measurement
- Figure 2.6:** The excitation and emission spectra of Indo-1
- Figure 2.7:** Schematic presentation of the protocol used for EC coupling gain measurements
- Figure 3.1:** The effects of $G\alpha_q$ KO on the electrophysiological characteristics of ventricular myocytes
- Figure 3.2:** The effect of Cd^{2+} on transient outward current (I_{toc}) density
- Figure 3.3:** The effect of $G\alpha_q$ KO on the transient outward current (I_{toc}) in ventricular myocytes
- Figure 3.4:** Tamoxifen pharmacokinetics

Figure 3.5: The effects of tamoxifen application on the electrophysiological characteristics of ventricular myocytes from wildtype and $G\alpha_{11}$ KO animals

Figure 3.6: The effect of tamoxifen application on the transient outward current (I_{toc}) of ventricular myocytes from wildtype and $G\alpha_{11}$ KO animals

Figure 3.7: The effects of miglyol application on the electrophysiological characteristics of ventricular myocytes from wildtype animals

Figure 3.8: The effects of miglyol application on the AP duration of ventricular myocytes from wildtype animals

Figure 3.9: The effects of miglyol application on the electrophysiological characteristics of ventricular myocytes from $G\alpha_{11}$ KO animals

Figure 3.10: The effects of miglyol application on the AP duration of ventricular myocytes from $G\alpha_{11}$ KO animals

Figure 3.11: The effects of Cre expression on the electrophysiological characteristics of ventricular myocytes from wildtype and $G\alpha_{11}$ KO animals

Figure 3.12: The effect of Cre expression on the transient outward current (I_{toc}) of ventricular myocytes from wildtype and $G\alpha_{11}$ KO animals

Figure 3.13: The effects of $G\alpha_q$ and/or $G\alpha_{11}$ KO on the electrophysiological characteristics of ventricular myocytes

Figure 3.14: The effect of $G\alpha_q$ and/or $G\alpha_{11}$ KO on the transient outward current (I_{toc}) in ventricular myocytes

Figure 3.15: The effects of HA on the electrophysiological characteristics of ventricular myocytes

Figure 3.16: The effect of HA on AP shape of ventricular myocytes

Figure 3.17: The effects of HA on the AP durations of ventricular myocytes

Figure 3.18: The effect of HA on the I_{toc} -voltage relationships

Figure 3.19: The effect of HA on the I_{toc} density in ventricular myocytes

Figure 3.20: The effect of I/E mutation on the L-type Ca^{2+} current ($I_{Ca,L}$) in ventricular myocytes

Figure 3.21: The effect of I/E mutation on the plasma membrane capacitance (C_M)

Figure 3.22: The effects of I/E mutation on EC coupling

Figure 3.23: The effects of I/E mutation on $I_{Ca,L}$ inactivation

Figure 3.24: The effect of expression of a constitutively active Rac1 on the L-type Ca^{2+} current ($I_{\text{Ca,L}}$) in ventricular myocytes

Figure 3.25: The effect of expression of a constitutively active Rac1 on EC coupling

Figure 3.26: The effect of expression of a constitutively active Rac1 on $I_{\text{Ca,L}}$ inactivation

Figure 3.27: The effect of 40 μM CytoD on the plasma membrane capacitance (C_M) of cultured adult cardiomyocytes

Figure 3.28: The effects of 40 μM CytoD on the electrophysiological characteristics of cultured adult ventricular myocytes

Figure 3.29: The effects of 40 μM CytoD on AP duration of cultured adult ventricular myocytes

Figure 3.30: The effect of 0.5 μM CytoD on the plasma membrane capacitance (C_M) of cultured adult cardiomyocytes

Figure 3.31: The effects of 0.5 μM CytoD in the culture medium on the electrophysiological characteristics of cultured adult ventricular myocytes

Figure 3.32: The effects of 0.5 μM CytoD on AP duration of cultured adult ventricular myocytes

Figure 4.1: Cre-ER/LoxP system

Figure 4.2: Survival curve of I/E and Ctr mice

Figure 4.3: Schematic illustration of I/E mutation effects in the heart

List of Tables

Table 1.1: Different distributions of Na^+ , K^+ , Ca^{2+} and Cl^- across the membrane and their Nernst potential

Table 1.2: genes encoding for the α and β subunits of potassium channels

Table 2.1: Composition of the solutions used for preparation of ventricular myocytes

Table 2.2: Composition of the solutions used for electrophysiological experiments

Table 3.1: Transgenic animals used to study the physiological role of $\text{G}\alpha_q$ and/or $\text{G}\alpha_{11}$ proteins

Table 3.2: $\text{G}\alpha_q$ KO by insertion of LoxP sites

Table 3.3: $\text{G}\alpha_q$ KO by employing Cre expression

1. Introduction

1.1. The heart anatomy

The heart is a muscular organ, which pumps the blood throughout the entire body. The blood provides O_2 and nutrients and removes excretory products in the vicinity of every single cell, thus ensures the cell survival. The pumping property originates from the intrinsic characteristics of the heart muscle. This muscle builds the walls of 4 heart chambers: *right and left atria*, *right and left ventricles*. The right atrium is separated from the right ventricle by the *tricuspid valve* whereas the left chambers (the left atrium and ventricle) are separated by the *mitral valve* (Figure 1.1).

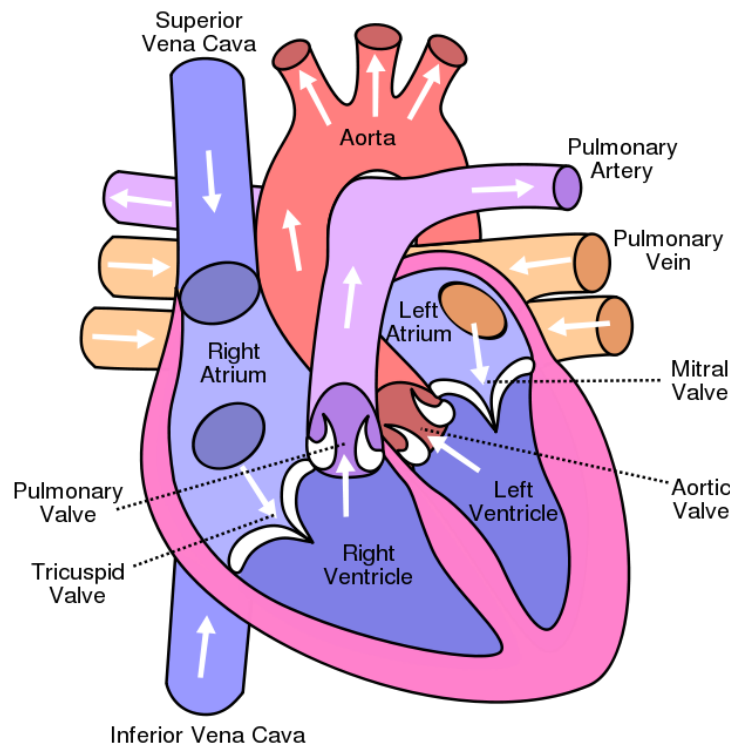


Figure 2.1: The graphical illustration of the anatomy of the heart. The heart chambers and valves as well as the blood circulation in the heart are shown. For detailed explanation see 1.1. Image taken from www.en.wikibooks.org

The atria have a thin wall and develop relatively low pressure. While the thicker muscular walls of the ventricles provide enough force for pumping of the blood to the arteries. A wave of contraction, which starts in the atria (atrial systole) and continues in the ventricles (ventricular systole), generate a heartbeat. Each heartbeat results in the ejection of blood to the arteries. The percentage of blood volume that is pumped out of a filled ventricle with each heartbeat, is called ejection fraction (EF) ⁶⁵. The beating frequency and EF are normally regulated in response to the body needs. For instance both heart rate and ventricular ejection are enhanced during exercise. After the contraction phase, all four chambers are relaxed (diastole).

1.2. The conduction system of the heart

In the previous section, the heartbeat was introduced as the driving force for blood ejection. But what is the trigger for the heartbeat? Does the cardiac muscle contract spontaneously or does it need a stimulus? The regular sequence of contraction of heart muscle contraction shows the necessity for a stimulus. The initial trigger for the heartbeat appears to be the electrical impulses, which originate from a group of specialized myocardial cells called the *sinoatrial (SA) node*. The electrical impulses initiated in the SA node propagate through the entire atrial muscle via the *intermodal atrial pathways*. After a delay in the *atrioventricular (AV) node*, the electrical excitation enters the ventricles via the *bundle of His*. The bundle of His has two branches: *right* and *left bundle branches* that enter the right and left ventricles, respectively. The wave of depolarization propagates into the ventricular muscle via the *Purkinje fibers*. The Purkinje network ensures the synchronized activation of both ventricles. Thus, the heartbeat is based on the function of the heart's conduction system (Figure 1.2).

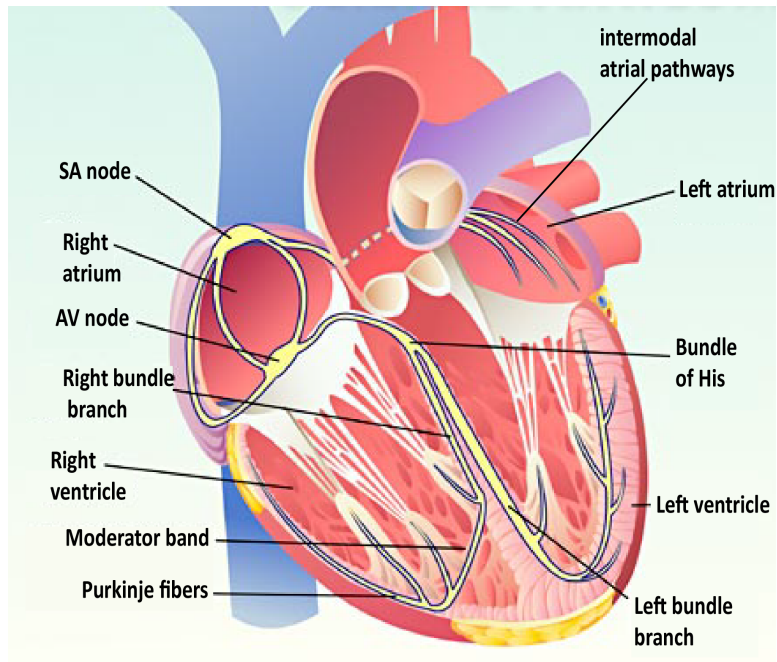


Figure 1.2: The graphical illustration of the heart conduction system. For detailed explanation see 1.2. Image taken from www.scienceart.com

1.3. Structure of a working cardiomyocyte

The cardiomyocytes are the working units of the heart. They have two important functional properties: (i) excitability and (ii) contractility. Both properties originate from their specialized structures.

The plasma membrane of the cardiomyocyte contains numerous ion channels and transporters that mediate ion influx and efflux and lead to the various ionic distribution across the membrane. These ionic movements are the basis for the cardiomyocytes' excitability, which will be explained in 1.4.

The other feature of the cardiomyocyte, are the invaginations of the plasma membrane that create the transverse tubular (t-tubular) system (Figure 1.3). This system is formed and stabilized by the cytoskeleton ¹⁰⁸ and ensures the rapid and synchronous contraction of the cardiomyocyte ³¹. Similar to the surface membrane, t-tubules contain different ion channels and transporters that facilitate the propagation of the electrical impulse into the cell interior. This process leads to the activation of a large number of

Ca²⁺ channels in the t-tubules ⁹⁹. The resulting Ca²⁺ influx is the main trigger for the increase in the intracellular Ca²⁺ concentration ([Ca²⁺]_i), which is the primary requirement for the activation of contraction. The sarcoplasmic reticulum (SR) is the main Ca²⁺ store of the cell and SR Ca²⁺ release is triggered by the Ca²⁺ influx across the membrane. As a result of the t-tubular system, the plasma membrane is located in the close proximity of the SR membrane, building the dyadic space that is about 15 nm wide ¹⁵⁶ to facilitate the Ca²⁺ induced Ca²⁺ release from the SR. Therefore, the t-tubules play an important role in the coupling of electrical excitation to the contraction, a phenomena called excitation-contraction (EC) coupling. A large number of cardiac diseases such as heart failure are associated with t-tubular disarray ²⁰⁷.

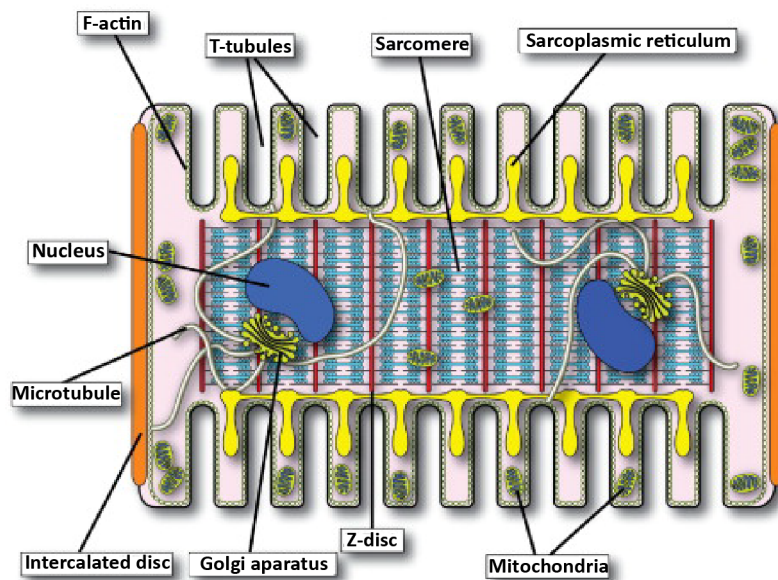


Figure 1.3: Schematic representation of cardiomyocyte's subcellular architecture. T-tubules are the invaginations of plasma membrane that proximate sarcolemmal Cav1.2 channels to SR Ca²⁺ release channels on the sarcoplasmic reticulum. The contractile filaments that are structured as sarcomeres are responsible for contractility in response to Ca²⁺ release from the sarcoplasmic reticulum. Taken from Smyth and Shaw, 2010 ¹⁸⁰.

In addition to the specialized features of the cell membrane, the cardiac myocyte contains thick (or myosin) and thin (or actin) filaments as well as associated contractile and skeletal components, which together build the contractile machinery of the cell. The special alignment of contractile filaments results in a cross-striated pattern in the cardiac cells (Figure 1.3). The remaining volume of cardiomyocyte is mostly occupied by the mitochondria, which are the energy supplies of the cell.

1.4. The electrophysiological properties of a cardiomyocyte

1.4.1. Resting membrane potential (V_R)

The membrane potential results from different distributions (Table 1.1) and conductances of ions across the membrane.

Table 4.1: Different distributions of Na^+ , K^+ , Ca^{2+} and Cl^- across the membrane and their Nernst potential ²³.

| Ion (x) | $[\text{x}]_o$ (mM) | $[\text{x}]_i$ (mM) | E_x (mV) |
|------------------|---------------------|---------------------|------------|
| Na^+ | 135-145 | 10 | +70 |
| K^+ | 3.5-5 | 155 | -89 |
| Ca^{2+} | 2 | 10^{-4} | +125 |
| Cl^- | 95-110 | 10-20 | -55 |

In cardiomyocytes, the plasma membrane is preferentially permeable to K^+ and the resting potential is mainly determined by the equilibrium potential of this ion. The equilibrium potential is the potential at which the chemical gradient of an ion is balanced by the electrical gradient across the membrane (net current flow=0) and can be described by the Nernst equation:

$$E_m = \frac{RT}{ZF} \ln \frac{P[x]_o}{P[x]_i} \quad \text{Nernst equation}$$

Where E_m is the membrane potential, R the gas constant, T the absolute temperature, Z the valence of the ion, F the Faraday constant, P the permeability to the ion, $[\text{x}]_o$ and $[\text{x}]_i$ extracellular and intracellular ion concentrations, respectively.

Despite the lower permeability of the membrane to other ions such as Na^+ and Ca^{2+} , they also contribute to the resting membrane potential (V_R). The resulting potential across the membrane can be quantified by the Goldman-Hodgkin-Katz (GHK) equation:

$$E_m = \frac{RT}{ZF} \ln \left(P_K \frac{[K]_o}{[K]_i} + P_{Na} \frac{[Na]_o}{[Na]_i} + P_{Cl} \frac{[Cl]_i}{[Cl]_o} \right) \quad \text{GHK Equation}$$

How are the resting concentration gradients of Na^+ and K^+ maintained across the membrane? The Na^+/K^+ -ATPase consumes one ATP to actively transport 3 Na^+ out of and 2 K^+ into the cell, which maintains the electrochemical gradients for Na^+ and K^+ , thus contributes to the V_R .

1.4.2. Action potential (AP)

The cardiac action potential (AP) comprises a wave of finely tuned coordinated openings and closings of multiple ion channels¹⁸¹. Voltage-gated ion channels e.g. Na^+ , K^+ , and Ca^{2+} channels contribute to the cardiac AP in a particular way. The shape and duration of the cardiac APs vary greatly among different regions of the heart (Figure 1.4) as well as specific areas within those regions (epicardium vs. endocardium)¹⁷.

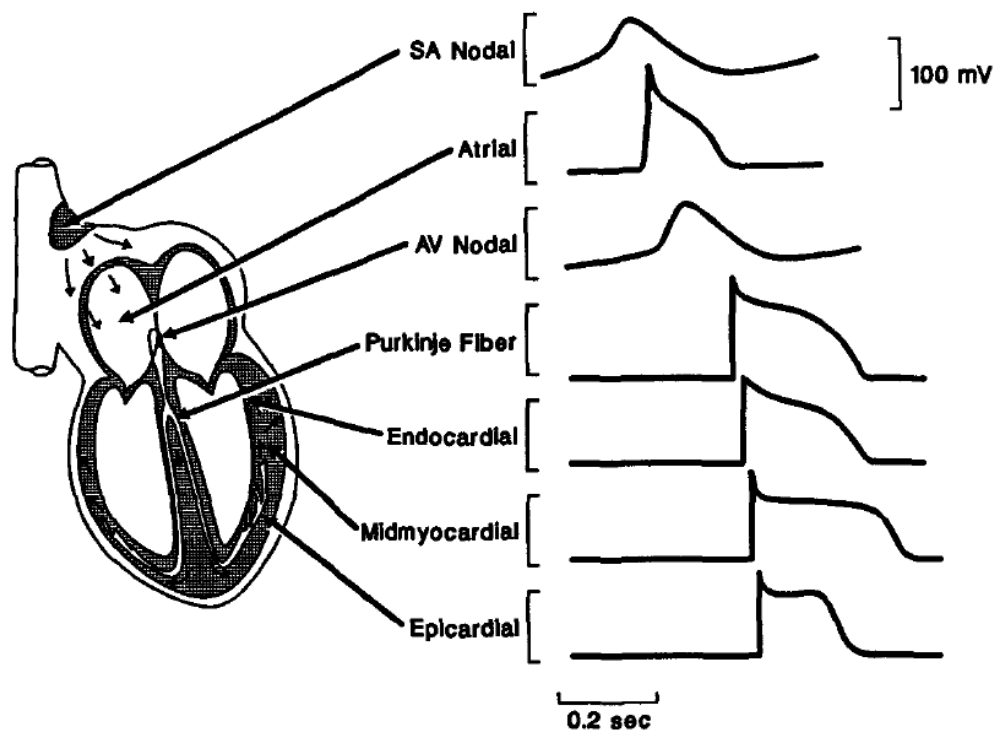


Figure 1.4: APs in different regions of the heart. The schematic illustration of different shapes and durations of APs in atria, ventricle and heart conduction system. The temporal sequence of AP propagation throughout the heart is reflected in the figure. Taken from Barry & Nerbonne, 1996¹⁷.

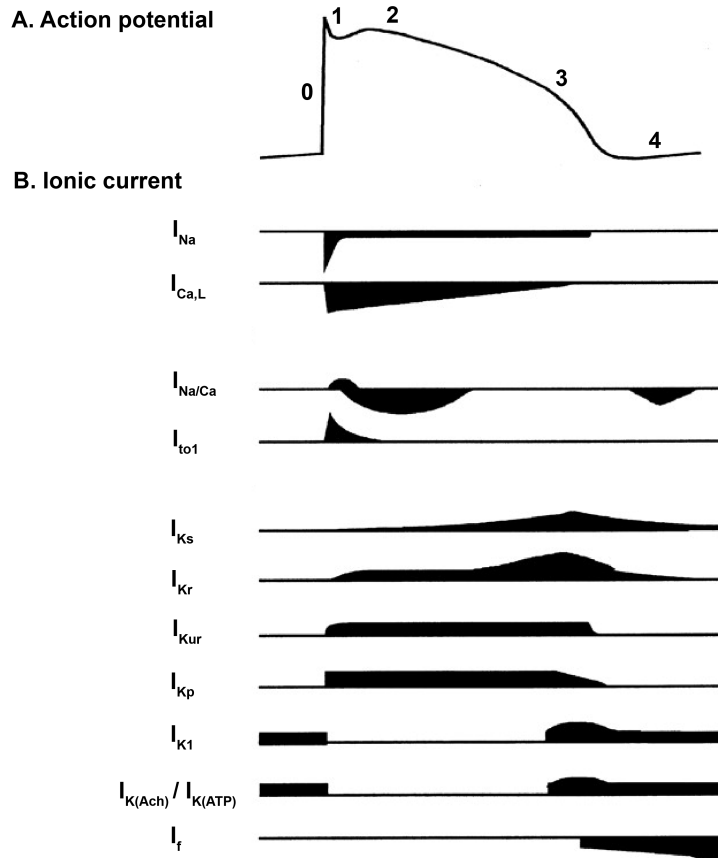


Figure 1.5: Cardiac AP and the major underlying ion currents. Different phases of cardiac AP (A) and the contribution of each current for shaping every phase (B), are displayed. The amplitudes of the depolarizing (downward) and repolarizing (upward) currents are not on the same scales. For abbreviations: see text. Modified from Snyder, 1999¹⁸¹

Figure. 1.5 illustrates a human ventricular AP and its underlying currents. As shown, the ventricular AP can be subdivided into 5 different phases. The initial upstroke (phase 0) results from the activation of the fast inward Na^+ current (I_{Na}). The transient rapid repolarization (phase 1) is a result of the activation of transient outward K^+ current (I_{to1}) and ultrarapid delayed rectifier K^+ current (I_{Kur}) along with the rapid voltage-dependent inactivation of I_{Na} . The size of this early repolarization (notch) greatly influences the time course of the other voltage-gated currents and, consequently controls the AP duration indirectly. Phase 2 results from a fine balance of inward depolarizing current ($I_{Ca,L}^*$) and outward currents through delayed rectifier K^+ channels (I_{Kur} , I_{Kr}^\dagger and I_{Ks}^*)¹⁸¹. The last

* L-type Ca^{2+} current

† Rapid delayed rectifier K^+ current

phase of repolarization (phase 3) is the product of the increase in the conductance of the I_{Kr} , I_{Ks} and I_{K1} ¹⁸⁸. The resting membrane potential (phase 4) is maintained by inwardly rectifying K^+ currents including I_{K1} , $I_{K(ATP)}$ [†] and $I_{K(Ach)}$ [‡]. The ventricular AP differs in shape and duration among different species²⁰⁰. While the AP in guinea pig cells displays a long-lasting plateau, the AP of mouse cells lacks phase 2 (Figure 1.6). In the following, the ionic currents shaping (underlying) the different phases of the AP will be described.

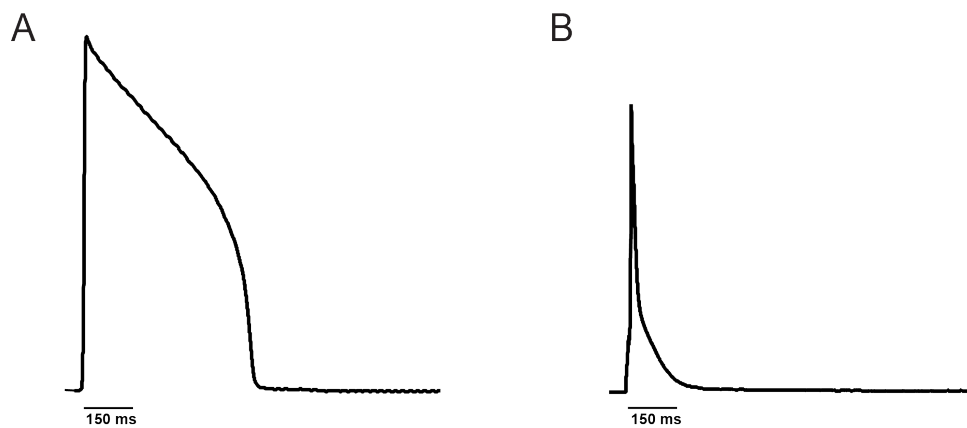


Figure 1.6: Guinea pig (A) and Mouse (B) ventricular AP. For description see 1.4.2.

1.4.3. Na^+ current

I_{Na} which generates the fast upstroke (phase 0) of cardiac AP was the focus of studies for more than half a century⁶². It has been shown that voltage-gated Na^+ channels underlie these currents and therefore are responsible for the AP upstroke as well as the rapid impulse conduction through cardiac tissue¹⁶.

These channels were the first voltage-gated ion channels to be cloned and sequenced in the 1980s¹⁴⁰. Voltage-gated Na^+ channels are composed of a principal large pore

* Slow delayed rectifier K^+ current

† inwardly rectifying K^+ current activated by ATP

‡ inwardly rectifying K^+ current activated by acetylcholine

forming α -subunit and small accessory β -subunits. By today, at least 6 separate genes encoding homologous α -subunit isoforms in human (Nav1.1- Nav1.6) have been cloned. These isoforms expressed in the brain, heart and skeletal muscle^{8,67}. The heart isoform, Nav1.5, which is encoded by the SCN5A gene, is the predominant α -subunit of the cardiac Na channels⁶⁶. Mutations in the SCN5A gene lead to various pathological phenotypes, such as long QT (LQT) syndrome type 3, Brugada syndrome, and the diseases of the heart conduction system²²⁶. Accessory β -subunits appeared to have a primary role in regulating the subcellular localization of the α -subunits⁸⁹.

The α -subunit is composed of four homologous domains (DI-DIV), each containing 6 transmembrane segments (S1-S6) and a pore loop (Figure 1.7). The pore through which Na^+ ions permeate, is formed by the S5-S6 segments along with their cytoplasmic linkers called pore loops (P-loop). Mutations in P-loop can completely disrupt the ion-channel function¹⁶¹. The fourth transmembrane segment (S4) in each of the 4 domains, which contains regularly arranged positive charges, works as a “voltage sensor” and responds to the membrane depolarization by a conformational change that results in channel pore opening and subsequent inward current¹⁶. In domain III, a lysine critically selects for Na^+ over Ca^{2+} and constructs the selectivity filter region¹⁴⁵.

Voltage-gated Na^+ channels inactivate rapidly after a very brief channel opening. A group of 3 hydrophobic amino acids in the linker between domains III and IV are proposed to be important for the channel inactivation⁸⁰ although other structures (S6 in domain IV and S4-S5 linkers) have also been suggested^{127,189}. Recovery from inactivation occurs when the membrane potential changes back to resting levels (negative E_m)²³.

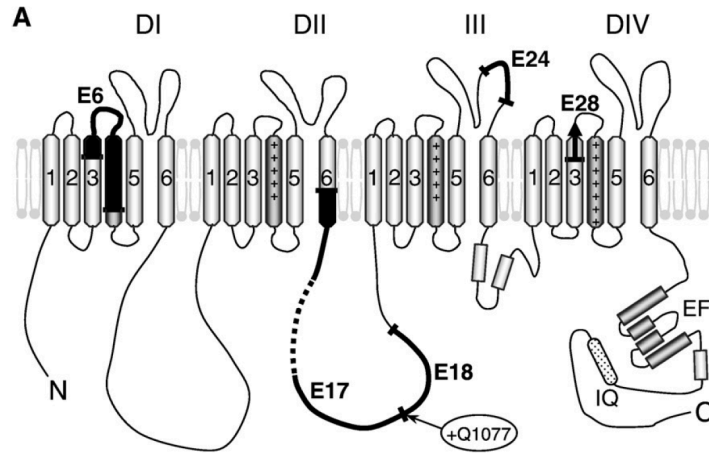


Figure 1.7: Structure of Nav1.5. Each of the four Na⁺ channel domains (DI–DIV) consists of six transmembrane α -helices. The fourth segment (S4) contains regularly arranged positive charges that function as the voltage sensor. The intracellular loop between DIII and DIV forms the inactivation gate. The proximal C terminus is composed of six helices forming an EF-hand domain (EF) and a downstream calmodulin binding motif (IQ motif). Black regions (E6, E17, E18, E24, E28) are channel regions affected by alternative splicing. Taken from Schroeter et al, 2010¹⁷⁴.

Unlike other voltage-gated Na⁺ channels, the cardiac Na⁺ channels are rather tetrodotoxin (TTX)-insensitive and can only be blocked by high concentrations (in mM range) of TTX. The Cys401 in the p-loop of the domain I of the cardiac Na⁺ channels, which is different from Phe or Tyr of the non-cardiac voltage-gated Na⁺ channels, has been proposed to underlie this low TTX sensitivity¹⁴. The type I antiarrhythmic agents such as quinidine, procainamide, lidocaine can also block cardiac I_{Na}. The PKA-dependent phosphorylation of the cardiac Na⁺ channels leads to a marked increase of I_{Na} by enhancing the maximal Na⁺ conductance¹⁷³.

1.4.4. L-type Ca²⁺ current

There are 2 types of Ca²⁺ currents in cardiac cells: T- and L-type Ca²⁺ currents. The channels responsible for these currents differ in their biophysical properties as well as drug sensitivity. L-type Ca²⁺ channels have a high conductance (~25 pS in 110 mM Ba²⁺), long openings, activation at larger depolarizations and sensitivity to 1,4-dihydropyridines (DHP). In contrast, T-type Ca²⁺ channels display a tiny conductance

(~8 pS in 110 mM Ba²⁺), transient openings, activation at more negative E_m and resistance to DHP²³.

Moreover they have different functions in cardiac myocytes. The L-type Ca²⁺ current (I_{Ca,L}) which is a depolarizing current does not play a considerable role in the rapid upstroke phase of AP in atria, ventricle and His-Purkinje system, but it balances the outward K⁺ currents which leads to a plateau during the early repolarization phase. On the other hand, I_{Ca,L} triggers SR Ca²⁺ release and contributes to the refilling of the SR Ca²⁺ stores. In addition to its role in working myocytes, I_{Ca,L} is responsible for the relatively slow depolarization phase of AP in SA and AV nodes.

Although T-type Ca²⁺ current (I_{Ca,T}) activation has the same E_m-dependency as I_{Na} (activation at -50 mV), it does not play an important role in the AP depolarization. A tiny channel conductance and transient openings cause only a very small inward current compared to the large Na⁺ influx. Moreover, they do not contribute to EC Coupling for two reasons: (i) I_{Ca,T} is very small and (ii) T-type channels are not located in close proximity to the Ca²⁺ release channels of the SR⁹⁸. Some studies suggest that I_{Ca,T} has a role in atrial pacemaking⁷⁶.

The L-type voltage-dependent Ca²⁺ channels (LVDCC) are composed of 4 subunits: the α₁, α₂/δ, β, and, in some tissues, γ²⁸ (Figure 1.8). The cardiac isoform lacks the γ subunit¹¹⁰. While α_{1c} builds the core of the cardiac LVDCCs (Cav1.2), the accessory (β₂, α₂/δ) subunits modulate the biophysical properties as well as trafficking of the α_{1c} to the membrane²⁸.

Similar to the α-subunit of other voltage-gated ion channels, α_{1c} consists of 4 homologous domains (I–IV), each composed of 6 transmembrane α-helices (S1 to S6). Various biophysical properties of the LVDCC such as channel pore (S5, S6 and their cytoplasmic linker), voltage sensor (S4), inactivation-related sequences (cytoplasmic C-termini) and the binding sites of the channel modulators³⁸ are all determined by the α_{1c} subunit. A congenital cardiac disease called Timothy Syndrome has been related to a mutation in the α_{1c} subunit and specifically in the exon 8 of the Cav1.2 gene¹⁸³.

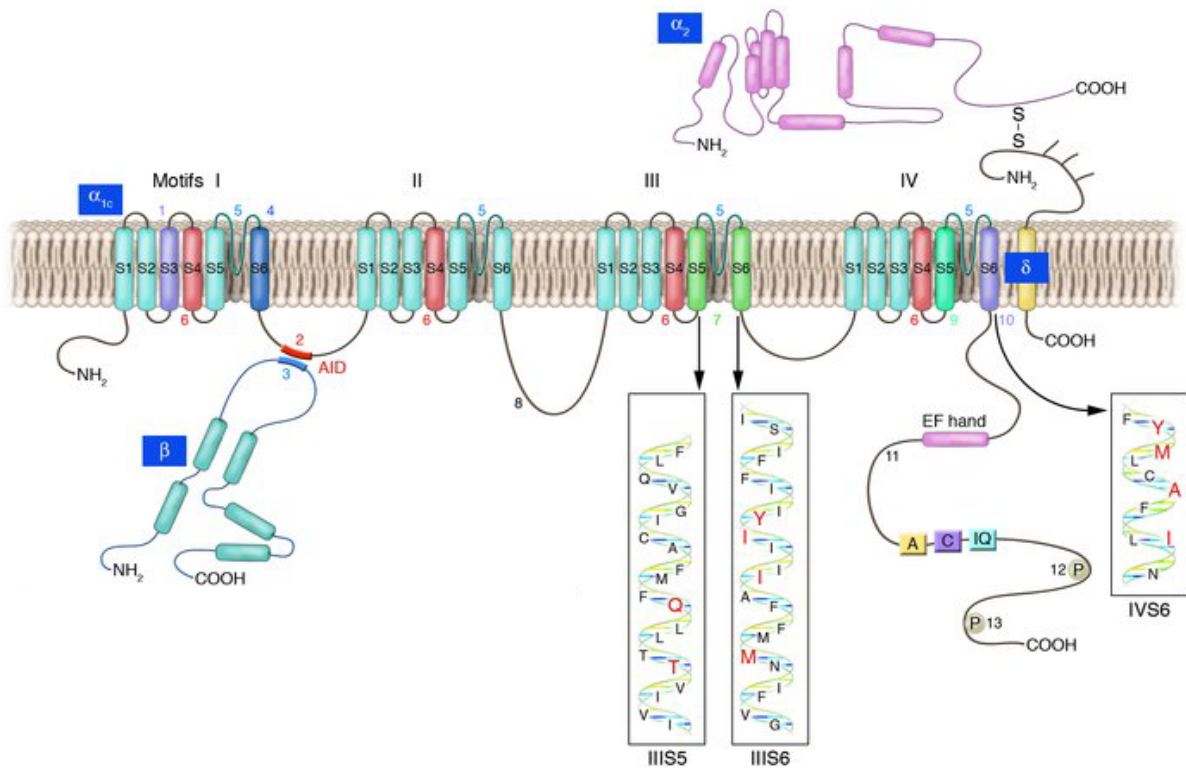


Figure 1.8: Structure of Cav1.2. The proposed membrane topology of the core subunit and interactions with auxiliary subunits are displayed. The pore-forming α -subunit consists of homologous domains (I–IV), each composed of 6 transmembrane α -helices (S1 to S6). The numbers indicate the following regions: 1- Voltage-dependent activation kinetics 2- Interaction with β -subunit (I-II cytoplasmic linker) AID 3- BID 4- Voltage-dependent inactivation (IS6 and flanking regions) 5- Ion selectivity (pore-forming S5-S6 linker regions) 6- Voltage sensor (IS4, IIS5, IIIS4, IVS4) 7- Binding sites for DHP 8- EC coupling (II-III linker) 9- Role in use-dependent block 10- Binding sites for BTZ, DHP, and PAA 11- Ca^{2+} -dependent inactivation (C terminal) 12- Phosphorylation site for CaMK-II (Ca^{2+} /calmodulin dependent protein kinase) 13- Phosphorylation site for PKA. Taken from Bodi et al, 2005²⁸.

The cardiac β_2 subunit, which consists of a single cytosolic domain (Figure 1.8), interacts with α_{1c} through a special sequence called the β -interaction domain (BID). It has been shown that the binding partner of BID on the α_{1c} is a highly conserved sequence in the cytoplasmic linker between domains I and II, called the α -interaction domain (AID)¹⁵⁴. While α_{1c} dictates the biophysical characteristic of the channel, β_2 is much more involved in the regulation of these properties¹⁷⁸. For instance, β_2 has been postulated to be important for the expression, assembly¹⁹⁰ and trafficking of the α_{1c} to the membrane²¹⁷. Moreover, the pore opening is augmented²¹⁷ and the DHP affinity is enhanced¹³³ by β_2 . The $I_{\text{Ca,L}}$ increase in response to β -adrenergic stimulation is also

mediated by the β_2 subunit¹³³. PKA-dependent phosphorylation of β_2 subunit at positions Ser478 and Ser479 resulted in an increase of peak $I_{Ca,L}$ ³⁴.

The α_2/δ subunits are the products of one gene and are separated posttranslationally⁴⁸. The α_2 is extracellular and is bound to the monomeric transmembrane δ subunit through a disulfid bridge²⁸. The α_2/δ are supposed to participate in the regulation of the biophysical properties of the channel with β_2 ²³. These subunits increased the DHP sensitivity of the channel by 4-fold and accelerated the channel opening and closing^{208,59}.

$I_{Ca,L}$ inactivates in a biphasic manner. Several studies proposed 2 different mechanisms for LVDCC inactivation: (i) Ca^{2+} -dependent inactivation (CDI) and (ii) voltage-dependent inactivation (VDI)¹⁰⁹. CDI is a regulatory mechanism with which Ca^{2+} limits its own influx via LVDCC. This helps to reduce the risk of Ca^{2+} overload in the cell. CDI is primarily dependent on the Ca^{2+} release from the Ca^{2+} release channels of SR (RyR)⁴⁹ and is the predominant mechanism for LVDCC inactivation on the time scale of an AP³². VDI On the other hand prevents a premature activation of the channel when CDI terminates¹⁵⁹.

CDI is mediated by a Ca^{2+} binding protein called calmodulin (CaM)^{227,229}. CaM has binding sites on the carboxy terminus of the α_{1c} subunit, one of them is called IQ motif². CaM binds to these binding sites with a very high affinity, even at rest and in unsaturated state (when less than 4 Ca^{2+} ions are bound to CaM)¹⁴⁹. E_m depolarization and intracellular Ca^{2+} increase lead to the binding of 4 Ca^{2+} ions to CaM. Ca^{2+} -saturated CaM changes its conformation along with α_{1c} , which leads to the closure of the channel pore¹⁹⁵.

LVDCCs appeared to be regulated by different types of protein kinases such as PKA and PKC. PKA which is activated downstream to β -adrenergic stimulation, enhances the $I_{Ca,L}$ by increasing the open probability as well as the open time of the channel¹⁹⁵.

α_{1c} has been shown to be the target for PKA-dependent phosphorylation⁴⁷. However, *in vitro* experiments showed a PKA-mediated phosphorylation of auxiliary β subunits, too⁶⁸. A source of readily usable PKA is provided by mAkap or AKAP15 in the vicinity of

LVDCCs⁹⁴. Activation of PKC downstream to various types of $G_{\alpha q/11}$ protein-coupled receptors may also lead to channel phosphorylation⁹⁴. Although, this effect on the $I_{Ca,L}$ can either be increasing¹¹ or decreasing²²¹. One possible explanation for this controversial effect is the GPCR-dependent production of IP_3 along with PKC activation. IP_3 could induce Ca^{2+} release from the SR which would induce CDI and counterbalance the $I_{Ca,L}$ increase by PKC phosphorylation¹⁰¹. Various pharmacological tools such as most of DHPs, phenylalkylamines (PAAs), and benzothiazepines (BTZs) can inhibit $I_{Ca,L}$ ²⁸. On the other hand, some DHPs such as Bay K 8644 and CGP 28392 are Ca^{2+} channel agonists and enhance $I_{Ca,L}$ ²³.

1.4.5. K^+ currents

Different types of K^+ currents have been described in cardiomyocytes. Cardiac K^+ currents have different biophysical properties such as various time- and voltage-dependence and/or drug sensitivity. This variety results in their different physiological functions. The K^+ currents shape the cardiac AP, drive E_m toward E_K , and regulate the heart rate. Furthermore, many hormones, neurotransmitters and drugs modulate the cardiac function by regulation of K^+ channels^{136,181}.

To simplify the study of K^+ channels, different types of classifications were introduced. According to Tamargo, K^+ channels can be classified as voltage-gated (Kv) and ligand-gated K^+ channels¹⁸⁸. The Kv channels were further categorized: (a) 4-AP sensitive, rapidly activating and inactivating currents, referred to as I_{to} (transient outward) and (b) TEA sensitive, slowly activating and inactivating outward currents referred to as delayed rectifier K^+ currents¹⁷. Table 1.2 shows members of each category and genes encoding for each channel.

Kv channels are formed by coassembly of four pore-forming α subunits and ancillary β subunits. The α subunit consists of six transmembrane-spanning segments (S1–S6) with cytoplasmic N- and C-termini and a pore loop between S5 and S6 carrying the K^+ selectivity filter signature TxGYG¹⁸¹. The voltage sensor resides in the S4 segment.

Accessory β subunits modulate membrane trafficking, gating properties and drug sensitivity of the channel ^{79,123}. Most Kv channels experience an inactivated state between open and close state and need a recovery phase for reactivation ¹⁸⁸.

Table 1.2: genes encoding for the α and β subunits of potassium channels. Taken from Tamargo et al, 2004 ¹⁸⁸.

| Current | α -Subunit | | β -Subunit | |
|--------------|-------------------|--------|-----------------------------|--------|
| | Name | Gene | Name | Gene |
| I_{Ks} | Kv7.1 (KVLQT1) | KCNQ1 | Mink | KCNE1 |
| I_{Kr} | Kv11.1 (HERG) | KCNH2 | Mink | KCNE1 |
| I_{Kur} | Kv1.5 (HK2) | KCNA5 | Kv β 1 (Kv β 3) | KCNAB1 |
| I_{K1} | Kir2.1 (IRK1) | KCNJ2 | | |
| | Kir2.2 (IRK2) | KCNJ12 | | |
| $I_{K(Ach)}$ | Kir3.1 (GIRK1) | KCNJ3 | | |
| | Kir3.4 (GIRK4) | KCNJ5 | | |
| $I_{K(ATP)}$ | Kir6.2 (BIR) | KCNJ11 | SUR2A | ABCC9 |
| I_{to1} | Kv4.3 | KCND3 | KChIP2 | KCNIP2 |
| | Kv1.4 | KCNA4 | | |
| | Kv4.1 | KCND1 | KChIP1 | KCNIP1 |
| | Kv4.2 | KCND2 | KChIP2 | KCNIP2 |

In cardiomyocytes inwardly rectifying K^+ currents have also been described, which include the members of ligand-gated K^+ currents. The channels responsible for these K^+ currents (Kirs) also contain α and β subunits, however the α subunit is different from those of Kv channels. Each Kirs' α subunit consists of two transmembrane segments (M1 and M2) and a cytoplasmic linker ¹⁸¹.

1.4.5.1. Transient outward K⁺ current (I_{to})

The early rapid repolarization (phase 1) is mediated by 2 repolarizing currents: I_{to1} and I_{to2}. The I_{to1} conducts K⁺, can be blocked by 4-AP and is Ca²⁺-insensitive⁷⁰. In contrast, I_{to2} conducts Cl⁻ more than K⁺, is 4-AP insensitive and Ca²⁺-dependent^{230,231}. The I_{to1} and I_{to2} modulate the gating of other repolarizing currents such as delayed rectifier K⁺ currents, by defining the height of the AP plateau (phase 2), thus determine the AP duration. The AP prolongation seen in heart failure, myocardial ischemia and infarction has been attributed to alterations of I_{to} such as reduced channel density¹⁴¹. Moreover, I_{to} currents indirectly contribute to EC coupling by modulating the AP duration¹⁴¹.

In addition to the human heart, I_{to1} has been also characterized in other species such as mouse²¹ and rat¹³. The I_{to1} density differs between different regions of the heart. For instance, in human, rat, rabbit and dog the epicardium has a higher I_{to} density compared to the endocardium¹⁴⁴. The gene encoding for I_{to1} was proposed to be Kv4.3 in human⁹² and Kv4.2 in rat⁵¹ and mouse²⁰.

PKC and PKA are candidates for I_{to1} channel's phosphorylation and regulation¹⁸⁸. While α-adrenergic stimulation showed a down-regulation of I_{to1} in rat¹², β-adrenergic agonist had no effects on the current density¹⁸⁸.

1.4.5.2. Delayed rectifier K⁺ currents (I_{Kur}, I_{Kr}, I_{Ks})

The members of delayed rectifier K⁺ currents contribute to the AP repolarization. They are classified as ultrarapid (I_{Kur}), rapid (I_{Kr}) and slow (I_{Ks}) currents based on their gating properties. Mutations of delayed rectifier K⁺ channels are involved in different types of human LQT syndrome²³.

Among delayed rectifier currents, I_{Kur} activates the fastest, does not inactivate and is blocked by 4-AP³⁰. The I_{Kur} channels are encoded by KCNA5⁶⁰.

Activation of I_{Kr} is faster than I_{Ks}, however they are both activated after I_{to} in the time course of an AP (I_{to} < I_{Kur} < I_{Kr} < I_{Ks}) (Figure 1.3). At positive potentials, I_{Kr} conducts an

inward current ²¹⁸. I_{Kr} channels are also called HERG channels since the α -subunit of the channel is encoded by human ether-a-go-go related gene (KCNH2) ¹. In HERG channels, the α -subunit is associated with accessory β -subunits such as mink and mirP1. The channel is highly expressed in human ventricular myocytes. Moreover higher I_{Kr} density has been also reported in rat atrial cells ¹⁵¹. Mutations in the HERG gene have been related to different types of LQT syndrome (See the Inherited Arrhythmia Database sponsored by Cardiovascular Genetics, New York University). For instance, cLQT syndrome, which is a complex disease described by massive QT interval prolongation and polymorphic ventricular tachycardia* is attributed to the mutations of KCNH2 ^{96,160}. β -adrenergic stimulation regulates HERG channels by 2 different mechanisms: (i) PKA-dependent phosphorylation and (ii) direct channel activation ²⁰⁵. Moreover, PIP_2 modulates the biophysical properties of the channel that results in more hyperpolarized E_m -dependent channel activation as well as I_{Kr} up-regulation ²⁴. Lanthanum and several members of class III antiarrhythmic drugs, including dofetilide, E-4031, and sotalol block I_{Kr} ^{167,168}.

I_{Ks} is composed of a pore forming α -subunit encoded by KCNQ1 and two accessory β -subunits ³⁹. The channel activation is very slow so that it never gets fully activated during a normal AP ²³. Therefore it does not markedly contribute to AP repolarization. However, $[Ca^{2+}]_i$ increase enhances I_{Ks} , and results in AP shortening that limits intracellular Ca^{2+} overload ¹⁹⁴.

1.4.5.3. Inwardly rectifying K^+ currents (I_{K1} , $I_{K(Ach)}$, $I_{K(ATP)}$)

In cardiomyocytes, inwardly rectifying K^+ currents (I_{K1} , $I_{K(Ach)}$, $I_{K(ATP)}$) contribute to the resting membrane potential (V_R) ¹⁷.

In addition to the resting membrane potential, I_{K1} also contributes to the phase 3 of repolarization. It activates at negative membrane potentials and closes very fast upon

* Torsades de Pointes (TdP)

E_m depolarization¹⁸⁸. Ba^{2+} is a strong I_{K1} blocker²¹³. In human ventricular myocytes, I_{K1} can be stimulated by PIP_2 and inhibited by isoproterenol and forskolin^{117,170}.

In contrast to Kv channels, the gating of $K_{(ATP)}$ and $K_{(ACh)}$ channels are E_m -independent. The gating of ATP-sensitive K^+ channels is controlled by the $[ATP]_i$. $I_{K(ATP)}$ is inhibited at physiological levels of $[ATP]_i$ ²¹⁹ and stimulated in situations of massive $[ATP]_i$ drops. For instance during myocardial ischemia in which $[ATP]_i$ decreases, $I_{K(ATP)}$ becomes activated¹³⁷. The resulting K^+ influx counterbalances the repolarizing currents and leads to AP shortening¹³⁷. This helps the cell to reduce its ATP expenditure by limiting excitation and subsequent contraction. This increases cell survival⁷³.

Acetylcholine activated K^+ currents ($I_{K(ACh)}$) are preferentially expressed in cells of the SA and the AV node where they hyperpolarize E_m and decelerate the heart rate. Some studies showed the presence of $I_{K(ACh)}$ in atrial cells¹²². The acetylcholine effect is mediated by the $\beta\gamma$ -subunits of members of the $G\alpha_{i/o}$ protein families⁴².

1.5. Action potential propagation in cardiac tissue

The heart is a functional *syncytium* in which electrical impulses can propagate between the cells. In heart tissue, the electrical impulse is transmitted from one cell to the other via a special type of nonselective ion channels in the gap junction region of intercalated discs⁹⁸ (Figure 1.3). These channels are called connexons and consist of six connexin subunits, each of which has four transmembrane α -helices. Two connexons from neighboring cells build the gap junction that allows the longitudinal ion flow between cells. $[Ca^{2+}]_i$ increase as well as acidosis lead to the closure of gap junction channels which is a safety mechanism to limit the distribution of toxic components to the neighbors.

The velocity of AP propagation is ~ 0.5 m/s in human atrial and ventricular muscle. The complete activation of atria takes ~ 90 ms, while all the ventricular mass is activated by ~ 230 ms¹⁰³.

1.6. Excitation-Contraction (EC) Coupling

The electrical impulse that is initiated in the SA node transmits to the ventricular myocytes and results in membrane depolarizations and APs. This AP in turn leads to cardiomyocyte's contraction. But how does this membrane depolarization cause activation of the contractile machinery? In cardiac cells, electrical excitation is coupled to contraction by the ubiquitous second messenger Ca^{2+} , a process called EC coupling.

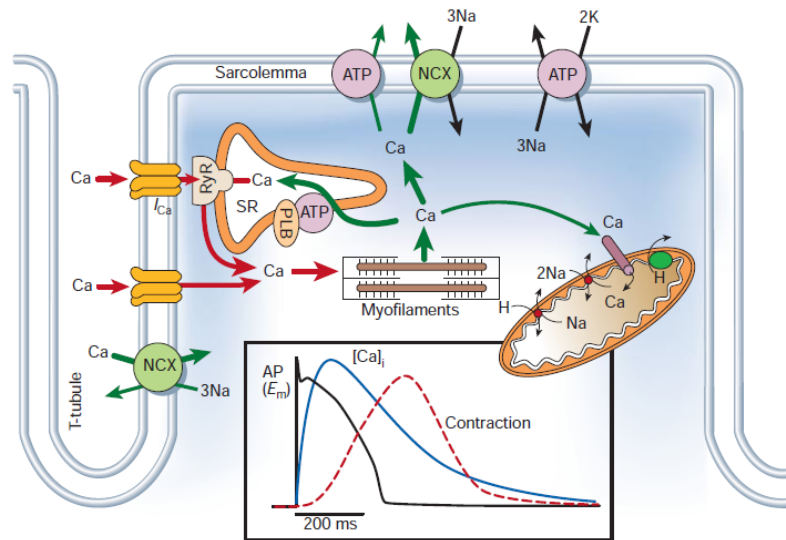


Figure 1.9: EC coupling in a cardiomyocyte. Several different ion channels, transporters, exchangers and contractile proteins contribute to this process. For description: see text. Taken from Bers 2002²².

The AP which is initiated in the surface membrane propagates along the surface and the t-tubules. The membrane depolarization causes the activation of LVDCCs, which results in Ca^{2+} influx. The LVDCC density is higher in t-tubules compared to surface membrane⁹⁹, which leads to the Ca^{2+} entry into the dyadic space. Therefore, the Ca^{2+} increases in the vicinity of RyRs and activates the Ca^{2+} release from the SR. This process is called Ca^{2+} -induced Ca^{2+} release (CICR)⁸⁸ and amplifies the Ca^{2+} influx to a degree required for the activation of the contractile filaments⁵⁰ and subsequent contraction. The contraction is followed by a relaxation period that requires Ca^{2+} removal from cytosol. This is achieved by members of the Ca^{2+} removal machinery

including: (i) SR Ca^{2+} -ATPase, (ii) sarcolemmal $\text{Na}^+/\text{Ca}^{2+}$ exchange, (iii) sarcolemmal Ca^{2+} -ATPase, (iv) mitochondrial Ca^{2+} uniport ²² (Figure 1.9).

β -adrenergic stimulation accelerates the contraction velocity by PKA-mediated phosphorylation of several proteins involved in EC Coupling such as LVDCC, RyR, phospholamban, troponin I and myosin binding protein C ²².

Phospholamban is a protein that binds the SR Ca^{2+} -ATPase and inhibits its activity. The phosphorylation of phospholamban results in its dissociation from the SR Ca^{2+} -ATPase and the relief of inhibition ⁹⁸. Troponin I as well as myosin binding protein C are the members of cardiomyocyte's contractile machinery, thus contribute in contraction.

1.6.1. SR Ca^{2+} release channels (RyR)

CICR is mediated by the SR Ca^{2+} release channels. These channels have high affinity to a neutral plant alkaloid, ryanodine, thus also called ryanodine receptors (RyR). A group of 6-20 RyRs are normally activated synchronously in response to a unitary Ca^{2+} influx, leading to a local Ca^{2+} increase called Ca^{2+} spark ⁴⁰. Ca^{2+} sparks are the elementary units of SR Ca^{2+} release during EC coupling. Tens of thousands of Ca^{2+} sparks are temporally synchronized by the AP to generate the global Ca^{2+} transient. In addition to their role as Ca^{2+} release channels, RyRs function as scaffolding proteins for other regulatory proteins involved in the CICR process. This helps to localize all important proteins for CICR at the sarcolemmal–SR junctions. For instance FKBP and calmodulin, which modulate the RyR gating properties and function respectively, are coupled to RyRs ⁶⁴. The SR Ca^{2+} buffer, calsequestrin, is also coupled to RyR on its SR luminal side ²²³.

1.6.2. Sarco/endoplasmic reticulum Ca^{2+} -ATPase

The Ca^{2+} , which is released into the cytosol during systole, should be removed from the cytosol and/or taken up by the internal stores for the next EC coupling cycle. This is

majorly mediated by the sarco/endoplasmic reticulum Ca^{2+} -ATPase type 2a (SERCA2a), the cardiac isoform of the SR Ca^{2+} pump²³. A small membrane protein called phospholamban regulates SERCA2a⁹⁸. Phospholamban inhibits the Ca^{2+} pump unless it is phosphorylated. Phosphorylation of phospholamban by either cAMP-dependent protein kinase (PKA) or calmodulin-dependent protein kinase (CaMK-II) terminates the inhibition, speeds up the Ca^{2+} reuptake²². The Ca^{2+} binding proteins in the SR lumen immediately buffer the pumped Ca^{2+} to maintain the normal SR Ca^{2+} concentration and avoid SERCA inhibition by Ca^{2+} -sensitive SERCA regulators. Calsequestrin, the major Ca^{2+} buffer of the SR, has been shown to have 18 to 50 Ca^{2+} binding sites⁹⁸.

1.6.3. $\text{Na}^+/\text{Ca}^{2+}$ exchange

Sarcolemmal $\text{Na}^+/\text{Ca}^{2+}$ exchange is the most important pathway for Ca^{2+} removal from the cardiac cell. This ion exchange is achieved by means of a plasma membrane antiporter called $\text{Na}^+/\text{Ca}^{2+}$ exchanger (NCX), which catalyzes the electrogenic transport of one Ca^{2+} for three Na^+ ⁵⁵. The Na^+ gradient across the membrane (which is maintained by Na^+/K^+ ATPase), is used as a driving force for Ca^{2+} efflux (forward mode). However NCX might also work in the reverse mode (Ca^{2+} influx) during high $[\text{Na}^+]_i$ or positive E_m ⁵⁰. KB-R7943, an isothiourea derivative, can selectively block NCX⁹⁰. NCX1 was cloned in cardiac cells and is the cardiac isoform¹³⁹.

1.7. Signal transduction in cardiomyocytes

At the cellular level, the communication with the environment is made possible by employing signal transduction. These signaling systems help the cell to sense the external stimuli and respond appropriately by modulating its function. In multicellular organisms or tissues, these responses are very important for the function of the whole system.

How do these systems work? An external stimulus, which could be a hormone or neurotransmitter, activates a receptor on the cell membrane. The ligand-receptor binding leads to the generation of different intracellular second messengers that stimulate a biological response either by activating or blocking cellular functions.

The heart is also finely regulated in response to the body needs. The cardiac cells employ many different signaling systems to fulfill this regulatory function⁹⁸. These signaling cascades integrate information from many sources, thus enabling the heart to switch on or off appropriate responses when needed.

The signaling-induced responses can be divided into two types. Non-genomic responses are developed rapidly in response to physiological stimuli such as exercise or blood loss. Whereas genomic responses are activated in response to chronic sustained stimuli such as cardiac overload induced by chronic hypertension. The latter is achieved by changes in gene expression and protein synthesis that results in structural and functional remodeling⁹⁸.

Thus, knowledge about these signaling systems helps us to understand the cardiac function. However it is not so easy to study these signaling cascades due to the fact that they are not linear pathways, in which each step activates a single downstream molecule, but instead they branch and interconnect with other pathways forming complex signaling networks.

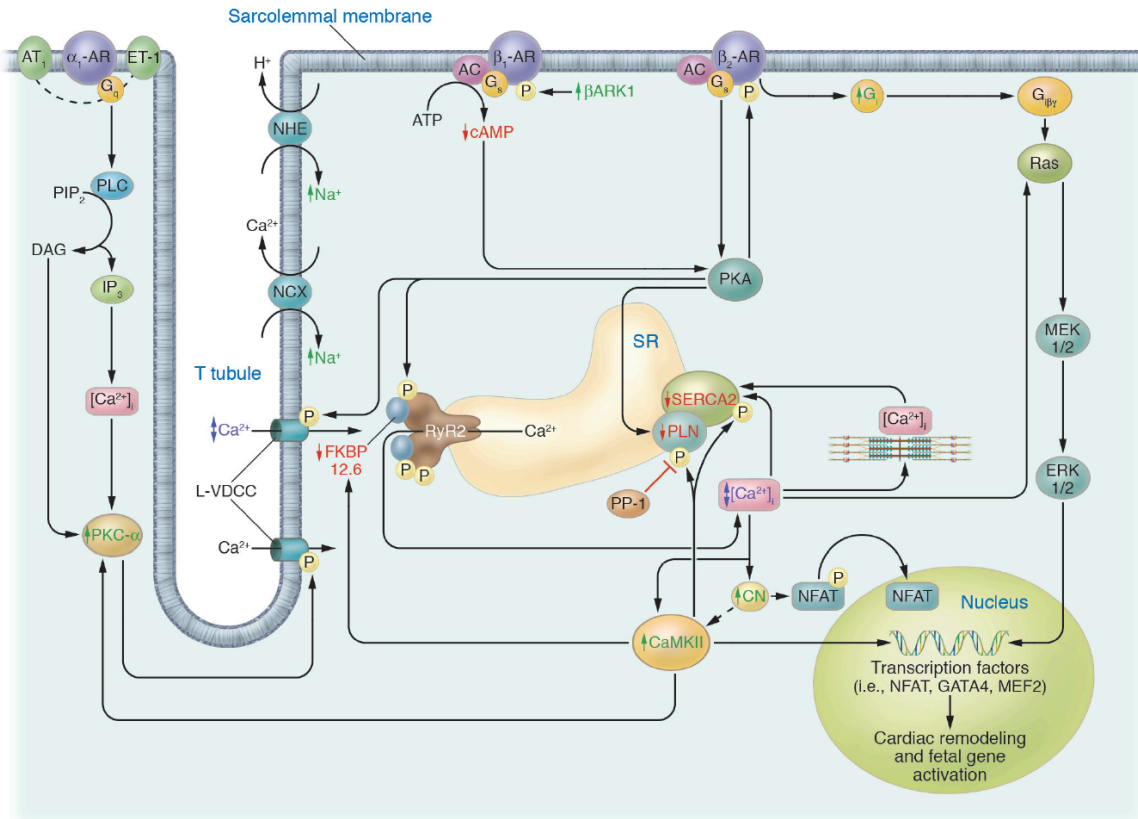


Figure 1.10: A model illustrating some signaling cascades in cardiomyocytes. Stimulation of β -adrenergic receptor (β -AR) activates G_{α_s} , which leads to the activation of PKA and subsequent phosphorylation of different members of EC coupling such as Cav1.2, RyR2 and PLN (phospholamban). The wave of phosphorylation enhances the $[Ca^{2+}]_i$ and contractility. Intracellular Ca^{2+} increase activates CN/NFAT (calcineurin/nuclear factor of activated T-cells) and CaMK-II signaling that contribute in myocyte hypertrophic response. Transcription factors, such as MEF2 (myocyte-enhancer factor 2) and GATA4 (cardiac zinc finger transcription factor) are located in the nucleus and serve as endpoints for hypertrophic-signaling pathways. Stimulation of α -AR activates G_{α_q} signaling, for description: see text. Image taken from Bodi et al, 2005²⁸.

1.7.1. $G_{\alpha_{q/11}}$ signaling pathway

G-protein mediated signaling contributes to various important physiological responses of cardiomyocytes. G-proteins are heterotrimeric GTP-binding proteins composed of α , β and γ subunits. G_{α} contains a bound guanine nucleotide. G-proteins are classified into 4 groups (G_{α_s} , $G_{\alpha_{i/o}}$, $G_{\alpha_{q/11}}$, $G_{\alpha_{12/13}}$) depending on the type of their α subunit²⁷⁰. While in cardiomyocytes the role of most of these G-protein mediated signaling are well understood, $G_{\alpha_{q/11}}$ signaling is still not investigated in great details. When ligands such as epinephrine, endothelin-1 or angiotensin-II bind to GPCRs, induce a conformational change in the receptor that allows the GPCR to function as a guanine nucleotide

exchange factor (GEF). Activated receptor exchanges the GDP bound to $G\alpha_q$ for GTP that leads to $G\alpha_q$ activation and dissociation from $\beta\gamma$ subunits⁹⁸. Activated $G\alpha_q$ stimulates PLC_β , an enzyme that hydrolyzes PIP_2 to IP_3 and DAG. IP_3 induces SR Ca^{2+} release and DAG activates cPKCs and nPKCs. Both effects, i.e. intracellular Ca^{2+} increase and PKC-mediated phosphorylations, modulate the cardiomyocyte's contractility (Figure 1.10).

The $G\alpha_{q/11}$ signaling scheme described above results in a non-genomic response to the body needs. However the physiological importance of this non-genomic response compared to $G\alpha_s$ signaling has not been well described in cardiomyocyte¹⁹². In contrast, many studies proposed an important role for the $G\alpha_{q/11}$ signaling cascade in pathological responses such as hypertrophy and heart failure⁸³. In humans, cardiac diseases develop over a long period of time, often years. Thus, the pathological responses of the $G\alpha_{q/11}$ signaling are genomic responses associated with structural and functional remodeling^{6,128}. The impact of $G\alpha_{q/11}$ signaling on the development of cardiac diseases has been the focus of study for many years and various biological tools were employed in these investigations. The overexpression of $G\alpha_q$ proteins in the heart resulted in hypertrophic response followed by heart failure^{6,44}. Inhibition of this signaling pathway by either expressing a $G\alpha_q/G\alpha_{11}$ -inhibitory peptide or $G\alpha_q/G\alpha_{11}$ protein knockout abolished the pressure-overload induced hypertrophy^{10,211}. RGS is a GTPase-activating protein that can inhibit $G\alpha_{q/11}$ signaling by inducing GTP hydrolysis. The overexpression of RGS4 in cardiac cells also reduced the hypertrophic response¹⁶³.

Besides the genomic responses, $G\alpha_{q/11}$ signaling appeared to cause non-genomic pathological responses, too¹²⁰. Activation of the IP_3 receptor type 2 (IP_3 -R2) downstream to $G\alpha_{q/11}$ signaling results in the SR Ca^{2+} release¹¹². Such a secondary mechanism modulating Ca^{2+} signals, could interfere with the highly orchestrated Ca^{2+} responses mediated by the SR Ca^{2+} release channels, RyR, and might thereby predispose the cell to arrhythmogenic events²¹⁶. IP_3 -R2 can also initiate ectopic Ca^{2+}

transients¹¹², a potential source of ectopic beats*. It has also been suggested that any IP₃-R2 located close to the sarcolemma, by causing local Ca²⁺ signals, could interfere with voltage-regulated Ca²⁺ channels to shorten AP duration. Local Ca²⁺ could also activate NCX to enhance Na⁺ entry¹⁶². Slow release of Ca²⁺ by IP₃-gated Ca²⁺ release channels is suitable for mediating the proliferative signals that regulate cellular processes such as protein synthesis, cell cycling and apoptosis⁸³. Unlike the short bursts of contraction and relaxation induced by CICR, IP₃-mediated Ca²⁺ signaling results in a sustained Ca²⁺ release that allows for the activation of genes related to the hypertrophic response⁵³.

These studies and many others focused on the relationship between cardiac diseases and G $\alpha_{q/11}$ signaling cascade. While the basic physiological impact of such a signaling in cardiac cells remained unexplored. In this thesis I investigated the impact of G $\alpha_{q/11}$ signaling on cardiac electrophysiology.

1.7.2. Rac signaling pathway

Rac1 belongs to the Rho family of small G-proteins. Rac1 and the other members of the Rho family (Rho and Ras) are activated downstream to integrin signaling (Figure 1.11). Integrin signaling contributes to protein synthesis and cell growth responses¹⁰⁵. Integrins are cell adhesion molecules that link the cytoskeleton to the extracellular matrix. Integrins activate members of the Rho family and many other signaling molecules such as various protein kinases (Akt, Raf, MEK and ERK)⁶⁹ in response to mechanical stress. The activation of these molecules initiates signaling pathways that modulate the interaction between integrins and the extracellular matrix⁹⁸. The integrin-extracellular matrix interactions are specifically modified during the hypertrophic response of the heart to overload. Thus, as part of hypertrophic response activation of Rho family members and their downstream signaling participate in the responses to mechanical stress.

* irregular cardiac rhythm

Activation of small G-proteins of the Rho family including Rac1 leads to the activation of different kinases such as PAK, MAPK, JNK family members^{9,222} and PKA^{121,209}, which in turn modify protein phosphorylation. MAPK and JNK signaling contribute to various cellular responses such as cell growth⁸³. In cardiomyocytes, activation of these kinases has been linked to hypertrophic responses²⁰⁴. Moreover, activation of PAK downstream to Rac1 signaling mediates the cytoskeletal reorganization at focal adhesion sites¹⁸⁴.

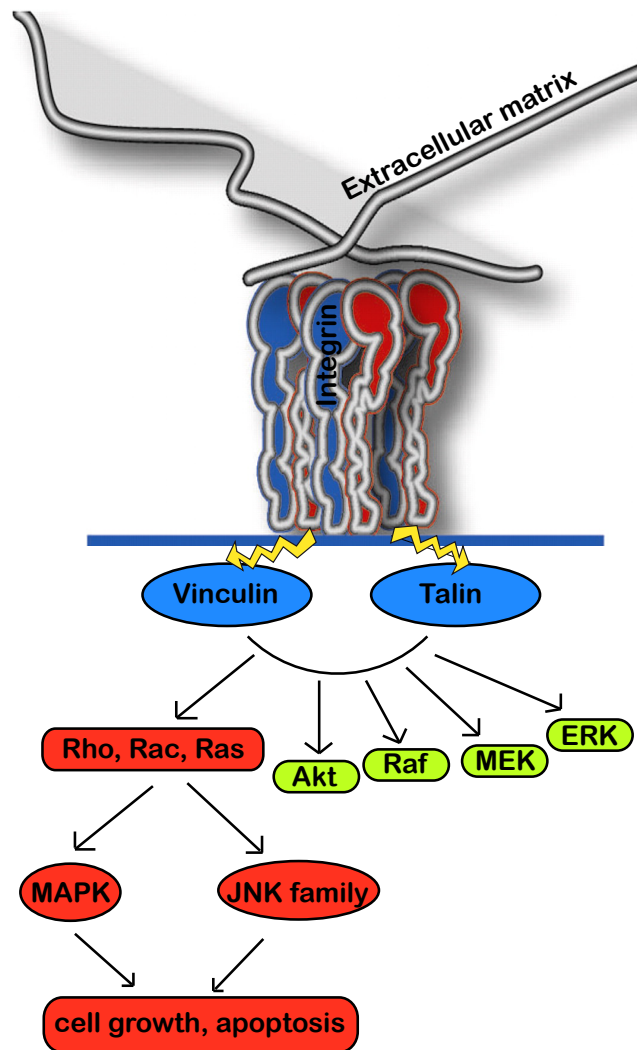


Figure 1.11: integrin signaling. Integrins activate the members of Rho family and many other signaling molecules such as various protein kinases (AKt, Raf, MEK, ERK) in response to the mechanical stress. Activation of Rho family members stimulates MAPK and JNK signaling which leads to cell growth and apoptotic responses.

The involvement of Rac1 in cardiac hypertrophic responses has been shown in both, *in vitro* and *in vivo* experiments ¹⁸⁴. However, the underlying mechanisms for such structural and functional remodeling remained to be explored.

Furthermore, Rac1 signaling leads to the activation of the NADPH oxidases (NOXes) that contribute to production of the reactive oxygen species (ROS). ROS are second messengers that induce both cellular physiological and pathological responses ⁸⁵.

Rac1 via ROS production activates downstream signaling molecules that modulate different cellular activities such as growth, differentiation and apoptosis. Moreover, ROS production has been linked to a plethora of cardiovascular diseases such as hypertension, inflammation and atherosclerosis ⁸⁵. Thus, Rac1 signaling has high importance in the cells of the cardiovascular system.

1.8. Cardiac diseases

Heart diseases are the most common diseases in the world and known to be the number one cause of death in western countries ⁹⁵. Cardiac diseases were the focus of studies for many years. To date, it is obvious that most of the pathological conditions are associated with the remodeling of cardiac cells. This remodeling presumably alters the cellular function and reflects in cardiac dysfunction in the context of the whole heart. Although the knowledge about heart diseases is growing rapidly, there are still several uncertainties, which need to be investigated. Especially studies on the cellular level would support clinical approaches in their effort to prevent and treat heart diseases.

1.8.1. Aldosterone

Aldosterone is a hormone that is produced by the adrenal gland in response to physiological stimuli such as a drop in blood pressure. Aldosterone secretion is stimulated via the activation of the renin-angiotensin-aldosterone system ⁶⁵ (Figure 1.12). Renin is a peptide, which is secreted from the juxtaglomerular apparatus of the kidney and activates the enzymatic conversion of angiotensinogen to angiotensin-I. Angiotensin-I is then converted to angiotensin-II by the angiotensin-converting enzyme found in the lungs. Angiotensin-II, in turn, stimulates the aldosterone secretion from the adrenal gland. In a compensatory response, aldosterone increases the blood volume and therefore the blood pressure by enhancing the renal reabsorption of Na⁺ and water and the release of K⁺ in the kidney's nephral tubes. When aldosterone is released in excess, a condition referred to as hyperaldosteronism in humans, it can cause hypertension. Sustained hypertension, in turn, increases cardiac workload and causes cardiac hypertrophy ¹²⁵.

In addition to hypertension-induced cardiac injury, aldosterone has been proposed to have direct insulting effects on the heart. Several studies suggested an important role for aldosterone in the development of cardiac diseases such as human congestive heart failure ²¹². Moreover, hypertrophy which developed in the hypertensive rat model with higher levels of angiotensin-II and/or aldosterone, could be suppressed by

mineralocorticoid receptor (MR) antagonists at doses lacking antihypertensive effects^{33,138}, suggesting a direct role for aldosterone in cardiovascular diseases²¹². Clinical studies showed a close relationship between plasma aldosterone level and the left ventricular hypertrophy²¹². MR antagonism could greatly rescue this phenotype. Although angiotensin-II and its downstream signaling have been studied extensively in the heart⁸³, little is known about aldosterone-mediated functions, and therefore it opened a new horizon in the field of cardiac research.

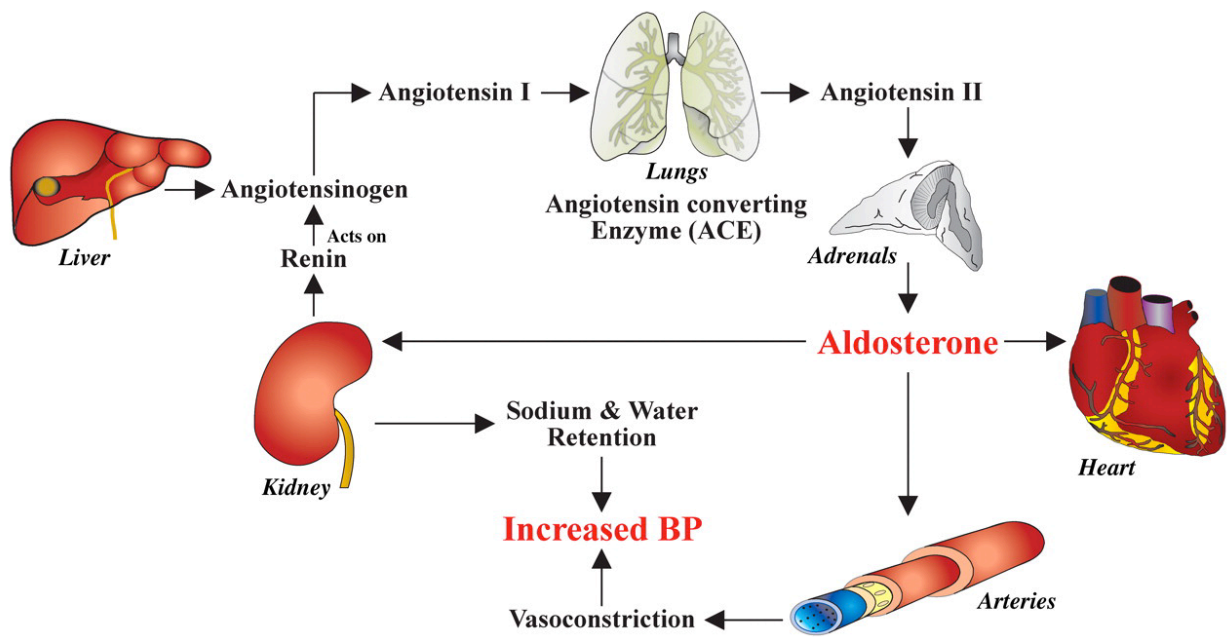


Figure 1.12: The schematic illustration of the Renin-Angiotensin-Aldosterone system. A drop in blood pressure (BP) stimulates the secretion of Renin from kidney which acts on Angiotensinogen and leads to the production of Angiotensin I. Angotesin converting enzyme (ACE) catalyzes the conversion of Angiotensin-I to Angiotensin-II that stimulates Aldosterone secretion from Adrenal gland. Aldosterone functions on three different target organs: (i) on Kidney it increases the reabsorption of sodium and water which results in the increased BP, (ii) on Arteries it induces vasoconstriction which leads to increased BP, (iii) on Heart its physiological impact is not well understood. Image taken from www.renalflow.blogspot.de

2. Materials & Methods

2.1. Chemicals and solutions

All chemicals used in this work were purchased, unless otherwise stated, from SIGMA-ALDRICH, Invitrogen or VWR.

All solutions used for preparation of ventricular myocytes and electrophysiological experiments are described in tables 2.1 and 2.2.

Table 2.1: Composition of the solutions used for preparation of ventricular myocytes.

| Chemicals | MW | Concentration (mM) | | |
|----------------------------------|--------|--------------------|------------|------------|
| | | CFS | LCS | CCS |
| NaCl | 58.44 | 134 | 134 | 134 |
| Glucose | 180.16 | 11 | 11 | 11 |
| KCl | 74.55 | 4 | 4 | 4 |
| MgSO ₄ | 120.37 | 1.2 | 1.2 | 1.2 |
| Na ₂ HPO ₄ | 141.96 | 1.2 | 1.2 | 1.2 |
| HEPES | 238.31 | 10 | 10 | 10 |
| DNase | | | 0.045 | 0.09 |
| CaCl ₂ | 147.02 | | 1 | 2 |
| pH | | 7.3 (NaOH) | 7.3 (NaOH) | 7.3 (NaOH) |
| Osmolarity | | 300±10 | 300±10 | 300±10 |

Table 2.2: Composition of the solutions used for electrophysiological experiments.

| Chemicals | MW | Concentration (mM) | | | |
|-------------------|--------|--------------------|--------------|--------------|---------------|
| | | Tyrode1 | Tyrode3 | IC1 | IC2 |
| NaCl | 58.44 | 135 | 135 | 10 | 10 |
| Glucose | 180.16 | 10 | 10 | | |
| KCl | 74.55 | 5.4 | | 135 | |
| HEPES | 238.31 | 10 | 10 | 10 | 10 |
| CaCl ₂ | 147.02 | 1.8 | 1.8 | | |
| MgCl ₂ | 95.22 | 1 | 1 | 2 | 2 |
| CsCl | 168.35 | | 5.4 | | 115 |
| 4-AP | 95.12 | | 5 | | |
| TEA | 165.7 | | 5 | | 20 |
| EGTA | 380.35 | | | 0.1 | 0.1 |
| MgATP | 507.18 | | | 3 | 3 |
| pH | | 7.3 (NaOH) | 7.3 (HCL) | 7.3 (KOH) | 7.3 (CsOH) |
| Osmolarity | | 300±10 | 300±10 | 300±10 | 300±10 |

2.2. Preparation of rat ventricular myocytes

Rat ventricular myocyte's isolation and culture were performed according to a standard method established in our lab¹⁹¹. Adult male Wistar rats (6 - 12 week old, 200 - 400 g) were anesthetized by an intraperitoneal injection (i.p.) of a mixture of 137 mg/kg ketamine hydrochloride (Ursotamin®, Serumwerk, Germany) and 6.6 mg/kg xylazine hydrochloride (Rompun®, Bayer Health Care, Germany). To prevent blood agglutination in the heart vessels, 20 mg/kg sodium citrate dihydrate was injected (i.p.) 10 min prior to surgery. After achieving deep anesthesia to suppress spinal cord reflexes, the animal

was killed by decapitation. The chest was opened; the heart was flushed with 10 ml of ice-cold Ca^{2+} -free solution (CFS) (for chemicals see Table 2.1). Thereafter, the aorta was pinched off, the heart was removed, attached to a Langendorff apparatus and perfused retrogradely for 5 min with O_2 saturated CFS containing 200 μM EGTA at room temperature. The perfusate was then changed to O_2 saturated CFS containing 0.17 mg/ml Liberase TM (Roche, Germany) for 20-25 min at 37 °C. After enzyme perfusion, the heart was removed from the apparatus. The ventricles were cleaned off of atria and vessels, cut to pieces and washed in O_2 saturated CFS. In the next step, the ventricular tissue was incubated in 20-25 ml of O_2 saturated CSF at 37 °C with gentle shaking for 5 min. Then the solution was discarded and the tissue was incubated in 20-25 ml of a low Ca^{2+} -solution (LCS). The last incubation and washing step was done by 20-25 ml of O_2 saturated Ca^{2+} -containing solution (CCS). After this, a gentle trituration was applied to release the ventricular myocytes. The cell suspension was plated on the cover slips of a 12-well plate, which were coated with extracellular matrix proteins (ECM gel from Engelbreth-Holm-Swarm murine sarcoma, diluted to 12.5% with M199 medium). The cells were allowed to settle down for approximately 1 h in medium M199* containing 100 $\mu\text{g}/\text{ml}$ Penicillin*, 100 $\mu\text{g}/\text{ml}$ Streptomycin* and 50 $\mu\text{g}/\text{ml}$ Kanamycin* (* PAA laboratories, Austria). The medium was supplemented with 870 nM insulin, 65 nM transferrin and 29 nM Na^+ -selenite (ITS supplemented medium). One hour after plating, the medium was changed for fresh medium supplemented with ITS. The myocytes were cultured in an incubator at 37 °C with a 5% CO_2 atmosphere. Animal care was approved by the Animal Ethics Committee of the Saarland University and was performed according to the European directive on Laboratory Animals (86/609/EEC) and the Guide for Care and Use of Laboratory Animals published by the US National Institute of Health (NIH Publication No. 85-23, revised 1996).

2.3. Generation of transgenic mice

2.3.1. Heart-specific inducible $G\alpha_q/G\alpha_{11}$ knockout

The heart-specific inducible $Cre^{tg/0}$ mice and the $G\alpha_q/G\alpha_{11}$ mutant mice were provided by Prof. Dr. Stefan Offermanns (Max-Planck-Institute for Heart and Lung Research, Bad Nauheim, Germany). Transgenic $G\alpha_q/G\alpha_{11}$ KO mice were generated according to the method described in paper by Pahlavan et al¹⁴³. Mice carrying the $gnaq^{flox/flox}$ and $gna11^{-/-}$ alleles²¹¹ were crossbred with the $Cre^{tg/0}$ mice to obtain $gnaq^{flox/flox}gna11^{-/-}Cre^{tg/0}$ mice. $Cre^{tg/0}$ mouse was a novel mouse line in which Cre was flanked by mutated estrogen receptor binding domain (Cre-ER) and controlled by the α -myosin heavy chain (α -MHC) promoter. $G\alpha_q$ knockout was induced by 5-day consecutive tamoxifen injection (50 mg/kg body weight, i.p.) and accomplished 21 days after injection.

2.3.2. Heart-specific inducible Cav1.2 I1624E mutation

Mice carrying Cav1.2 I1624E mutation (I/E mice) were provided by Prof. Dr. Frank Hofmann (Institut für Pharmakologie und Toxikologie, Technische Universität München, Germany).

Transgenic I/E mice were generated according to the method described in paper by Poomvanicha et al¹⁵². To generate these mice, the heterozygous $Cav1.2^{+/I1624E}$ mice were crossbred with $Cav1.2^{flox/flox}$ ¹⁷⁶ and MerCreMer^{*} mice¹⁸². The resulting offspring included $Cav1.2^{flox/flox}$ x MerCreMer (identified as knockout), $Cav1.2^{flox/I1624E}$ x MerCreMer (I/E), $Cav1.2^{+/flox}$ x MerCreMer (control) and $Cav1.2^{+/flox}$ (wildtype). A 4-day tamoxifen injection regime (100 mg/kg body weight, i.p.) was employed to induce Cav1.2 KO. All experiments were performed 10 days after the first tamoxifen injection, which was proved to be sufficient for the Cav1.2 KO²⁷.

* tamoxifen inducible Cre recombinase under the control of the α -MHC promoter

2.3.3. Heart-specific constitutively active Rac1

Transgenic RacET mice (expressing constitutively active Rac1 under the control of the α -MHC promoter) were generated¹⁸⁴ and provided by Prof. Dr. Mark Sussman group (Heart institute, San Diego state university, CA). RacET mice were compared with age-matched FVB-N mice (genetic background for RacET mice, designated as WT) in all experiments.

2.4. Aldosterone Pump implantation

Pump implantation was performed by Dr. Kathrina Wiesen (Institute for Molecular Cell Biology, Saarland University Homburg). Osmotic mini-pumps (**Alzet**[®], DURECT corporation, model 2002) were filled with 200 μ L of aldosterone (2 mg/mL; 25 mg aldosterone diluted in 10.875 ml propylenglycol, 1.175 ml ethanol and 0.5 ml distilled water) and were implanted subcutaneously in 8-week old mice in order to provide a constant release rate of 7.2 μ g/day for 42 days. In control mice, empty pumps (dummy) were implanted. In the end of 42-day hormone infusion period, plasma aldosterone level was assessed using ELISA test (DRG instruments, Germany).

2.5. Preparation of mouse ventricular myocytes

The isolation of mouse ventricular myocytes was performed according to a standard method established in our lab¹⁴³. Mice (10 - 14 weeks old, 25 - 30 g) were anesthetized by injection of a mixture of 85 mg/kg ketamine hydrochloride and 15 mg/kg xylazine hydrochloride (i.p.). Sodium citrate dehydrate (10 mL/kg body weight) was used to prevent blood clot in the heart vessels. After achieving deep anesthesia to suppress spinal cord reflexes, the animal was killed by decapitation. The chest was opened and the lungs were removed. The remaining blood in the heart was washed out by flushing 2 mL ice-cold CSF into the ventricles. Then the aorta was cut off; the heart was cannulated to allow retrograde Langendorff-perfusion. The heart was primarily perfused

with CFS (O₂ saturated, containing 200 μM EGTA) at room temperature for 5 min and then with Liberase TM (0.085 mg/ml, diluted in O₂ saturated CFS) at 37 °C for 12 min. After enzymatic digestion, the atria and vessels were removed; the ventricles were cut open and incubated in 10-20 mL O₂ saturated CFS containing 0.09% DNase for 5 min at 37 °C. Then, the solution was discarded and the ventricles were incubated in 5 mL CFS containing 0.09% DNase for another 5 min. After these washing steps, ventricles were gently triturated and diluted with O₂ saturated CCS gradually (10 x 150 μL CCS, every 5 min). The cell suspension was plated on ECM-coated coverslips of a 12-well plate and incubated for 1 hour at 37 °C, 5% CO₂. After 1 hour, the supernatant was replaced by fresh medium M199. Animal care was performed according to the Guide for Care and Use of Laboratory Animals published by the US National Institute of Health (NIH Publication No. 85-23, revised 1996).

2.6. Patch-clamp setup

The patch-clamp setup consisted of an inverted microscope (TE-2000, Nikon, Japan) residing on a vibration isolation table (CVI Melles Griot, Germany) inside a Faraday cage, an EPC 10 patch-clamp amplifier (HEKA Elektronik, Germany), a micromanipulator (Luigs & Neumann, Germany) holding the amplifier probe and a computer. The vibration isolation table was used to reduce vibrations beyond a few Hz, which is usually sufficient for the purpose of patch clamping. The patch-clamp preamplifier was surrounded by a Faraday cage to shield the sensitive amplifier probe from the electrical noise.

EPC 10 system consisted of the head stage (or probe) and the amplifier main unit. The probe, which was in a small enclosure, was mounted on the micromanipulator. The main unit contained the signal processing electronics, the A/D and D/A converters and the connectors for analog and digital input/output.

The micromanipulator was used to control the movements of the patch pipette (beyond submicrometer range) in order to finely position the patch pipette tip on the cell.

Data acquisition and analysis was performed using “Patchmaster” and “Fitmaster” softwares (HEKA), respectively.

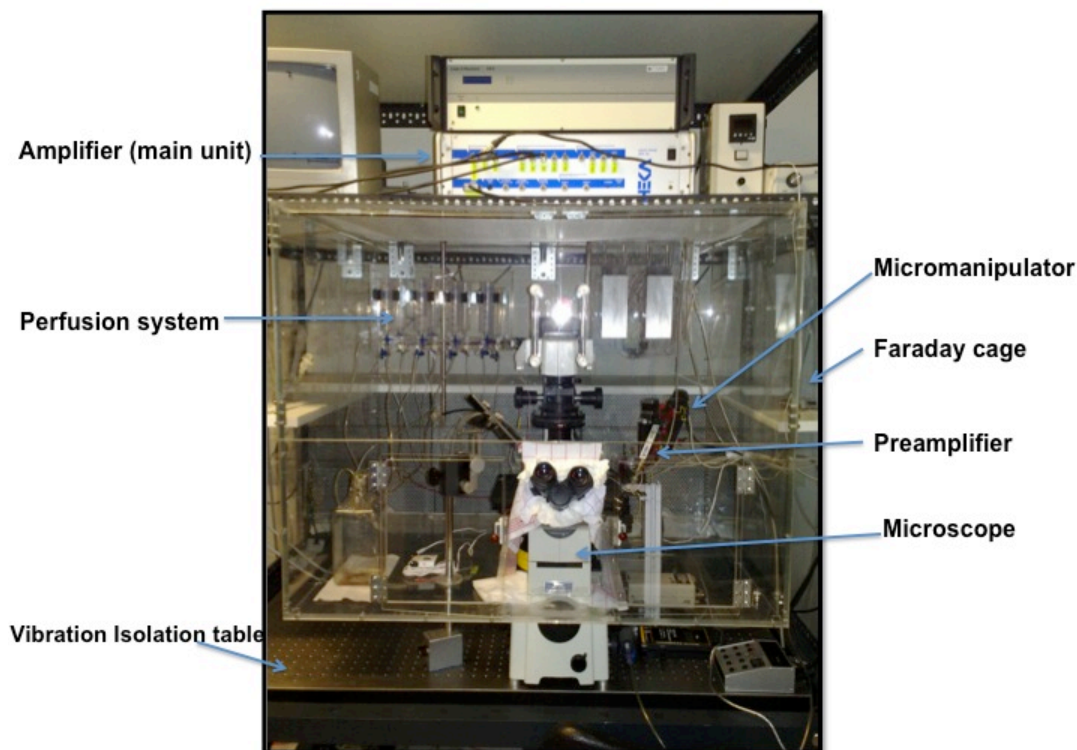


Figure 2.1: Patch-clamp setup.

2.7. Patch-clamp technique

The patch-clamp technique enables us to record macroscopic whole-cell or microscopic single-channel currents through the ion channels of biological membranes ¹⁶⁵. In the patch-clamp technique, it is possible to experimentally control and modify the voltage of membrane patches or the whole cell (voltage-clamp), which allows us to investigate the voltage dependence of ion channels. Furthermore, the experimenter can monitor the changes of membrane potential in response to membrane currents (current-clamp). Therefore, the patch-clamp technique is a powerful tool to study cells electrophysiologically.

2.7.1. Electrophysiological experiments

The electrophysiological experiments were performed using an EPC10 patch-clamp amplifier controlled by “Patchmaster” software (HEKA).

The experiment was started by transferring the cells into the patch-clamp setup. To do so, the coverslip containing the ventricular myocytes were mounted into a custom-made chamber and transferred onto the stage of an inverted microscope. During the experiment, the cells were visualized using a CCD color camera (JVC professional products, USA). The cells were supplied by a bath solution, which had the ionic composition very similar to the interstitial fluid. This solution was permanently refreshed by a gravity-fed, valve-controlled perfusion system in combination with a custom-made suction system. Depending on the type of the experiment, different compositions of bath solution were used (see Table 2.2). Then the patch-pipette with the tip opening of 2-2.5 μm was prepared by a pipette puller (DMZ Universal puller, Zeitz instruments, Germany) and filled with the pipette solution. Similar to the bath solution, various compositions of pipette solutions were used depending on the type of the experiment (see Table 2.2). The pipette was then connected to the preamplifier via a pipette holder and approached to the chamber by a micromanipulator. As soon as the pipette entered the bath solution, a current could be observed in the oscilloscope window (Figure 2.2) resulting from repetitive application of a -5 mV voltage pulse to the electrode by the amplifier. After entering the bath solution, a positive pressure was applied to get rid of cell debris and to avoid the occlusion of the pipette tip. Liquid junction potential i.e., potential differences between bath and intracellular solutions, was calculated for each pair of Tyrode and IC using a junction potential calculator and corrected from the voltage readings of the amplifier. The pipette was then approached to the cell. Then the pipette was positioned on the cell membrane and a gentle suction was applied to the pipette to form a gigaseal.

The gigaseal was formed when the resistance between the pipette and the cell membrane increased to the values $>10^9 \Omega$ (Figure 2.2). Additional suction was applied to rupture the membrane patch under the pipette and to provide access to the cell

interior. By doing so, the “whole cell configuration” was obtained which could be identified by a current change in the oscilloscope window (Figure 2.2). This current had two components: (i) capacitive transients (I_c) and (ii) steady-state current (I_{ss}) that the former should be omitted from the measurements. Capacitive transients could be estimated and cancelled by the amplifier. The cancellation was done by supplying the current needed to charge the capacitor (plasma membrane) ¹⁶⁵. After establishing a successful whole cell configuration and before starting the measurements, a 2-4 min interval was considered for complete exchange of the intracellular solution with pipette solution. Then the AP and various ionic currents were recorded in the current-clamp and voltage-clamp mode, respectively.

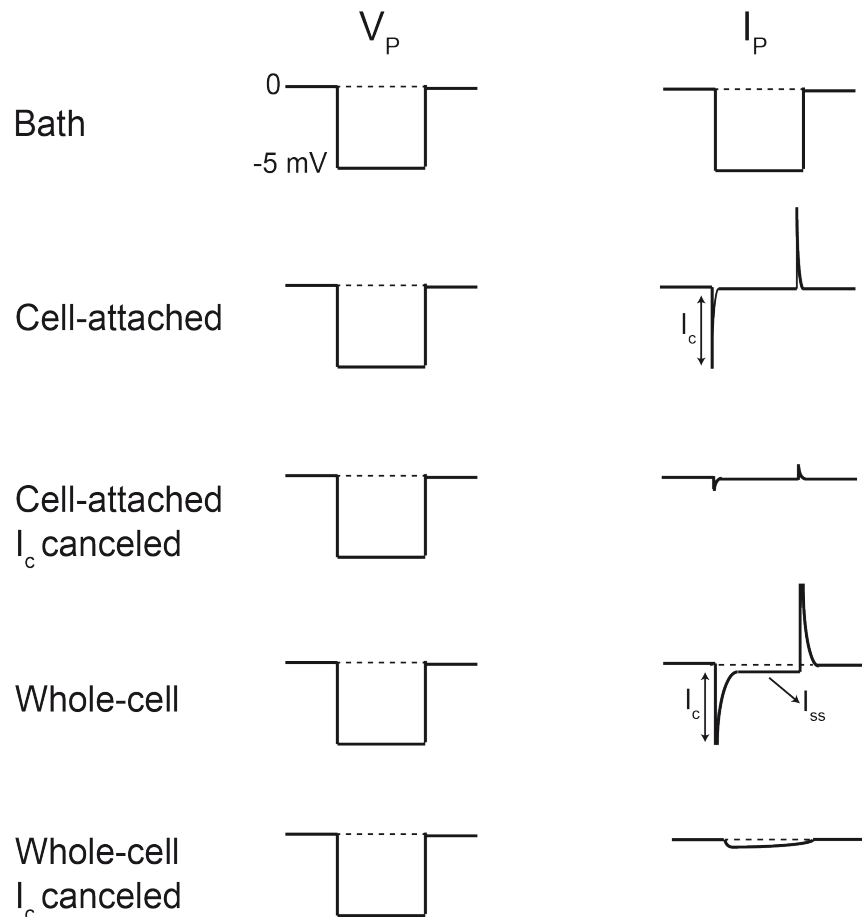


Figure 2.2: Sequence of pipette potentials (V_p) and pipette currents (I_p) during establishment of the whole cell configuration. Taken from the laboratory manual of the graduate school calcium signaling and cellular nanodomains, 2009.

In the voltage-clamp experiments, the access resistance between the pipette and the cell interior should be considered, while it constitutes a resistance (R_s) in series with the membrane resistance (ion channels) that results in inaccurate membrane voltage readings. Therefore, in all voltage-clamp experiments, the R_s was compensated by the amplifier up to 70%.

2.7.2. Action potential recording in ventricular myocytes

The pipette solution and the bath solution for AP recording were IC1 and Tyrode1, respectively (Table 2.2). After establishing the whole cell configuration, the amplifier was switched to the current-clamp mode. AP was evoked by the repetitive injections of 4-ms depolarizing currents, starting from $I=100$ pA with 100 pA increments at 1 Hz (RT) and 4 Hz (37 °C), until an overshoot > 5 mV is reached. Signals were acquired at 50 kHz sampling frequency, filtered at 2.9 kHz and 10 kHz, and 3 consecutive APs were saved for further analysis.

V_R was determined by the voltage recorded at rest in the current-clamp mode (Figure 2.3). AP amplitude was calculated as the voltage difference between V_R and AP overshoot (Figure 2.3). Time to peak (TTP) was calculated as the time required for reaching the AP overshoot. Signal 4.02 (Cambridge electronic design Ltd, Cambridge, UK) was used for analysis of AP durations. AP durations at 30%, 50%, 70% and 90% of repolarization (APD_{30} , APD_{50} , APD_{70} , APD_{90}), were analyzed using a custom-made macro of Signal software.

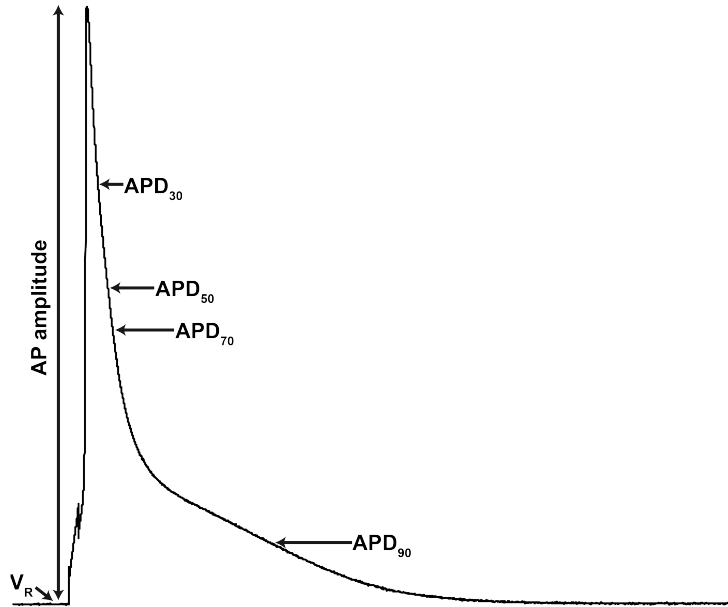


Figure 2.3: Schematic illustration of AP amplitude and AP durations.

2.7.3. Transient outward current (I_{toC}) measurement

For I_{toC} measurements, the pipette was filled with IC1 and the cells were perfused with Tyrode1. I_{toC} was activated by a series of 500 ms test pulses ranging from -30 to +60 mV with 10 mV increments from a holding potential of -120 mV (50 ms). Each test pulse was preceded by a depolarizing step to -40 mV (50 ms) to voltage inactivate I_{Na}^{23} (Figure 2.4).

Data were recorded at 20 kHz sampling frequency and filtered at 2.9 kHz and 10 kHz.

I_{toC} was obtained by subtraction of the end current from the peak current amplitude (Figure 2.4). The current amplitude was normalized to the C_M in order to facilitate the comparison of the I_{toC} recorded in different cells with various sizes, and presented as current density (pA/pF). The current densities were plotted against the applied voltage pulses in Prism (GraphPad Software Inc., La Jolla, USA) and presented as current-voltage (IV) relationships.

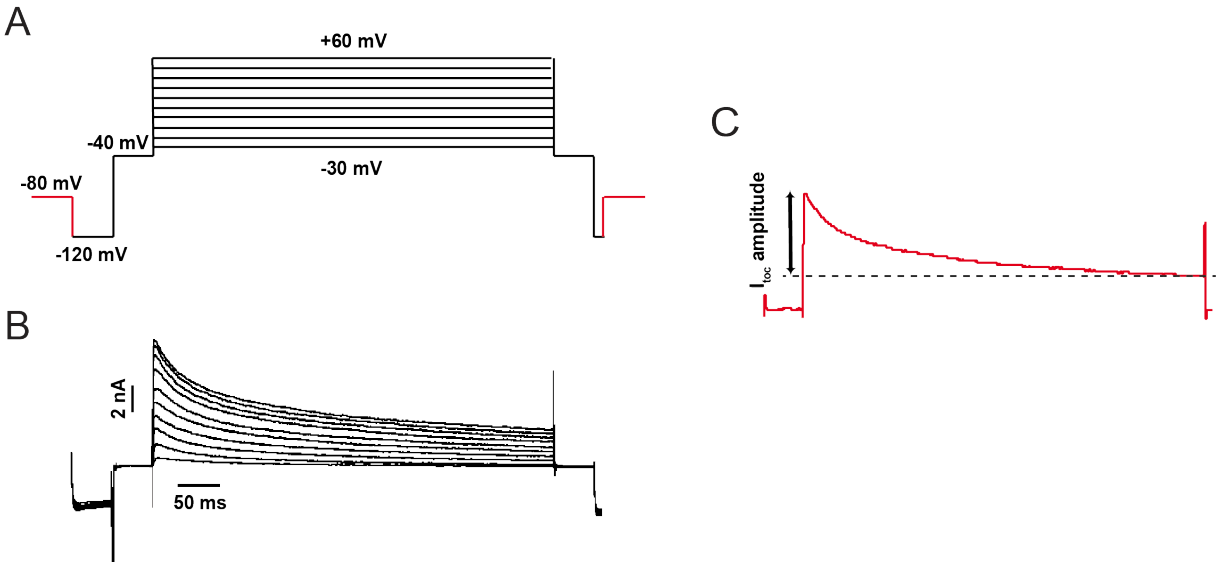


Figure 2.4: I_{toc} measurement. Illustration of protocol used for the I_{toc} recording (A), typical I_{toc} recording (B), and analysis of the I_{toc} amplitude (C).

2.7.4. L-type Ca^{2+} current ($I_{Ca,L}$) measurement

To record L-type Ca^{2+} currents, IC2 was used as pipette solution (Table 2.2). Ventricular myocytes were perfused with Tyrode 3 (Table 2.2). In whole cell configuration and voltage-clamp, a series of 250 ms test pulses ranging from -50 to +50 mV with 10 mV increments were used to activate $I_{Ca,L}$. Each test pulse was preceded by a depolarizing step to -40 mV (150 ms) to voltage inactivate I_{Na}^{23} . To gain $I_{Ca,L}$, the end current was subtracted from the peak current (Figure 2.5 C). The resulting currents were normalized to the C_M and plotted against the applied voltage pulses as IV relationships. To have more accurate $I_{Ca,L}$ amplitude, leak current was measured prior to each $I_{Ca,L}$ recording and subtracted from the Ca^{2+} current. Leak current was activated by application of a +30 mV test pulse in a voltage range where voltage-dependent channels are not active. Therefore, 4-time depolarizing pulses from -120 to -90 mV for 250 ms were applied; the resulting currents were averaged, scaled and subtracted from the current activated by the main test pulse. $I_{Ca,L}$ was obtained as the peak current amplitude, normalized to C_M and plotted as IV relationships (IV curve).

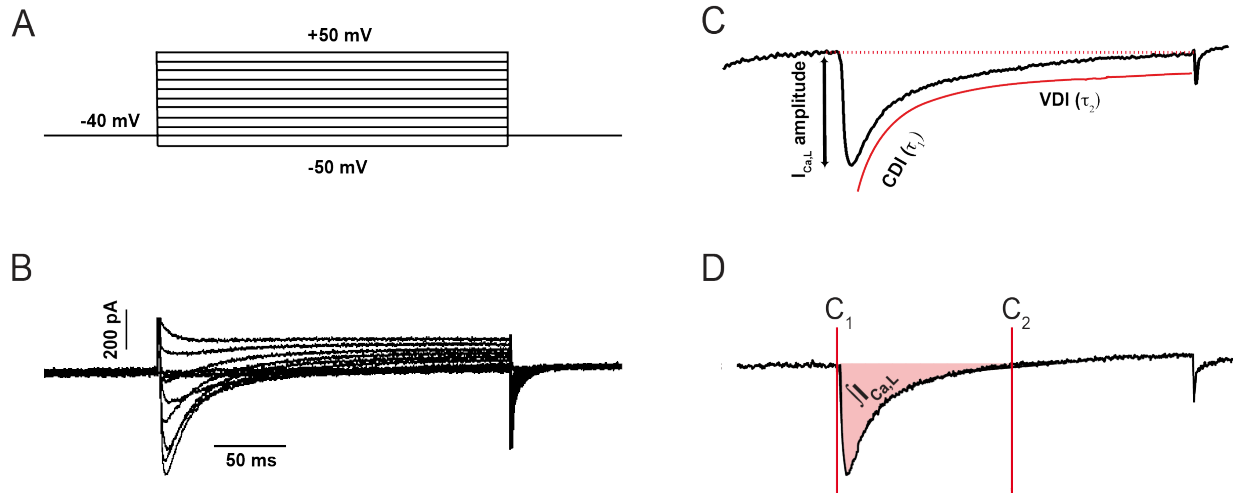


Figure 2.5: $I_{Ca,L}$ measurement. Illustration of pulse protocol used for the $I_{Ca,L}$ recording (A), typical $I_{Ca,L}$ recording (B), analysis of the $I_{Ca,L}$ amplitude and $I_{Ca,L}$ inactivation (C), and integration of $I_{Ca,L}$ (D). For detailed description see 2.7.4.

The time constants of $I_{Ca,L}$ inactivation (τ_1 and τ_2) were obtained by a non-linear fit from the peak current to the end current ($I_{Ca,L}$ at 0 mV test pulse) using a two-exponential function of “Patchmaster” software:

$$y(x) = Amp_0 + \sum_{i=1}^2 Amp_i e^{\frac{-x}{\tau_i}} \quad \text{Equation 2.1}$$

The amount of charge entry via $I_{Ca,L}$ was calculated by integration of $I_{Ca,L}$ trace ($I_{Ca,L}$ at 0 mV test pulse). The integration has been done using the online analysis methods of “Fitmaster” software (HEKA). To define the range for integration, the left cursor (C_1) was set at the beginning and the right cursor (C_2) at the position where the current was completely inactivated (Figure 2.5 D). In figure 2.5 D, the integral is shown as the signed area bounded by $I_{Ca,L}$ trace.

2.8. Photometry system

The photometry system (TILL Photonics, Germany) consisted of a monochromator (polychrome IV), two Avalanche photodiode-based fluorescence detectors, the fluorescence detection unit (a microprocessor controller board) and a polychrome manual controller (PMC). For CICR gain measurements, this system was incorporated into the Patch-clamp setup and interfaced to the “Patchmaster” software. Indo-1, an emission ratiometric fluorescence dye, was used to measure $[Ca^{2+}]_i$. To excite this fluorescence probe, excitation light at 355 ± 7 was produced by a monochromator, reflected into the objective by dichroic mirror 1 (DM 380 LP) and focused on the dye-loaded cell through an immersion objective (40x /1.30 oil, Plan Fluor, Nikon). The emission light was collected by the same objective and splitted into two channels by dichroic mirror 2 (DM 440 LP). The two emission wavelengths were detected by photodiodes (Figure 2.6), digitized at 0.5 KHz by the EPC10 amplifier and saved for further analysis.

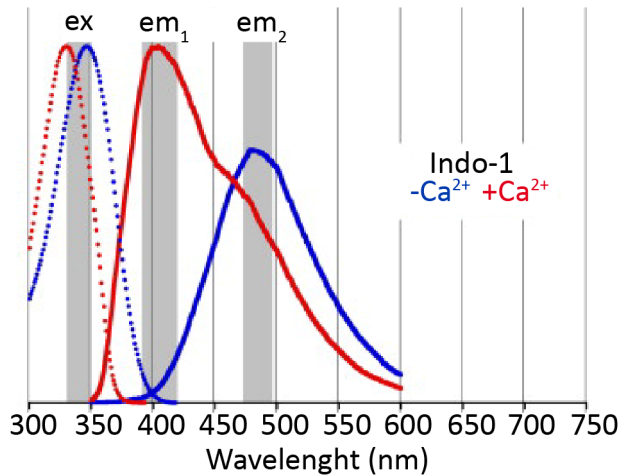


Figure 2.6: The excitation and emission spectra of Indo-1. Modified from Carlson and Campbell, 2009³⁷.

2.9. Excitation-contraction coupling gain measurements

For EC coupling gain measurements, ventricular myocytes were perfused with Tyrode3. The pipette was filled with EGTA-free IC2 containing 0.1 mM Indo-1 pentapotassium salt (Indo-1). Indo-1 was dissolved in water and kept as 10 mM stock solutions at -20°C . After establishing the whole cell configuration and before recording, a 7-min loading time was considered to ensure complete exchange of the intracellular solution with the pipette solution according to the test experiments. $I_{\text{Ca,L}}$ and SR Ca^{2+} release were activated and recorded simultaneously using combination of patch-clamp and photometry system. $I_{\text{Ca,L}}$ was activated by a pulse protocol similar to that explained in 2.7.4. Additionally, each test pulse was preceded by 10 times 250-ms depolarizing pulses to 0 mV from a holding potential of -40 mV (Figure 2.7). In the gain measurements these prepulses were applied to obtain steady-state SR Ca^{2+} loading. During $I_{\text{Ca,L}}$ recording, the Indo-1 was excited by photometry system and fluorescence was measured from a field slightly larger than the cell under study. The fluorescence signals were digitized at 0.5 KHz by an analog-to-digital converter of the EPC-10. Indo-1 based Ca^{2+} signals were analyzed in Igor Pro 6.22 (WaveMetrics Inc., Oregon, USA) software. After background correction, two emitted wavelengths were ratioed and the amplitude of the resulting signal was calculated. EC coupling gain was calculated by ratioing of the Ca^{2+} signal amplitude over $I_{\text{Ca,L}}$ density. The resulting Ca^{2+} current density, Ca^{2+} signal amplitude and EC coupling gain were plotted against the corresponding voltage pulses in Prism (Graphpad).

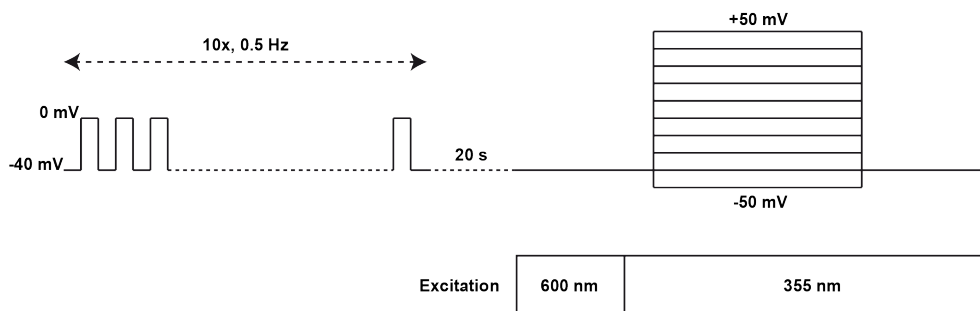


Figure 2.7: Schematic presentation of the protocol used for EC coupling gain measurements. Ten times depolarization to 0 mV to induce steady-state SR Ca^{2+} loading and $I_{\text{Ca,L}}$ recording after 20 s interval. Recording of the Intracellular Ca^{2+} transients was performed simultaneous with $I_{\text{Ca,L}}$ measurements.

2.10. Data statistics

Statistical analysis was performed in Prism (Graphpad) by using the appropriate tests (unpaired t-test, Mann-Whitney-Test, one-way ANOVA, Kruskal-Wallis-Test and two-way ANOVA) chosen depending on the results of the normality test (D'Agostino & Pearson omnibus normality test).

Data are displayed as mean \pm SEM for Gaussian distributed and median \pm 25/75 percentiles for non-Gaussian distributions. Asterisks indicate significant differences. $p < 0.05$ (*), $p < 0.01$ (**), $p < 0.001$ (***)).

3. Results

3.1. The effects of $G\alpha_q/G\alpha_{11}$ knockout on the basic electrophysiological properties of ventricular myocytes

In cardiomyocytes, $G\alpha_{q/11}$ signaling mediates the regulatory function of many hormones such as endothelin-1, angiotensin-II and epinephrine. Although its physiological relevance may not be as well established as $G\alpha_s$ signaling, $G\alpha_{q/11}$ signaling has been shown to play an important role in the development of cardiac diseases such as hypertrophy and heart failure^{130,166}. Pathological $G\alpha_{q/11}$ signaling has been investigated extensively using different biological tools, from *in vitro* assays to the generation of transgenic animals⁸³. However most of these studies did not consider the contribution of $G\alpha_{q/11}$ signaling to basic physiology of a cardiomyocyte, including excitability and contractility. Here we used a novel transgenic mouse model with cardiac specific inducible $G\alpha_q/G\alpha_{11}$ KO (see 2.3.1) to study the possible contribution of these signaling cascades to the basic physiological properties of ventricular myocytes.

3.1.1. $G\alpha_q$ knockout modulates the electrophysiological properties of ventricular myocytes

Heart-specific $G\alpha_q$ KO mice were generated using the inducible Cre/LoxP system (see 2.3.1). The $G\alpha_q$ KO was induced on $G\alpha_{11}$ null-background mice, since $G\alpha_q$ and $G\alpha_{11}$ showed to have overlapping functions⁵. To do so, mice with a $Gq^{fl}G11^{-}Cre^{+}$ genotype (abbreviations in Table 3.1), either received a tamoxifen injection ($G\alpha_q/G\alpha_{11}$ double KO [DKO], red) or were kept without any treatment ($G\alpha_{11}$ KO, turquoise). $G\alpha_q$ KO effects were studied by comparing DKO with $G\alpha_{11}$ KO.

Table 3.1: Transgenic animals used to study the physiological role of $G\alpha_q$ and/or $G\alpha_{11}$ proteins. wt, wildtype; tg, transgenic; 0, no Cre expression. Color-code in figures is identical.

| Label | <i>gnaq</i> | <i>gna11</i> | Cre status | Tamoxifen | Miglyol |
|--|-------------|--------------|------------|-----------|---------|
| Gq ^{fl} G11 ⁻ Cre ⁺ Tam ⁻ | flox/flox | -/- | tg/0 | - | - |
| Gq ^{fl} G11 ⁻ Cre ⁺ Tam ⁺ | flox/flox | -/- | tg/0 | + | - |
| Gq ^{wt} G11 ^{wt} Cre ⁻ Tam ⁻ | wt/wt | wt/wt | 0/0 | - | - |
| Gq ^{wt} G11 ^{wt} Cre ⁻ Tam ⁺ | wt/wt | wt/wt | 0/0 | + | - |
| Gq ^{fl} G11 ⁻ Cre ⁻ Tam ⁻ | flox/flox | -/- | 0/0 | - | - |
| Gq ^{fl} G11 ⁻ Cre ⁻ Tam ⁺ | flox/flox | -/- | 0/0 | + | - |
| Gq ^{wt} G11 ^{wt} Cre ⁺ Tam ⁻ | wt/wt | wt/wt | tg/0 | - | - |
| Gq ^{fl} G11 ^{wt} Cre ⁻ Tam ⁺ | flox/flox | wt/wt | 0/0 | + | - |
| Gq ^{fl} G11 ^{wt} Cre ⁺ Tam ⁺ | flox/flox | wt/wt | tg/0 | + | - |
| Gq ^{wt} G11 ^{wt} Cre ⁻ Mig ⁺ | wt/wt | wt/wt | 0/0 | - | + |
| Gq ^{fl} G11 ⁻ Cre ⁺ Mig ⁺ | flox/flox | -/- | tg/0 | - | + |

In electrophysiological experiments, AP was studied as an integrative parameter since its shape reflects the contribution of all voltage-gated ion currents. Therefore, AP can be used as an indicator for changes in ion channel contributions. Furthermore, plasma membrane capacitance (C_M), which provides information about the cell membrane area including the surface membrane and the t-tubular system, was assessed. Deletion of the $G\alpha_q$ protein resulted in a 12% reduction of the cell membrane area (Figure 3.1A, red). One of the possible reasons underlying C_M reduction might be t-tubular loss, which was observed in many cardiac diseases²⁰⁷. T-tubular loss could affect functional properties of cardiac myocytes such as EC coupling. However, C_M measurements alone are not sufficient to verify this but could motivate further experiments investigating this possibility.

V_R was determined in both DKO and $G\alpha_{11}$ KO cells and the results showed no effect of $G\alpha_q$ KO on this particular parameter (Figure 3.1B).

APs were evoked in ventricular myocytes of DKO and $G\alpha_{11}$ KO mice. All AP

measurements were performed at room temperature. The AP analysis showed a 10% reduction of the AP amplitude in DKO (Fig.3.1C, red). Figure 3.1Da demonstrates an exemplified AP from each group indicating AP prolongation in DKO cells. This observation was further confirmed by analyzing the time course of APs, quantitatively. APD₃₀ and APD₅₀ were used as indicators for studying the early repolarization while APD₇₀ and APD₉₀ served to characterize the late repolarization. The statistical analysis of early and late repolarization showed the prolongation of late repolarization, as depicted in figure 3.1Db and Dc, respectively.

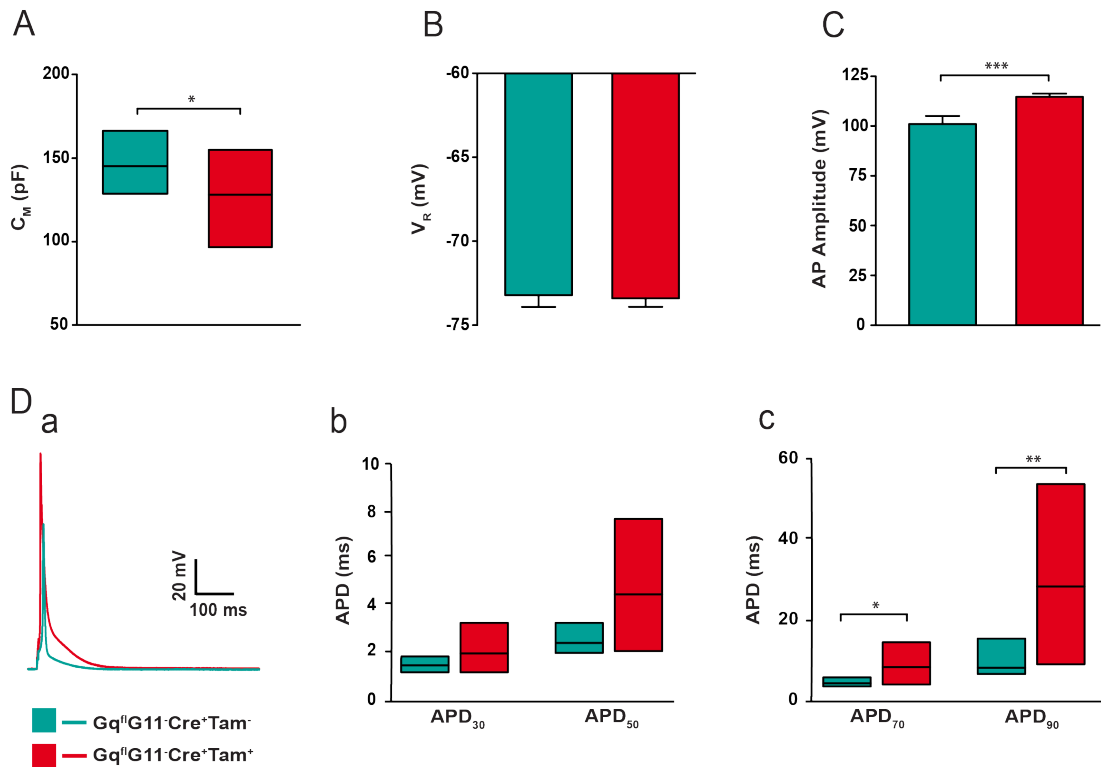


Figure 3.1: The effects of G α_q KO on the electrophysiological characteristics of ventricular myocytes. Membrane capacitance (C_M), resting membrane potential (V_R), and action potential amplitude (AP amplitude) (A–C). Representative APs (Da) and action potential durations after 30, 50, 70 and 90% repolarization, APD₃₀ and APD₅₀ (Db), APD₇₀ and APD₉₀ (Dc). Number of animals and cells are shown in Supplementary table 1. Error bars represent mean \pm SEM. The box plots show median (middle band) and 25/75 percentiles (lower/upper quartiles, respectively).

The repolarization of the AP is brought about by the activation of many different K^+ currents of which a few might be under the control of $G\alpha_q/G\alpha_{11}$ -protein signaling as suggested previously^{25,131}. Wagner et al. showed recently that the $G\alpha_{11}$ protein might contribute to the regulation of I_{to} ²⁰². Therefore I also investigated the effects of $G\alpha_q$ on I_{to} by recording this current in ventricular myocytes lacking this protein.

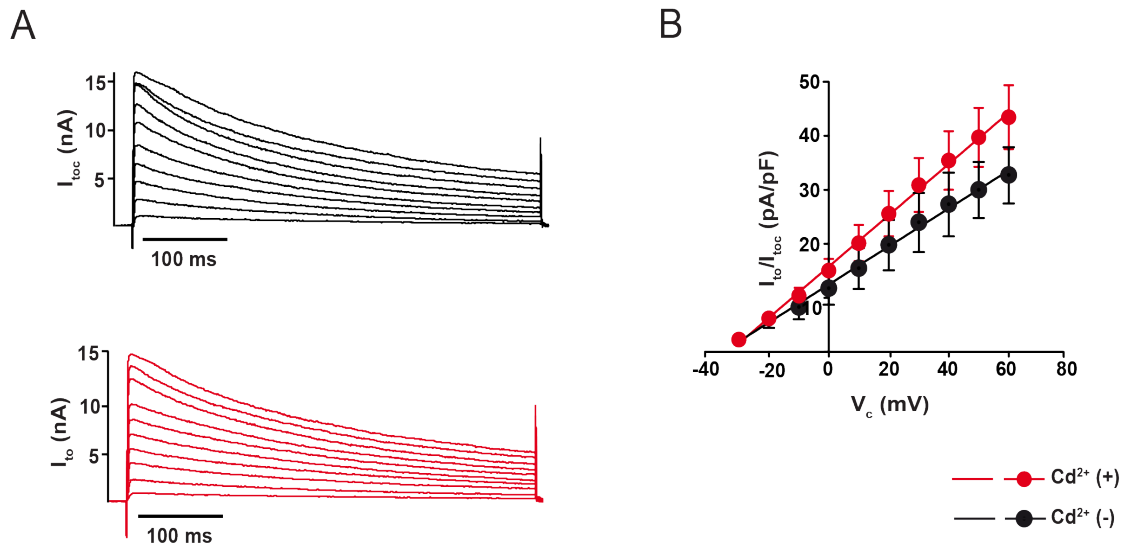


Figure 3.2: The effect of Cd^{2+} on transient outward current (I_{toC}) density. Representative I_{toC} traces (A) and corresponding current-voltage (IV) relation curve of I_{toC} (B) in the presence and absence of Cd^{2+} in the bath solution to block $I_{Ca,L}$. Error bars represent mean \pm SEM.

I_{to} recording requires a special composition of bath and pipette solutions. These solutions are needed to block contaminating currents, in particular $I_{Ca,L}$. Consequently, AP and I_{to} recordings would require different sets of bath and pipette solutions. In order to optimize the throughput of measured cells, I decided to use the same solutions anyhow. Since $I_{Ca,L}$ displayed an almost 5-fold lower current density, this approach appeared appropriate. Nevertheless, I performed control experiment with the $I_{Ca,L}$ blocker, Cd^{2+} * (0.1 mM) to verify this (Figure 3.2) and indeed found very little contamination by $I_{Ca,L}$. I refer to this current as I_{toC} (transient outward current) throughout this thesis due to the possible minor contaminations.

* $CdCl_2$

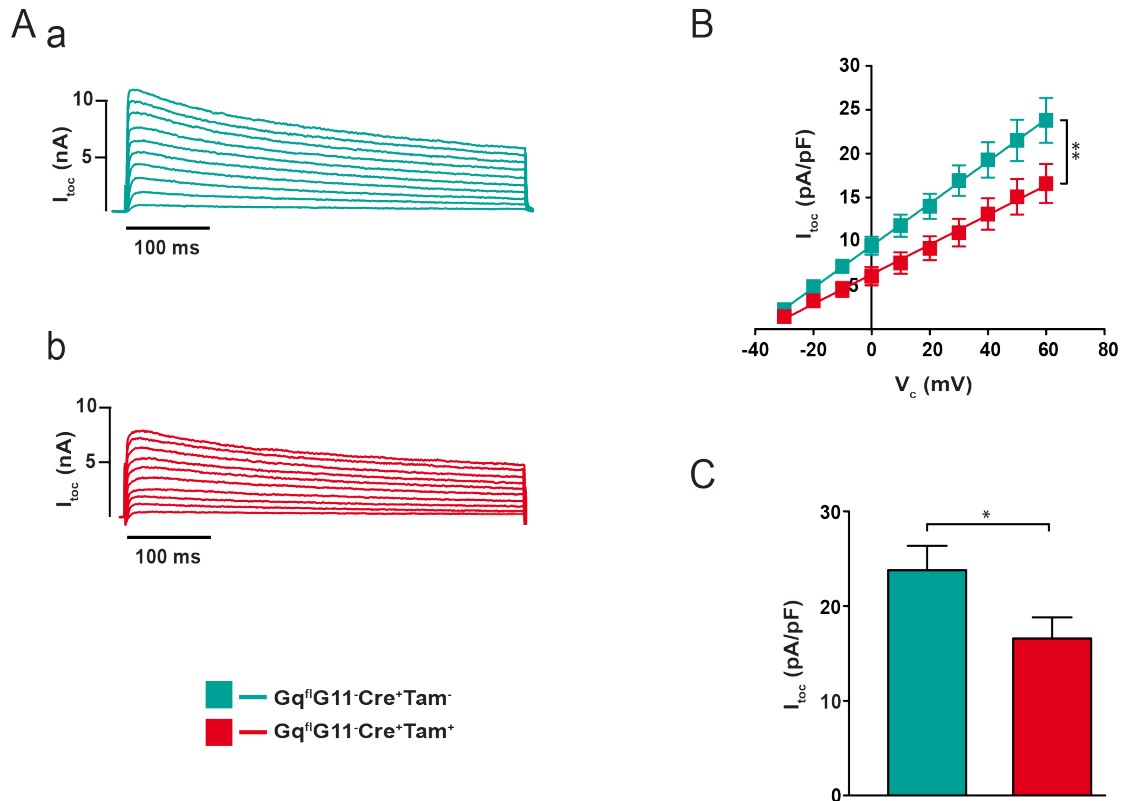


Figure 3.3: The effect of $G\alpha_q$ KO on the transient outward current (I_{toc}) in ventricular myocytes. Typical I_{toc} traces (A), corresponding current-voltage (IV) relationships (B), and the I_{toc} density at +60 mV test potential (C). Number of animals and cells are shown in Supplementary table 1. Error bars represent mean \pm SEM.

Interestingly, $G\alpha_q$ KO reduced the I_{toc} density and altered its IV relationships (Figure 3.3B, red). The maximum reduction of current density was at +60 mV, 16.6 ± 2 (pA/pF) in DKO compared to 23.8 ± 3 (pA/pF) in $G\alpha_{11}$ KO (Figure 3.3C).

In summary, heart-specific inducible $G\alpha_q$ KO modulated many of the investigated electrophysiological parameters (C_M , AP amplitude, APD_{70} , APD_{90} and I_{toc}). At this point, I was concerned whether all effects that I have seen were solely caused by the $G\alpha_q$ KO, or other experimental conditions such as tamoxifen injection, the $G\alpha_{11}$ KO and/or Cre expression were contributing to the observed phenotype. Therefore, another set of experiments was designed to specifically address the following questions: (i) the impact of tamoxifen (ii) the effects of Cre expression (iii) the effects of $G\alpha_{11}$ KO and (iv) the optimized set of genotypes to study $G\alpha_q$ KO effects.

3.1.2. Tamoxifen alters the electrophysiological properties of ventricular myocytes

Tamoxifen is a selective estrogen receptor modulator (SERM) ⁶⁵ and is widely used in the treatment of breast cancer ⁶¹. Previously, scientists developed an inducible knockout system based on tamoxifen for temporal control of gene knockout ⁸¹. In this technique, Cre is bound to a mutated form of the estrogen receptor that is no longer responsive to estrogen but is activated by tamoxifen. Tamoxifen activates Cre-ER* recombinase that removes genomic DNA between the two loxP sites ⁸¹. In our Cre/LoxP system, we used an injection regime comprising administration of tamoxifen on five consecutive days (see 2.3.1) to induce $G\alpha_q$ KO. All experiments were performed 28 days after the last injection. As suggested previously, tamoxifen's half-life is supposed to be five days ($t_{1/2}=5$ days) ¹¹⁵; therefore, its concentration should be reduced to below 2% after 28 days (Figure 3.4). This remaining tamoxifen concentration was assumed to be inefficient. However, we checked this hypothesis by application of a similar tamoxifen injection regime in wildtype mice. As mentioned before, we performed our inducible $G\alpha_q$ KO on a $G\alpha_{11}$ -null background to avoid overlapping functions of these proteins. To further investigate the possible effects of tamoxifen in our system, the same strategy was used in $G\alpha_{11}$ KO mice.

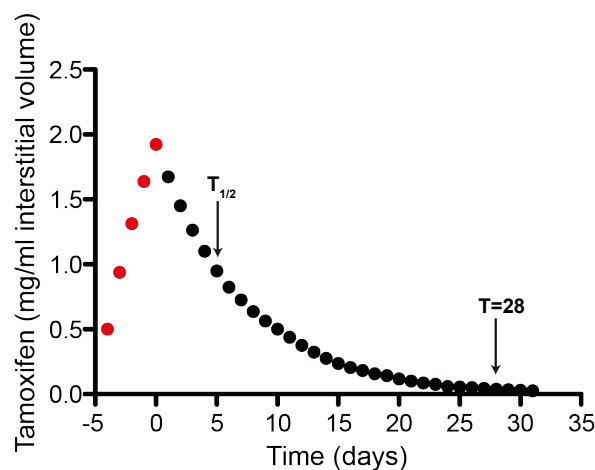


Figure 3.4: Tamoxifen pharmacokinetics. $T_{1/2}$ shows the half-life of tamoxifen and $T=28$ indicates the start of electrophysiological experiments.

* Cre bound to a mutated form of the estrogen receptor (ER)

Tamoxifen injection in wildtype mice did not affect C_M , V_R , AP amplitude and AP shape (Figure 3.5, brown vs. grey). Although APD_{30} and APD_{50} were not altered, I_{toC} showed a significant increase in tamoxifen treated wildtype mice (Figure 3.6A, brown vs. grey), which is reflected in IV curve, too (Figure 3.6B, brown vs. grey).

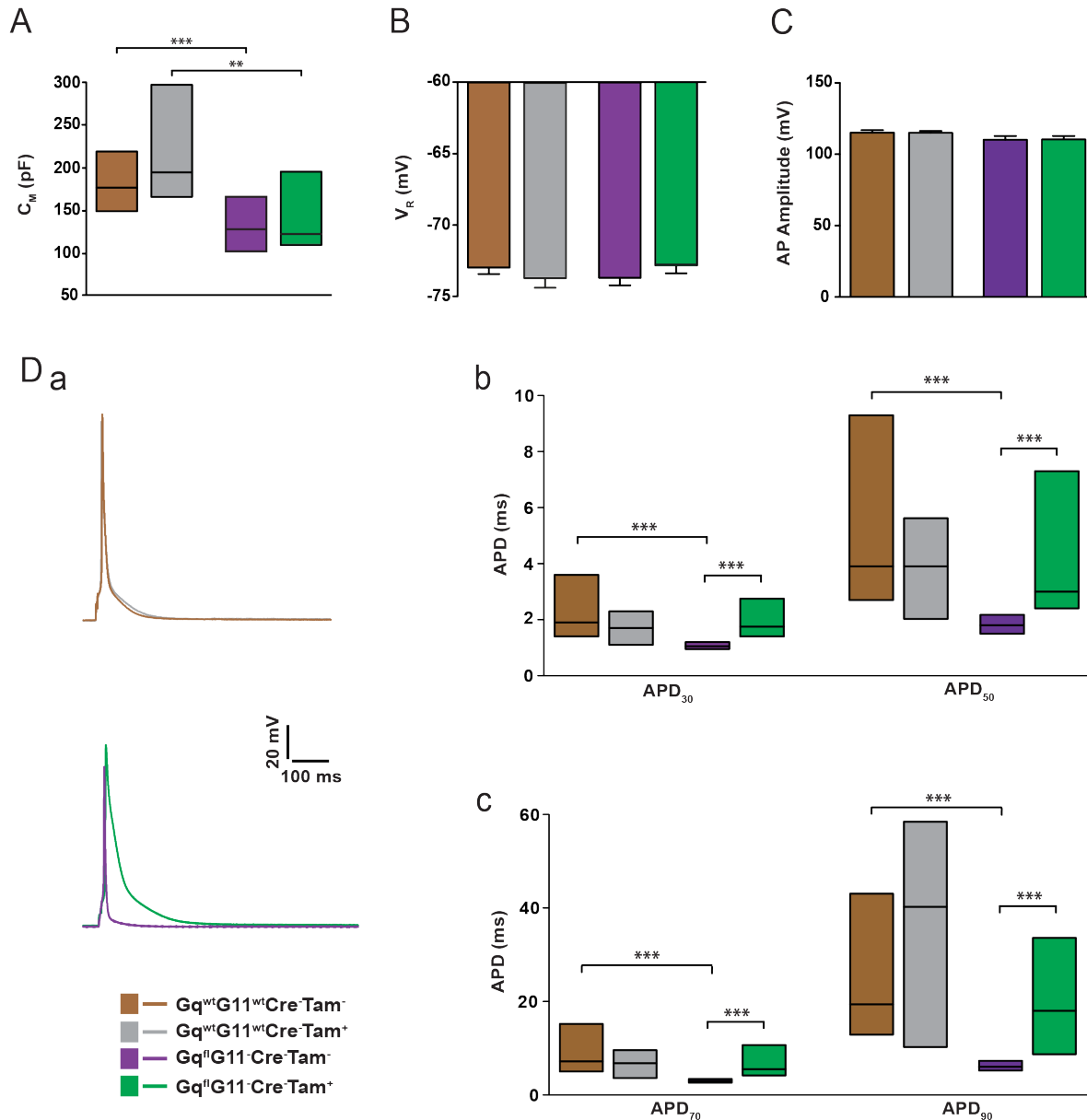


Figure 3.5: The effects of tamoxifen application on the electrophysiological characteristics of ventricular myocytes from wildtype and $G\alpha_{11}$ KO animals. Membrane capacitance (C_M), resting membrane potential (V_R), and action potential amplitude (AP amplitude) (A–C). Representative APs (Da) and action potential durations after 30, 50, 70 and 90% repolarization, APD_{30} and APD_{50} (Db), APD_{70} and APD_{90} (Dc). Number of animals and cells are shown in Supplementary table 1. Error bars represent mean \pm SEM. The box plots show median (middle band) and 25/75 percentiles (lower/upper quartiles, respectively).

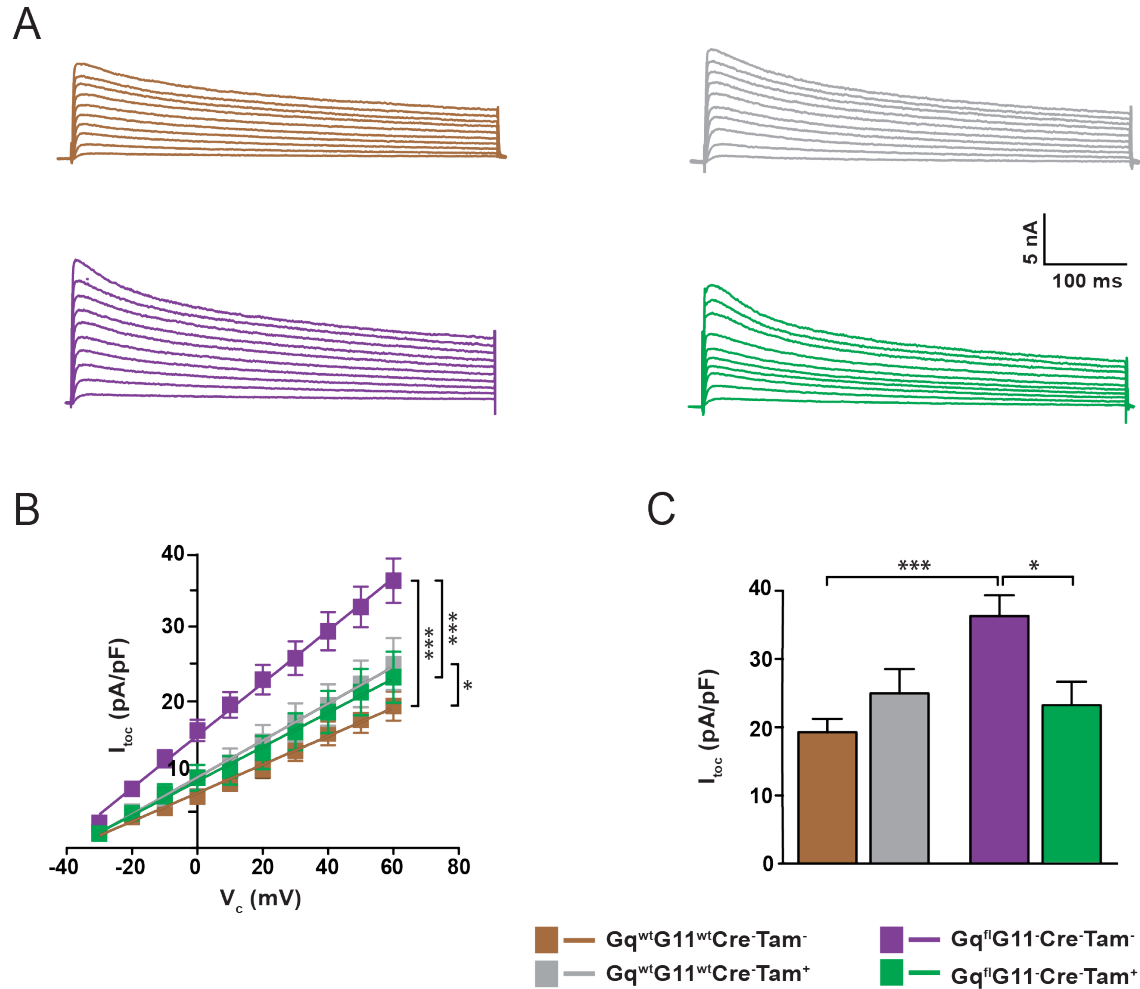


Figure 3.6: The effect of tamoxifen application on the transient outward current (I_{toc}) of ventricular myocytes from wildtype and $G\alpha_{11}$ KO animals. Typical I_{toc} traces (A), corresponding current-voltage (IV) relationships (B), and the I_{toc} density at +60 mV test potential (C). Number of animals and cells are shown in Supplementary table 1. Error bars represent mean \pm SEM.

The results of electrophysiological characterization in $G\alpha_{11}$ KO mice were rather unexpected since they showed some discrepancies to the results found in wildtype mice. While, the tamoxifen treatment did not alter C_M , V_R and AP amplitude (Figure 3.5A-C, violet vs. green), AP was prolonged in $G\alpha_{11}$ KO mice (Figure 3.5Da, violet vs. green). This was further confirmed by analyzing the time course of AP repolarization (APDs). Both early and late repolarization periods were significantly slowed down in cells from tamoxifen-injected mice (Figure 3.5Db & Dc, violet vs. green). I_{toc} was significantly reduced in tamoxifen treated- $G\alpha_{11}$ KO mice (Figure 3.6A, violet vs. green), which was in agreement with the results of early repolarization (Figure 3.5Db, violet vs.

green). While the current-voltage relationships were significantly different in tamoxifen-injected wildtype mice (Figure 3.6B, brown vs. grey), the I_{toC} density at +60 mV was not (Figure 3.6C, brown vs. grey). A possible explanation for this apparent discrepancy could be that the sample size at +60 mV might be the limiting factor for statistical analysis.

I also investigated the impact of miglyol, the tamoxifen solvent, on the electrophysiological characteristics of ventricular myocytes. Similar to tamoxifen experiments, miglyol effects were studied in both wildtype and $G\alpha_{11}$ KO mice following the same injection regime.

Miglyol injection into wildtype mice (2.5 ml/kg body weight) resulted in a significant decrease of C_M compared to tamoxifen treatment (Figure 3.7A, sapphire vs. grey). Similar to tamoxifen, V_R , AP amplitude (Figure 3.7B & C, sapphire vs. brown) and AP shape (Figure 3.8, sapphire vs. brown) were not altered by the miglyol treatment in wildtype mice. Furthermore, miglyol injection did not modulate the electrophysiological properties of $G\alpha_{11}$ KO cardiomyocytes (Figure 3.9 and 3.10).

Moreover, these sets of experiments enabled us to obtain information about the electrophysiological effects of $G\alpha_{11}$ KO in ventricular myocytes. $G\alpha_{11}$ KO resulted in a substantial decrease in C_M (28%) (Figure 3.5A, brown vs. violet). While V_R and AP amplitude remained unchanged, the repolarization phase of the AP was significantly faster in $G\alpha_{11}$ KO cells (Figure 3.5B-D, brown vs. violet). One of the potential reasons for this faster repolarization phase appeared to be I_{toC} up-regulation (~2-fold) in $G\alpha_{11}$ KO cells (Figure 3.6, brown vs. violet).

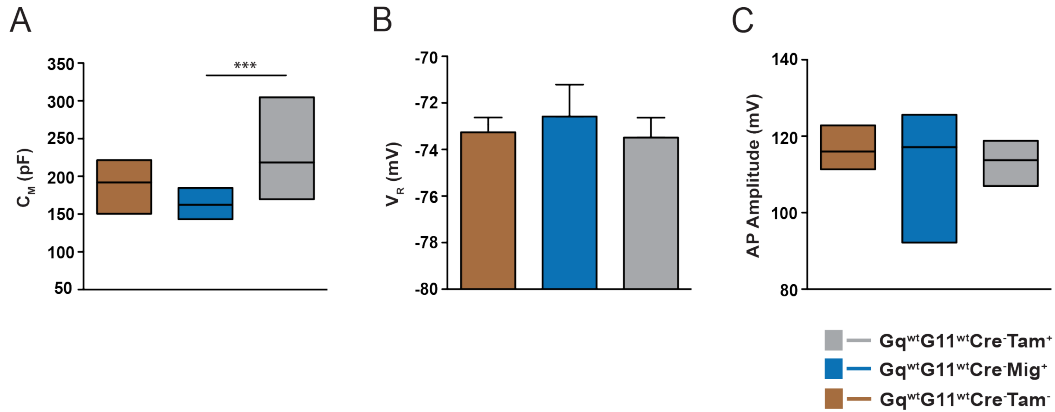


Figure 3.7: The effects of miglyol application on the electrophysiological characteristics of ventricular myocytes from wildtype animals. Membrane capacitance (C_M), resting membrane potential (V_R), and action potential amplitude (AP amplitude) (A–C). Number of animals and cells are shown in Supplementary table 1. Error bars represent mean \pm SEM. The box plots show median (middle band) and 25/75 percentiles (lower/upper quartiles, respectively).

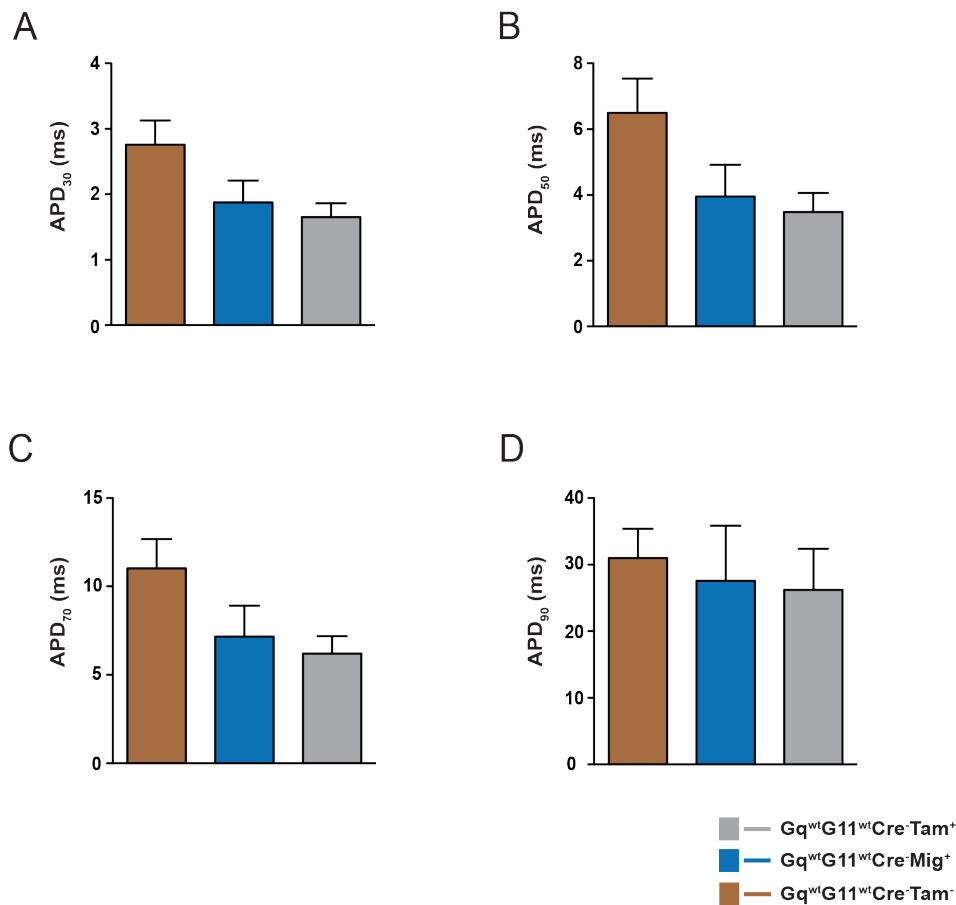


Figure 3.8: The effects of miglyol application on the AP duration of ventricular myocytes from wildtype animals. AP durations after 30, 50, 70 and 90% repolarization, APD₃₀ (A), APD₅₀ (B), APD₇₀ (C), and APD₉₀ (D), respectively. Number of animals and cells are shown in Supplementary table 1. Error bars represent mean \pm SEM.

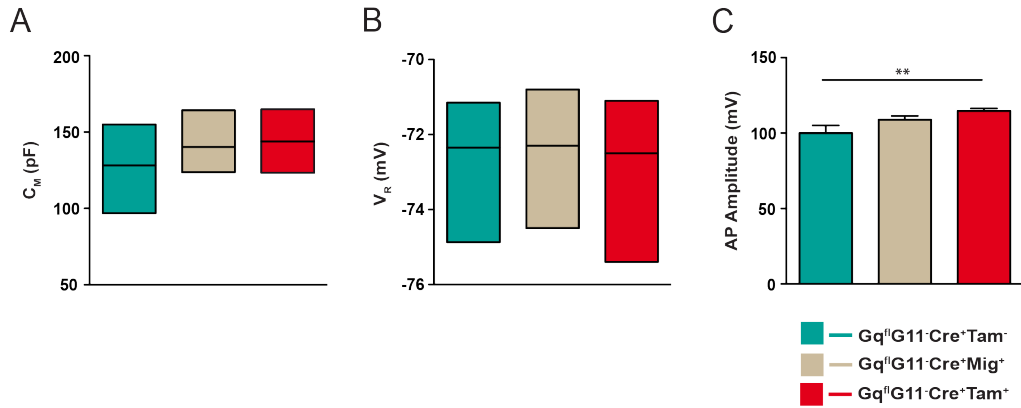


Figure 3.9: The effects of miglyol application on the electrophysiological characteristics of ventricular myocytes from $G\alpha_{11}$ KO animals. Membrane capacitance (C_m), resting membrane potential (V_R), and action potential amplitude (AP amplitude) (A–C). Number of animals and cells are shown in Supplementary table 1. Error bars represent mean \pm SEM. The box plots show median (middle band) and 25/75 percentiles (lower/upper quartiles, respectively).

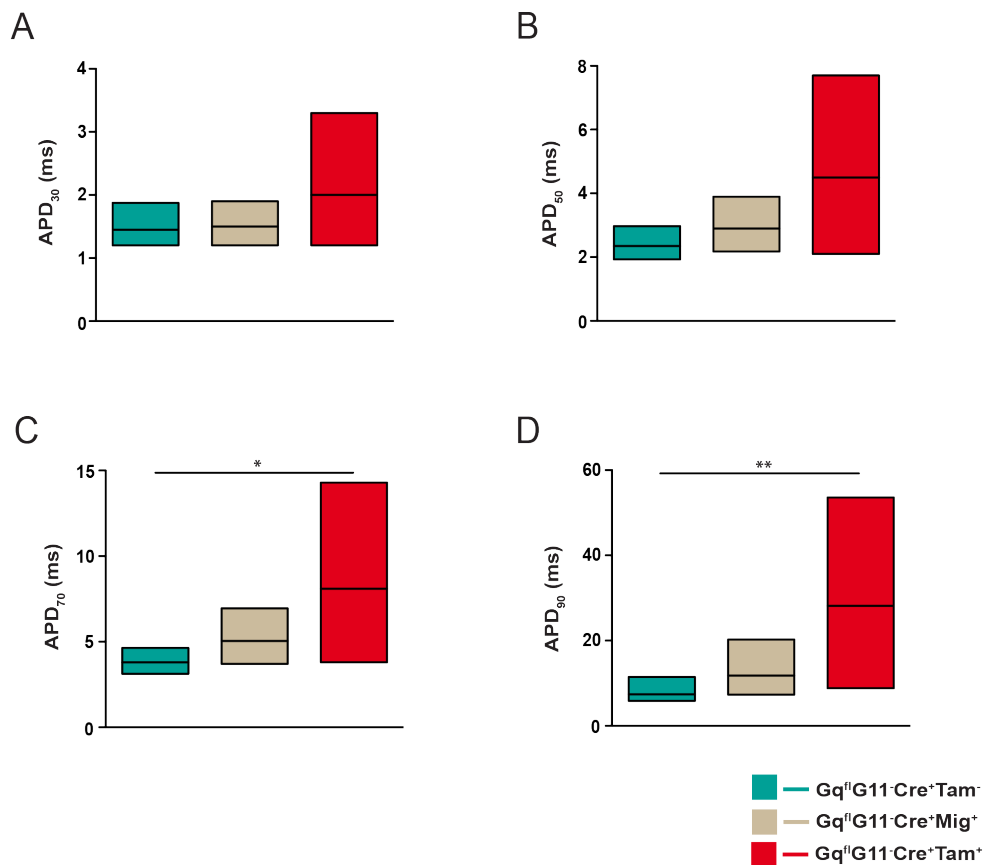


Figure 3.10: The effects of miglyol application on the AP duration of ventricular myocytes from $G\alpha_{11}$ KO animals. AP durations after 30, 50, 70 and 90% repolarization, APD₃₀ (A), APD₅₀ (B), APD₇₀ (C), and APD₉₀ (D), respectively. Number of animals and cells are shown in Supplementary table 1. The box plots show median (middle band) and 25/75 percentiles (lower/upper quartiles, respectively).

In summary,

1. Tamoxifen injection resulted in a rather complex, genotype-dependent alteration of electrophysiological properties (I_{toC} up-regulation in wildtype, AP prolongation and I_{toC} down-regulation in $G\alpha_{11}$ KO) even though its injection had been terminated at least 28 days prior to the actual experiment
2. Miglyol injection did not modify the electrophysiological properties of ventricular myocytes, nor in wildtype neither in $G\alpha_{11}$ KO
3. $G\alpha_{11}$ KO resulted in substantial C_M reduction, AP shortening and I_{toC} up-regulation in ventricular myocytes

3.1.3. Cre recombinase expression causes only minor changes in myocyte properties

Nowadays, Cre/LoxP system is widely used in gene targeting. Improvements in this system enabled us to restrict the gene manipulation down to a specific cell type. For instance, to generate a cardiomyocyte-specific gene knockout, the Cre expression was accomplished under the control of a cardiomyocyte-specific promoter e.g. α -MHC. Despite this great power, high levels of Cre expression reported to have toxic effects in cardiomyocytes⁷. Therefore, we investigated the effects of Cre expression on the AP characteristics and I_{toC} of ventricular myocytes in our Cre/LoxP system. Similar to tamoxifen experiments, the effects of Cre expression were studied in wildtype mice and mice with $G\alpha_{11}$ null-background.

As shown in figure 3.11 and 3.12 the only electrophysiological parameter that was affected by the Cre expression was the magnitude of I_{toC} in the $G\alpha_{11}$ -deficient mice (Figure 3.12, turquoise vs. violet). Interestingly, this Cre-induced decrease in I_{toC} did not change the APD_{30} and APD_{50} (Figure 3.11Db, turquoise vs. violet). It has to be noted that the boxes or bars with the same colors as figures 3.5 and 3.6 represent the same dataset.

In summary, Cre expression did not greatly alter the electrophysiological properties of ventricular myocytes.

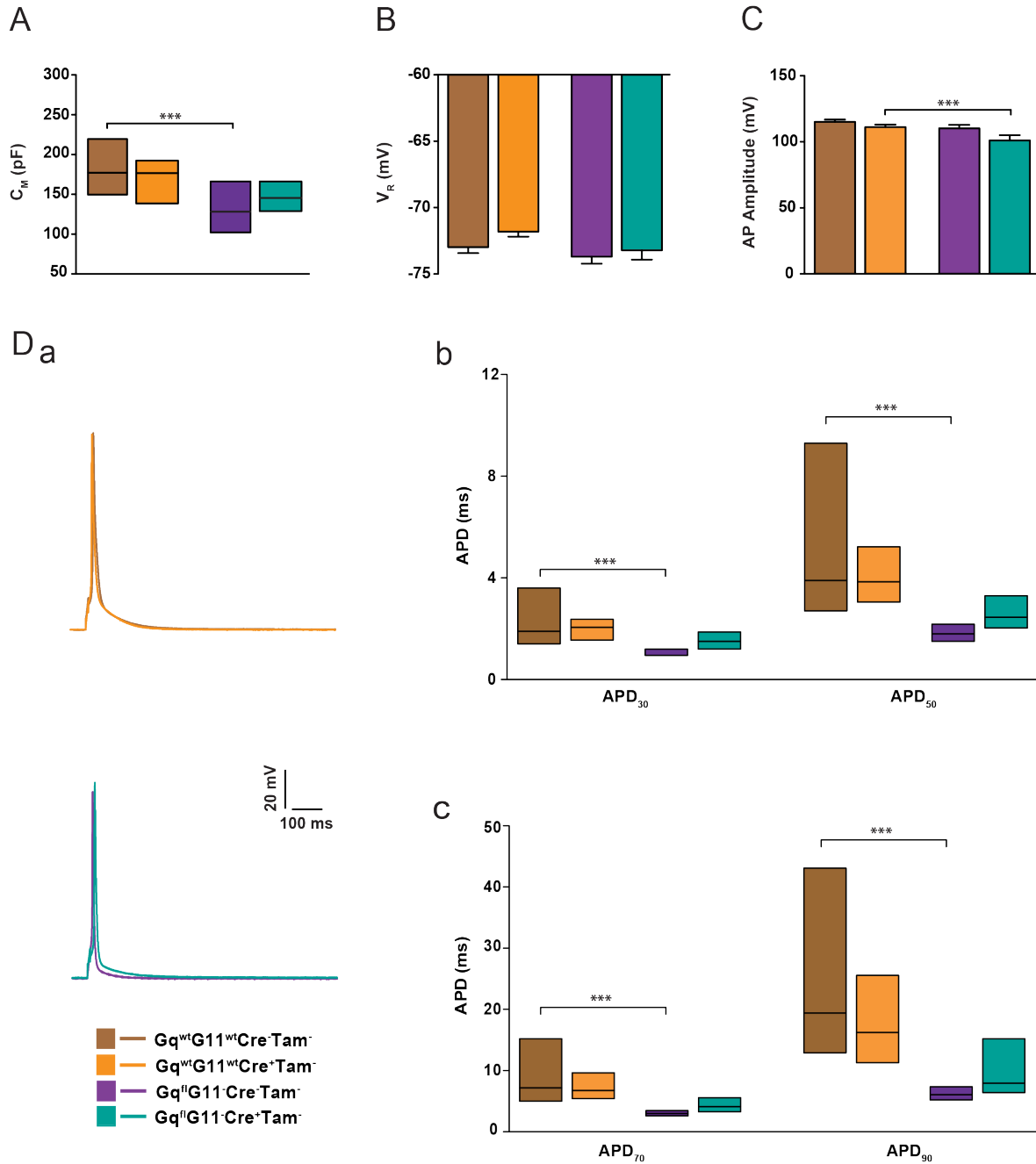


Figure 3.11: The effects of Cre expression on the electrophysiological characteristics of ventricular myocytes from wildtype and $G\alpha_{11}$ KO animals. Membrane capacitance (C_m), resting membrane potential (V_R), and action potential amplitude (AP amplitude) (A–C). Representative APs (Da) and action potential durations after 30, 50, 70 and 90% repolarization, APD₃₀ and APD₅₀ (Db), APD₇₀ and APD₉₀ (Dc). The boxes or bars with the same colors as figure 3.5 represent the same dataset. Number of animals and cells are shown in Supplementary table 1. Error bars represent mean \pm SEM. The box plots show median (middle band) and 25/75 percentiles (lower/upper quartiles, respectively).

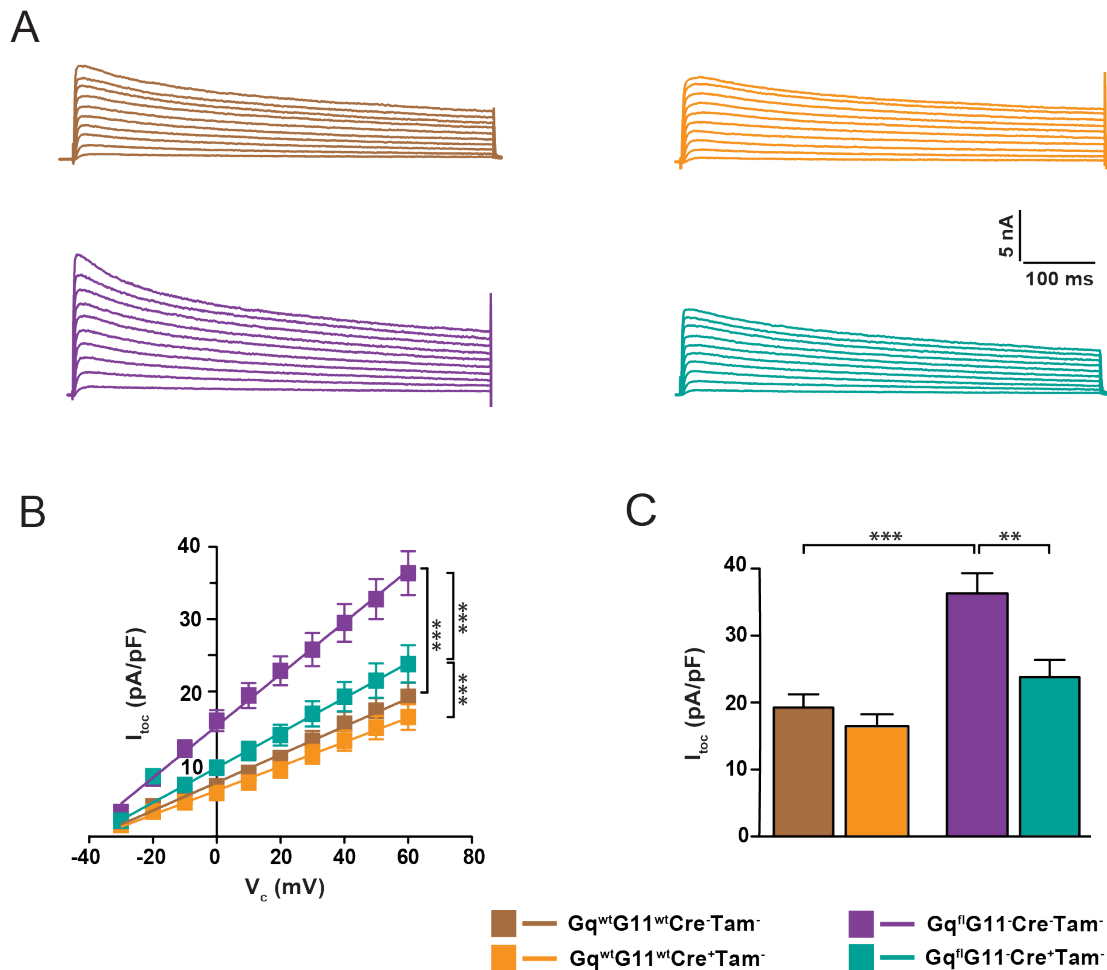


Figure 3.12: The effect of Cre expression on the transient outward current (I_{toc}) of ventricular myocytes from wildtype and $G\alpha_{11}$ KO animals. Typical I_{toc} traces (A), corresponding current-voltage (IV) relationships (B), and the I_{toc} density at +60 mV test potential (C). The boxes or bars with the same colors as figure 3.6 represent the same dataset. Number of animals and cells are shown in Supplementary table 1. Error bars represent mean \pm SEM.

3.1.4. Two sets of genotypes are sufficient to study the effects of $G\alpha_q/G\alpha_{11}$ knockout in ventricular myocytes

I performed two sets of experiments to study the effects of tamoxifen and Cre expression on the AP characteristics and I_{toc} of ventricular myocytes. The results showed a modulatory effect of tamoxifen in most of the investigated parameters, which was surprisingly dependent on the genetic background (Figure 3.5 and 3.6). In contrast, Cre expression did not induce severe changes in most of the electrophysiological

parameters (Figure 3.11 and 3.12). Therefore, we concluded that the tamoxifen injection on a constant genetic background, similar to what I introduced in figures 3.1 and 3.2, is not the best approach to study the effects of $G\alpha_q$ KO. Rather, Cre or loxP insertion would better serve this purpose.

Therefore we designed two genetic approaches to address the role of $G\alpha_q$; they are summarized in tables 3.2 and 3.3. The basic idea behind the set of genotypes presented in table 3.2 was to generate $G\alpha_q$ KO by inserting the loxP sites, while table 3.3 introduces the idea of employing Cre expression. While loxP insertion would require the breeding of four separate mouse lines with an increasing genetic distance over time, the genotypes introduced in table 3.3 (Cre expression with tamoxifen injection) would require the breeding of only two mouse lines, enabling us to compare the $G\alpha_q$ KO effects in litter-mates. Therefore, we decided to perform the final set of experiments using the genotypes detailed in table 3.3, which all included tamoxifen injection.

Table 3.2: $G\alpha_q$ KO by insertion of LoxP sites. wt, wildtype; tg, transgenic; 0, no Cre expression.

| Label | <i>gnaq</i> | <i>gna11</i> | Cre status | Tamoxifen |
|--------------------------------|--------------------|---------------------|-------------------|------------------|
| $Gq^{wt} G11^{wt} Cre^+ Tam^+$ | wt/wt | wt/wt | tg/0 | + |
| $Gq^{fl} G11^{wt} Cre^+ Tam^+$ | flox/flox | wt/wt | tg/0 | + |
| $Gq^{wt} G11^- Cre^+ Tam^+$ | wt/wt | -/- | tg/0 | + |
| $Gq^{fl} G11^- Cre^+ Tam^+$ | flox/flox | -/- | tg/0 | + |

Table 3.3: $G\alpha_q$ KO by employing Cre expression. wt, wildtype; tg, transgenic; 0, no Cre expression.

| Label | <i>gnaq</i> | <i>gna11</i> | Cre status | Tamoxifen |
|--------------------------------|--------------------|---------------------|-------------------|------------------|
| $Gq^{fl} G11^{wt} Cre^- Tam^+$ | flox/flox | wt/wt | 0/0 | + |
| $Gq^{fl} G11^{wt} Cre^+ Tam^+$ | flox/flox | wt/wt | tg/0 | + |
| $Gq^{fl} G11^- Cre^- Tam^+$ | flox/flox | -/- | 0/0 | + |
| $Gq^{fl} G11^- Cre^+ Tam^+$ | flox/flox | -/- | tg/0 | + |

3.1.5. $G\alpha_q$ knockout modifies the electrical properties of cardiomyocytes, but its effects depend on $G\alpha_{11}$ expression

Using the genotypes introduced in table 3.3, I studied the impact of $G\alpha_q$ and/or $G\alpha_{11}$ KO on the AP and I_{toC} in ventricular myocytes. While $G\alpha_q$ and $G\alpha_{11}$ KO alone did not significantly change the cell membrane capacitance (Figure 3.13A, blue and green vs. black), $G\alpha_q/G\alpha_{11}$ DKO resulted in a 15% reduction of C_M (Figure 3.13A, red vs. black). This C_M alteration might be to a great extent due to the $G\alpha_{11}$ rather than $G\alpha_q$ KO (compare blue & green and blue & red in Figure 3.13A). $G\alpha_q$ KO resulted in a more hyperpolarized V_R (Figure 3.13B, blue vs. black) and significantly larger AP amplitudes (Figure 3.13C, blue vs. black). The AP amplitudes were significantly enhanced in $G\alpha_q/G\alpha_{11}$ DKO, too (Figure 3.13C, red vs. black) that could be attributed to $G\alpha_q$ KO effect rather than $G\alpha_{11}$ -deficiency (Figure 3.13C, green vs. black and blue vs. black).

In contrast to most of the alterations of AP shape introduced so far (Fig 3.5 and 3.11), I did not find any significant changes in the repolarization phase of AP while investigating myocytes from our optimized genotypes (Figure 3.13D), despite significant but minor alterations in the I_{toC} -voltage relationships (Figure 3.14, green vs. red and black).

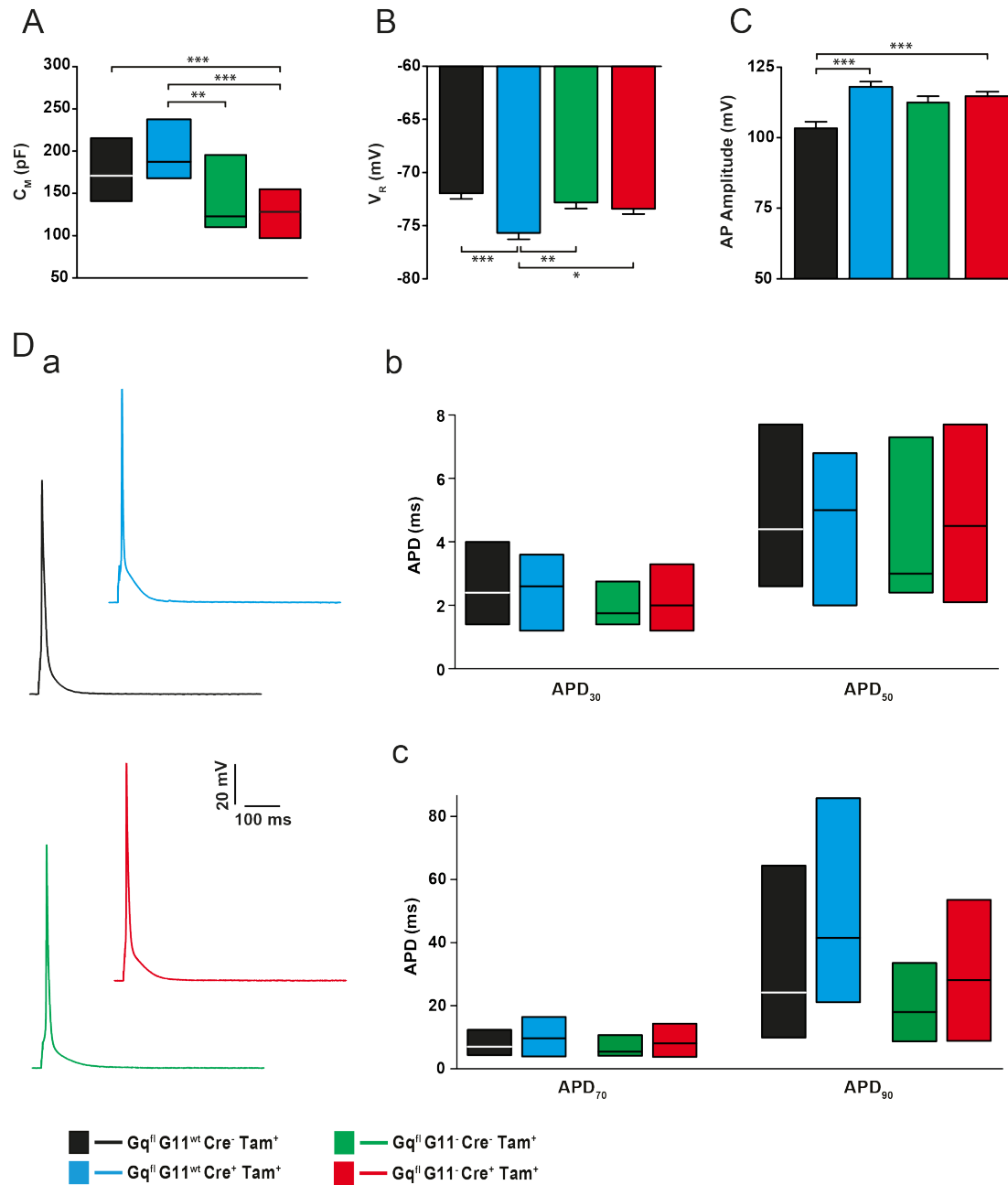


Figure 3.13: The effects of $G\alpha_q$ and/or $G\alpha_{11}$ KO on the electrophysiological characteristics of ventricular myocytes. Membrane capacitance (C_m), resting membrane potential (V_R), and action potential amplitude (AP amplitude) (A–C). Representative APs (Da) and action potential durations after 30, 50, 70 and 90% repolarization, APD₃₀ and APD₅₀ (Db), APD₇₀ and APD₉₀ (Dc). The boxes or bars with the same colors as figures 3.1 and 3.5 represent the same dataset. Number of animals and cells are shown in Supplementary table 1. Error bars represent mean \pm SEM. The box plots show median (middle band) and 25/75 percentiles (lower/upper quartiles, respectively).

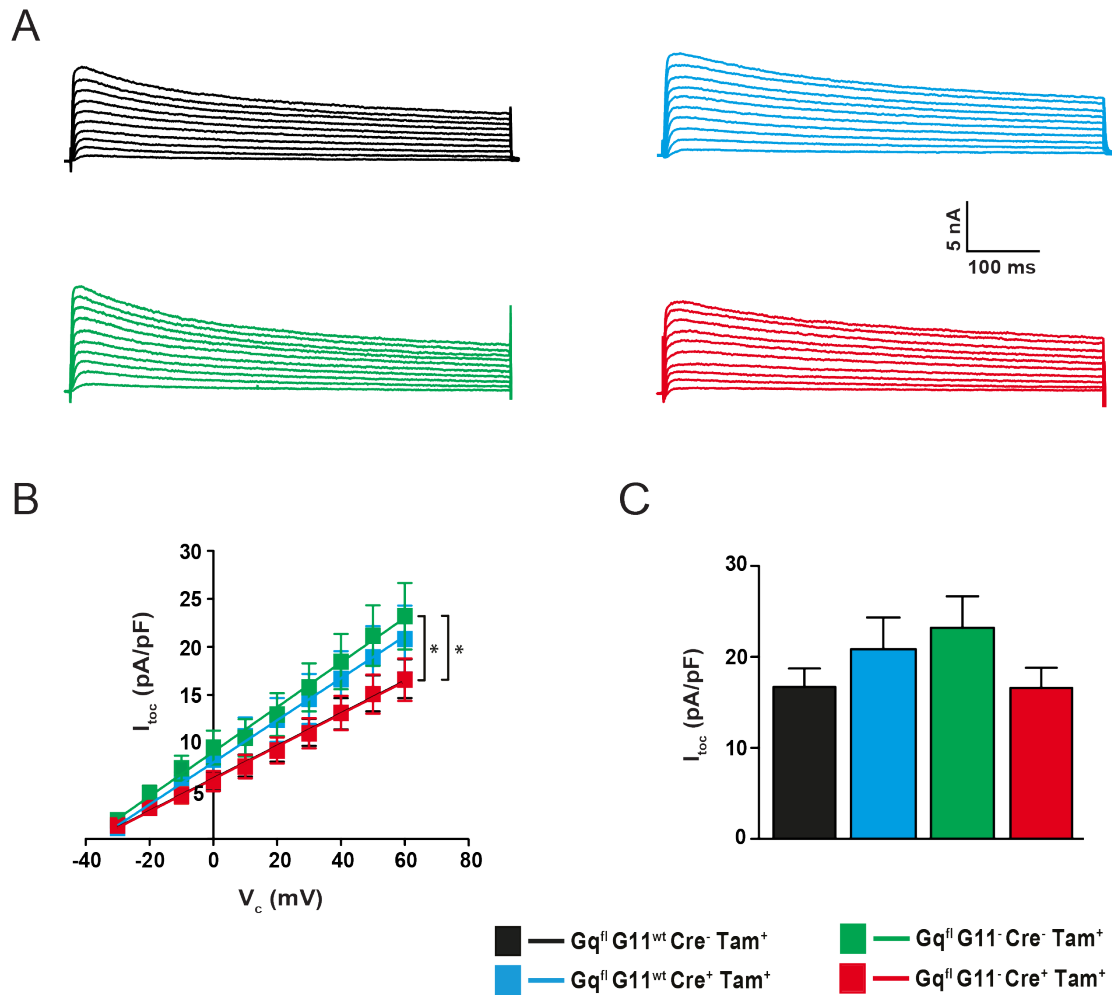


Figure 3.14: The effect of $G\alpha_q$ and/or $G\alpha_{11}$ KO on the transient outward current (I_{toc}) in ventricular myocytes. Typical I_{toc} traces (A), corresponding current-voltage (IV) relationships (B), and the I_{toc} density at +60 mV test potential (C). The boxes or bars with the same colors as figures 3.3 and 3.6 represent the same dataset. Number of animals and cells are shown in Supplementary table 1. Error bars represent mean \pm SEM.

In summary,

1. $G\alpha_q/G\alpha_{11}$ DKO resulted in C_M reduction.
2. $G\alpha_q$ KO resulted in significantly more negative V_R .
3. $G\alpha_q$ KO as well as $G\alpha_q/G\alpha_{11}$ DKO resulted in significantly higher AP amplitudes.
4. The repolarization phase of AP remained unchanged in all genotypes.
5. $G\alpha_{11}$ KO altered the I_{toc} -voltage relationships.

3.2. Hyperaldosteronism-induced electrical remodeling in ventricular myocytes of wildtype and $G\alpha_q/G\alpha_{11}$ KO mice

Hyperaldosteronism is a risk factor for cardiac diseases because it induces hypertension²²⁰. It was recently reported that aldosterone induces cardiac remodeling independent of the effects on the arterial blood pressure⁴⁶. Since then many studies investigated the physiological and pathological effects of aldosterone on the heart²¹². Recently our group in a collaborative work with Neuberger group, reported an important role for aldosterone in the development of atrial fibrillation¹⁵⁸. In the current study, we aimed to investigate the putative role of $G\alpha_{q/11}$ coupled signaling pathways in aldosterone-induced on the heart. We also studied cellular remodeling process in response to hyperaldosteronism.

To address the possible involvement of $G\alpha_{q/11}$ signaling in the aldosterone effects, I took the advantage of our four optimized genotypes described in table 3.3. Hyperaldosteronism (HA) was induced in mice (see 2.4) and was confirmed by ELISA tests indicating a 8-fold increase in the plasma aldosterone level (from 292.5 pg/ml to 2400 pg/ml). We studied remodeling on the level of the heart as well as on the isolated ventricular myocytes. Various morphological and functional properties of the heart were assessed using echocardiography. On the cellular level, the electrophysiological properties and Ca^{2+} handling were investigated. In this thesis I will present the results of electrophysiological studies. The effects of HA on the AP characteristics and I_{toC} were assessed in ventricular myocytes from $G\alpha_q$ and/or $G\alpha_{11}$ KO mice.

3.2.1. Aldosterone effects on C_M and V_R is mediated by $G\alpha_q/G\alpha_{11}$ proteins

The sustained increase in the plasma aldosterone level has shown to enhance the risk of human left ventricular hypertrophy²¹². In a rat model of induced HA, the hypertrophic response was associated with larger cardiomyocyte size¹⁸⁶. I also investigated this in

the mouse model of induced HA by measuring C_M . While chronic HA did not affect C_M in wildtype cells, $G\alpha_{11}$ KO and $G\alpha_q/G\alpha_{11}$ DKO resulted in ~ 15% HA-mediated decrease of the C_M (Figure 3.15A, red & green). Since C_M remained unchanged in $G\alpha_q$ KO following HA (Figure 3.15A, Blue), thus the effects seen in $G\alpha_q/G\alpha_{11}$ DKO might be attributed to the aldosterone- $G\alpha_{11}$ KO interaction.

The chronic HA induced minor changes on V_R . While following HA, V_R shifted to more negative potentials in wildtype cells, the absence of either $G\alpha_q$ or $G\alpha_{11}$ abolished this hyperpolarization (Figure 3.15B).

In summary,

- 1- HA resulted in C_M reduction in $G\alpha_{11}$ and $G\alpha_q/G\alpha_{11}$ DKO ventricular myocytes.
- 2- HA resulted in more negative V_R in wildtype cells and this effect was abolished by deletion of either $G\alpha_q$ and/or $G\alpha_{11}$ proteins.

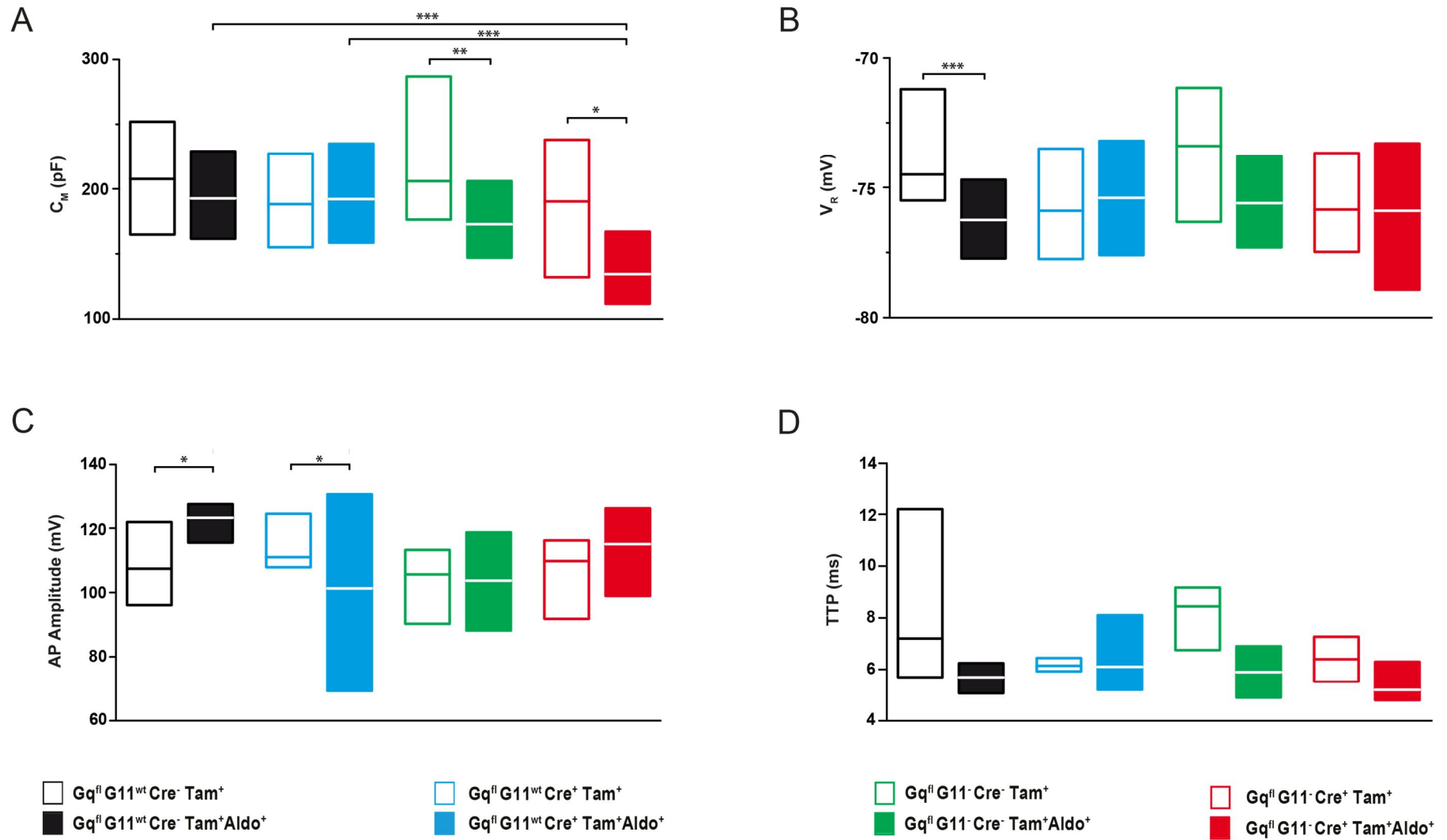


Figure 3.15: The effects of HA on the electrophysiological characteristics of ventricular myocytes. Membrane capacitance (C_M), resting membrane potential (V_R), and action potential amplitude (AP amplitude) and time to peak (TTP) (A–D). Number of animals and cells are shown in Supplementary table 2. The box plots show median (middle band) and 25/75 percentiles (lower/upper quartiles, respectively).

3.2.2. Cardiac action potential is greatly altered by hyperaldosteronism

Many cardiac diseases are accompanied by cellular electrophysiological remodeling that is often manifested in alterations of APs⁴³. In our study we aimed to investigate the putative role of HA in electrophysiological remodeling of cardiac cells and the AP was chosen as a parameter integrating many electrical characteristics of the cell. Similar to 3.2.1, the putative HA-induced alterations of AP were investigated in various genotypes to study the contribution of $G\alpha_q$ and $G\alpha_{11}$ signaling.

All AP measurements were performed in steady-state at 4 Hz and 37 °C. The depolarization phase of the AP was studied by analyzing two important parameters: (i) AP amplitude and (ii) time to peak (TTP). The AP amplitude was significantly enhanced (~13%) by HA in ventricular myocytes of wildtype mice (Figure 3.15C, black). Similar result was obtained in the $G\alpha_q$ -deficient myocytes (Figure 3.15C, blue). In contrast, deletion of either $G\alpha_{11}$ or $G\alpha_q/G\alpha_{11}$ proteins abolished this HA-mediated effect on the AP amplitude (Figure 3.15C, green & red, respectively).

The TTP was not affected by HA in wildtype cells (Figure 3.15D, black). $G\alpha_q$ and/or $G\alpha_{11}$ KO did not alter this AP parameter, too (Figure 3.15D, green & red).

HA-induced hypertrophic responses were shown to be associated with AP prolongation in cardiac myocytes^{18,142}. In contrast, I found that APD_{30} , APD_{50} and APD_{70} were significantly shortened in wildtype cells following HA as reflected in exemplified APs, too (Figure 3.16, black). While this effect was completely blunted by either $G\alpha_q$ or $G\alpha_{11}$ protein deletion, removal of both proteins ($G\alpha_q/G\alpha_{11}$ DKO) reversed that (Figure 3.16, blue, green & red). AP durations were substantially prolonged in ventricular myocytes of $G\alpha_q/G\alpha_{11}$ DKO cells following HA (Figure 3.17B-D red).

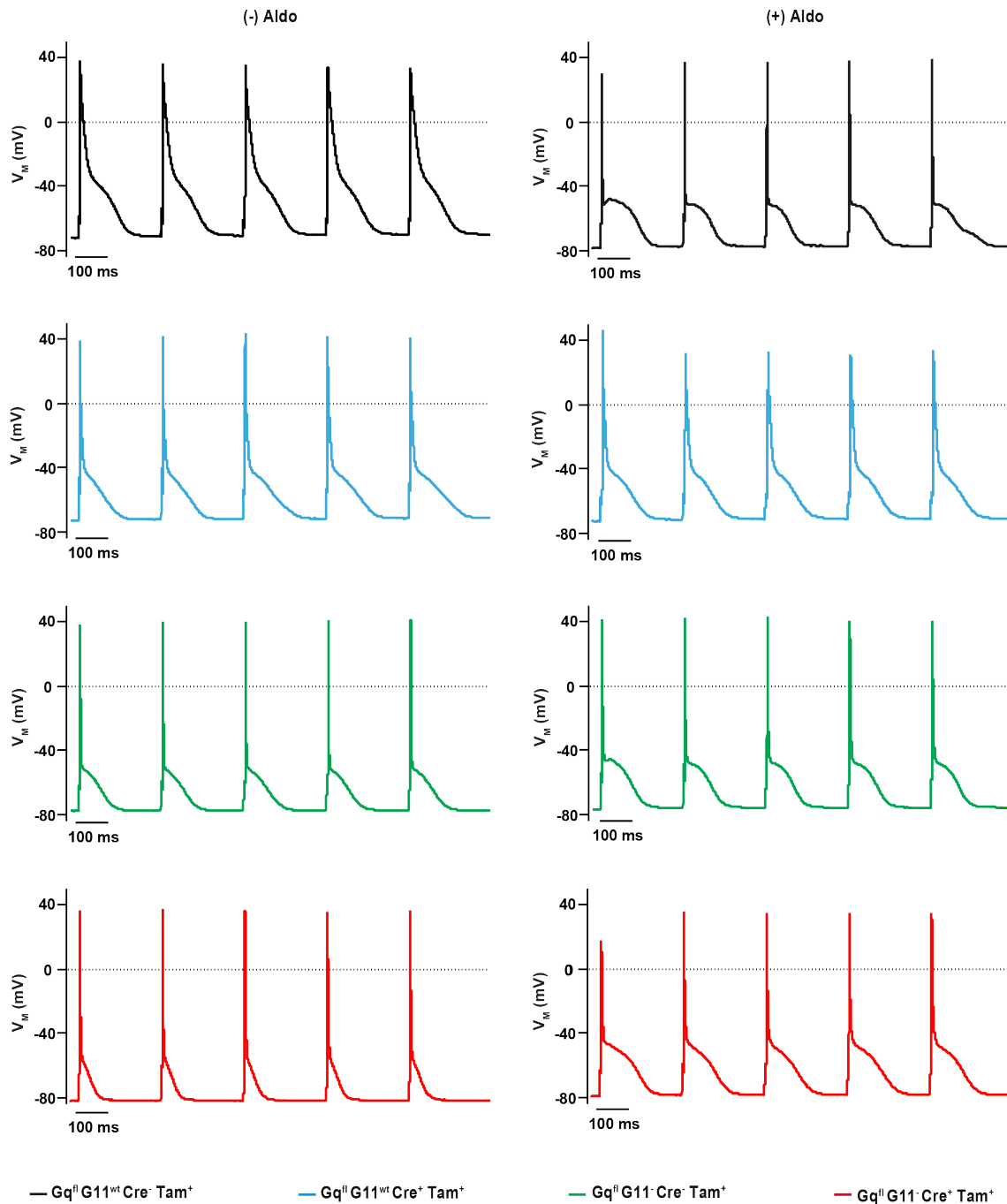


Figure 3.16: The effect of HA on AP shape of ventricular myocytes. Representative APs in wildtype, $G\alpha_q$ KO, $G\alpha_{11}$ KO, and $G\alpha_q/G\alpha_{11}$ DKO in control (left column) and following HA (right column). Number of animals and cells are shown in Supplementary table 2.

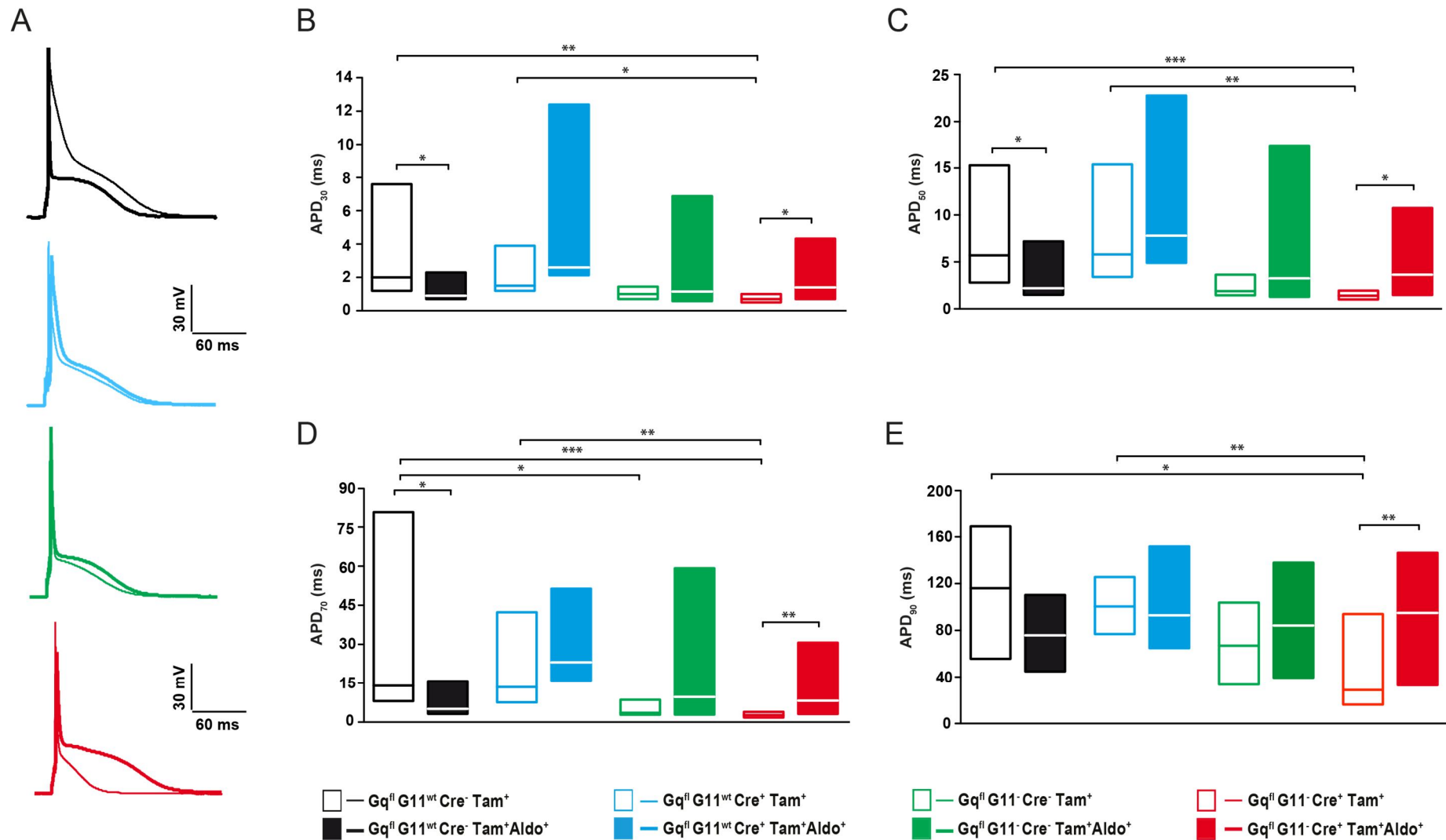


Figure 3.17: The effects of HA on the AP durations of ventricular myocytes. Representative APs (A) and statistical analysis of AP durations at 30, 50, 70 and 90% repolarization, APD₃₀ (B), APD₅₀ (C), APD₇₀ (D), and APD₉₀ (E), respectively. Number of animals and cells are shown in Supplementary table 2. The box plots show median (middle band) and 25/75 percentiles (lower/upper quartiles, respectively).

In summary,

1. HA caused larger AP amplitudes in wildtype and $G\alpha_q$ KO cells but no effects in cells from $G\alpha_{11}$ or $G\alpha_q/G\alpha_{11}$ DKO.
2. HA did not alter time to peak of depolarization phase of AP in all genotypes studied.
3. HA resulted in a shortened AP repolarization when investigating wildtype cells, an unchanged AP in single KOs but a prolonged AP repolarization in DKO.

3.2.3. I_{toC} is the target of aldosterone effects in ventricular myocytes

In the following, I investigated putative ionic currents contributing to these AP alterations. Changes in the I_{to} density as well as alterations in mRNA expression of Kv4.2 and KV4.3 have been attributed to HA^{18,46}. Thus, I studied I_{toC} to investigate their putative contribution to changes in APD_{30} .

I_{toC} was greatly altered in wildtype cells following HA (Figure 3.18A). Interestingly, HA caused an increased I_{toC} density that was absent in single KO animals (Figure 3.18A & B & C and 3.19 black, blue and green). Unexpectedly, the density of I_{toC} was reduced following HA in the cells from animals with $G\alpha_q/G\alpha_{11}$ DKO (Figure 3.18D and 3.19 red). This was in agreement with the behavior of APD_{30} in these genotypes (Figure 3.17A & B, blue and green). While the current-voltage relationships were significantly different in $G\alpha_{11}$ following HA (Figure 3.18Cb), the I_{toC} density at +60 mV was not (Figure 3.19, green). A possible explanation for this apparent discrepancy could be that the sample size at +60 mV might be the limiting factor for statistical analysis.

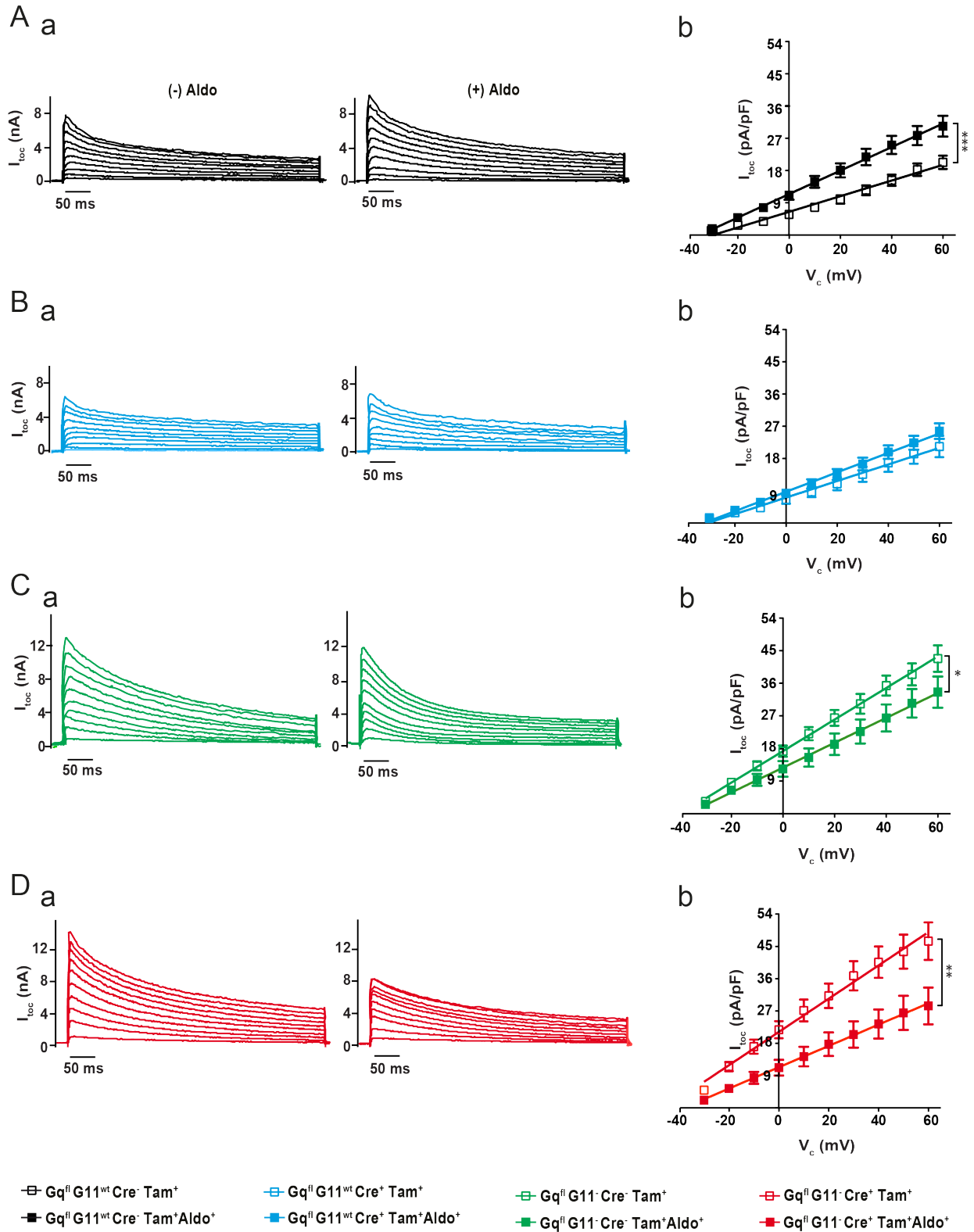


Figure 3.18: The effect of HA on the I_{toc} -voltage relationships. Typical I_{toc} traces and corresponding current-voltage (IV) relationships in wildtype (Aa-b), $G\alpha_q$ KO (Ba-b), $G\alpha_{11}$ KO (Ca-b) and $G\alpha_q/G\alpha_{11}$ KO (Da-b). Number of animals and cells are shown in Supplementary table 2. Error bars represent mean \pm SEM.

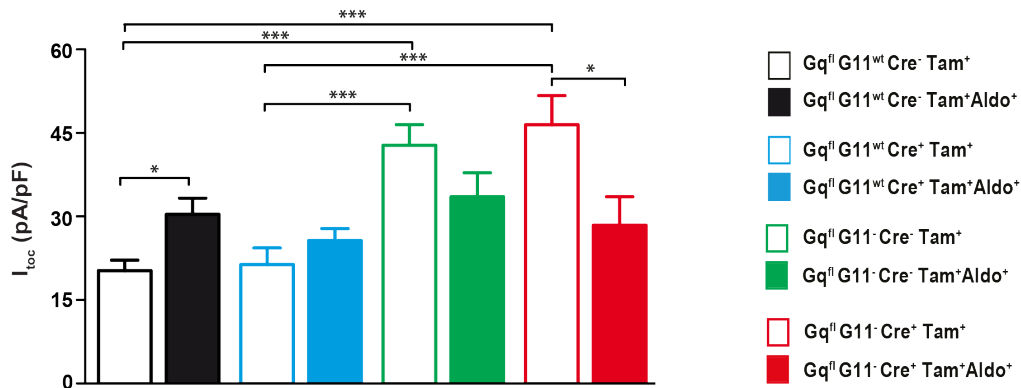


Figure 3.19: The effect of HA on the I_{toc} density in ventricular myocytes. I_{toc} density at +60 mV test potential. Number of animals and cells are shown in Supplementary table 2. Error bars represent mean \pm SEM.

In summary :

- 1- HA altered the I_{toc} density and current-voltage relationships in ventricular myocytes from wildtype and $G\alpha_q/G\alpha_{11}$ DKO mice.
- 2- In wildtype cells, I_{toc} density was enhanced and the I_{toc} -voltage relationships were altered.
- 3- In $G\alpha_q/G\alpha_{11}$ cells, the I_{toc} density was decreased and current-voltage relationships were modulated.
- 4- While HA altered the I_{toc} -voltage relationship, it did not induce significant changes in current densities in $G\alpha_{11}$ KO cells.
- 5- The results of I_{toc} measurements were in great agreement with the results of early repolarization (APD_{30}) in all genotypes studied.

3.3. I1624E mutation in the IQ motif of Cav1.2 and the effects on the $I_{Ca,L}$ and EC Coupling gain

In contrast to the skeletal muscle, contraction of cardiomyocyte is majorly dependent on the extracellular Ca^{2+} . LVDCCs mediate the Ca^{2+} influx and provide the initial trigger for further Ca^{2+} release from SR. The LVDCC is regulated precisely to control the contractility of cardiomyocyte. One regulatory mechanism that originates from the intrinsic properties of the channel is the Ca^{2+} -dependent inactivation (CDI), which is mediated by CaM. There are growing body of evidences showing that CaM binds to the IQ motif of Cav1.2 which is located at amino acids 1624–1635^{77,227,229}. Ile-1624 was especially characterized as the determinant of CaM binding to Cav1.2¹⁵². Mutation of Ile-1624 to Glu (I/E mutation) decreased the affinity of IQ sequence for CaM by ~100-fold⁴⁹ and abolished CDI of $I_{Ca,L}$ expressed in *Xenopus* oocytes²²⁸. However the physiological relevance of the IQ motif in the channel regulation has not been clarified in the hearts of living animals. To address this question, transgenic I/E mice were generated (see 2.3.2). To study the physiological and pathological impacts of I/E mutation, the morphological and functional properties of the heart as well as single ventricular myocytes were assessed. In this thesis I will present the results of $I_{Ca,L}$ and EC coupling gain measurements.

3.3.1. Mutation in IQ motif of Cav1.2 modifies the channel function

To study the physiological relevance of the I/E mutation in the Cav1.2 function and regulation, $I_{Ca,L}$ was recorded in ventricular myocytes of I/E and control (Ctr) mice (for genotypes see 2.3.2). The IV relationships showed a substantial reduction of the current density in I/E cells (Figure 3.20 B), which is evident in the representative current traces, too (Figure 3.20Aa & Ab). The peak current amplitude was reduced by 33% in I/E cells at 0 mV. The I/E mutation did not cause any alterations of the membrane area (C_M) (Figure 3.21B). Since the Western blot analysis showed reduced Cav1.2 levels in the ventricles of I/E mice compared to Ctr mice¹⁵², there might be some alterations of the channel assembly due to this mutation.

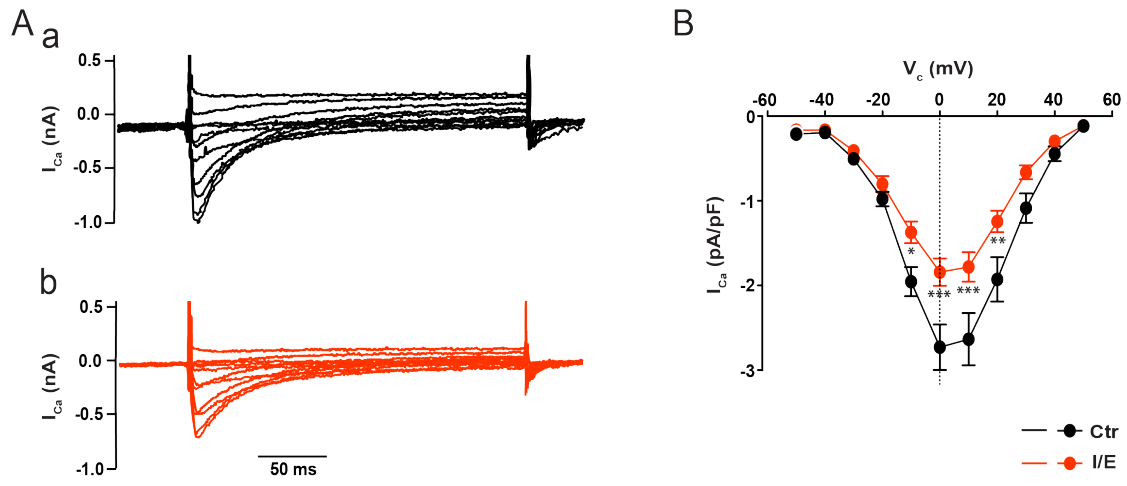


Figure 3.20: The effect of I/E mutation on the L-type Ca^{2+} current ($I_{Ca,L}$) in ventricular myocytes. Typical $I_{Ca,L}$ traces in control (Ctr) (Aa) and I/E (Ab), and corresponding current-voltage (IV) relationships (B). Number of animals and cells are shown in Supplementary table 3. Error bars represent mean \pm SEM.

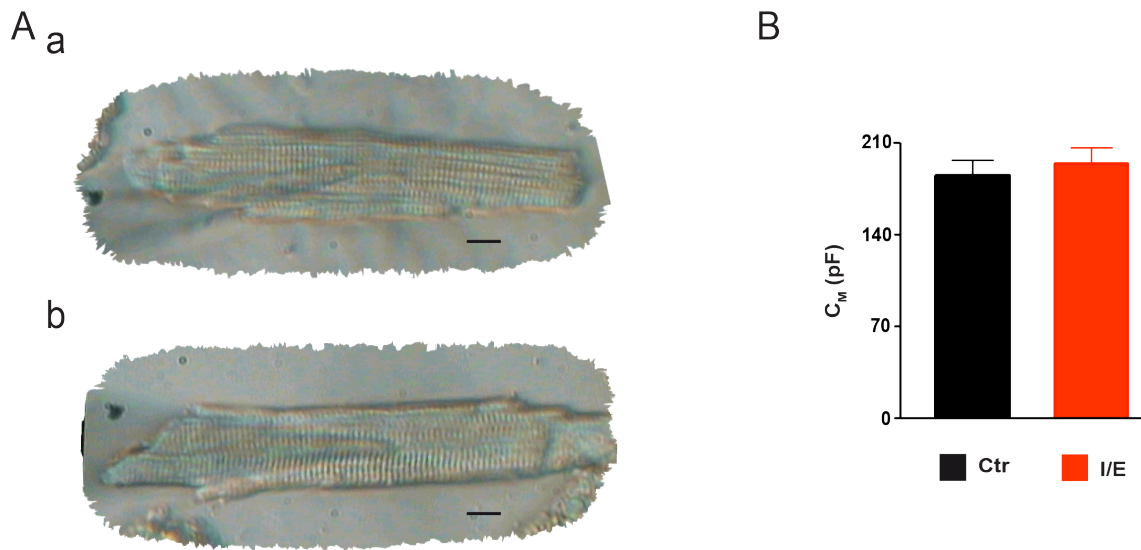


Figure 3.21: The effect of I/E mutation on the plasma membrane capacitance (C_M). Representative transmission images of ventricular cells from Ctr (Aa) and I/E (Ab) mice, scale bar=100 μ m. Statistical analysis of C_M measurements (B). Number of animals and cells are shown in Supplementary table 3. Error bars represent mean \pm SEM.

3.3.2. The I/E mutation results in alterations of EC coupling gain

EC coupling links the electrical excitation of the cell membrane to the mechanical contractile machinery of the cardiomyocyte. $I_{Ca,L}$ is a major mediator of this process. Since the KO mouse only expressing Cav1.2^{I1624E} in the heart, displayed a much smaller $I_{Ca,L}$ but unaltered global Ca^{2+} transients and single cell contractility²⁷, I wondered whether in a compensatory fashion, the EC coupling gain was altered. To study this, I performed simultaneous $I_{Ca,L}$ and Ca^{2+} measurements. Indo-1 was used to monitor cellular Ca^{2+} transients. Briefly, cardiomyocytes were voltage clamped and repetitively depolarized (10 times at 0.5 Hz) to obtain steady-state conditions (see 2.9). This prepulse was followed by a series of test pulses (from -50 mV to +50 mV with 10 mV increments) to activate $I_{Ca,L}$. The resulting Ca^{2+} transients (CICR) were recorded simultaneously. Figure 3.22Aa shows the typical bell-shaped V_m dependence of $I_{Ca,L}$ and the resulting Ca^{2+} transients. The steady-state $I_{Ca,L}$ was reduced over the entire voltage range (Figure 3.22Aa). Unexpectedly, under voltage-clamp conditions, the Ca^{2+} transient amplitudes were substantially increased in cells from I/E mice (Figure 3.22Aa), which is also evident in the representative Ca^{2+} signals (Figure 3.22Ad).

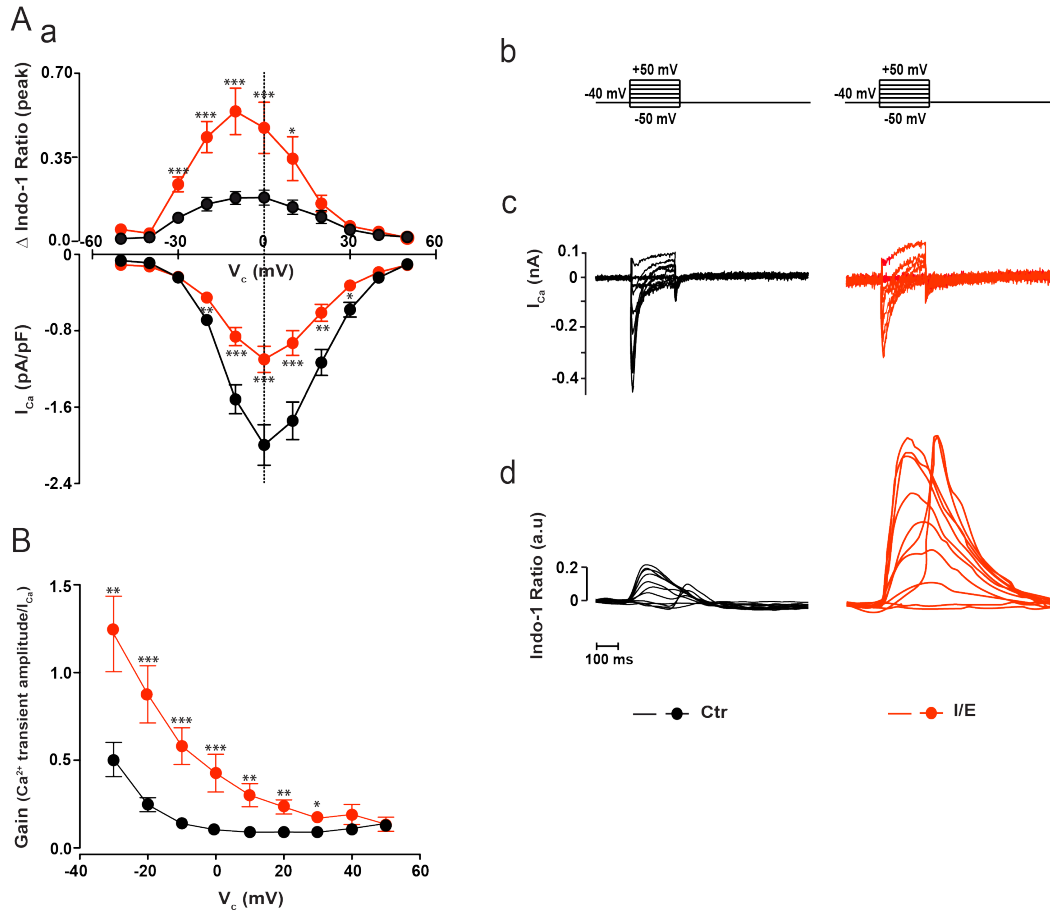


Figure 3.22: The effects of I/E mutation on EC coupling. V_m -dependencies of $I_{Ca,L}$ and global Ca^{2+} transients (Aa), schematic illustration of the protocol used for the measurements (Ab), representative examples for $I_{Ca,L}$ (Ac), and Ca^{2+} transients (Ad) in ventricular myocytes from Ctr and I/E mice. V_m -dependence of EC coupling gain calculated from the data in Aa (B). Number of animals and cells are shown in Supplementary table 4. Error bars represent mean \pm SEM.

In order to further quantify EC coupling, I calculated the ratio of Ca^{2+} transient amplitude over $I_{Ca,L}$ amplitude, the so called EC coupling gain (see 2.9). The results of such an analysis are depicted in figure 3.22B and strongly indicated a substantially augmented EC coupling gain, particularly for lower membrane potentials.

Under control conditions, there was a left shift in the voltage-dependence of the whole cell Ca^{2+} transient compared to $I_{Ca,L}$. While the IV relationships for $I_{Ca,L}$ peaked at around 0 mV, the cellular Ca^{2+} transients displayed the largest amplitude 10 mV more negative, at -10 mV (Figure 3.22Aa). This discrepancy originates from the fact that the whole cell $I_{Ca,L}$ is the sum of single channel currents (i_{Ca}) through thousands of individual open channels ($I_{Ca} = i_{Ca} \times NP_0$). On the other hand, individual Ca^{2+} channels

trigger local Ca^{2+} release events so called Ca^{2+} sparks from the SR. Thus, locally, the Ca^{2+} release probability to a large degree critically depends on the single channel current (i_{Ca}) rather than global $I_{\text{Ca,L}}$. Due to a large driving force for Ca^{2+} influx at negative membrane voltages, i_{Ca} is higher at more negative potentials. As a consequence, the probability that i_{Ca} could trigger a Ca^{2+} spark increases at these voltages. Therefore the EC Coupling gain is higher at more negative V_m ^{36,169}.

In the native Ca^{2+} channel, the IQ motif was reported to be the site for CaM binding and this supposed to mediate CDI. The I/E mutation introduced here prevents CaM binding. I thus analyzed the inactivation properties of $I_{\text{Ca,L}}$ in the ventricular myocytes of I/E mice. Time constants of $I_{\text{Ca,L}}$ inactivation (τ_1 , τ_2) were calculated according to the formula described in 2.6.4. While τ_1 characterizes the fast inactivation, which can be attributed to the CDI, τ_2 describes the slow component of inactivation resulting from VDI. Both, CDI and VDI remained unchanged in I/E mutated cardiomyocytes compared to Ctr cells at 0 mV test pulse (Figure 3.23A & B). However further studies using Ba^{2+} as the charge carrier showed that the I/E mutation resulted in Ca^{2+} channels permanently locked in CDI¹⁵². Interestingly, although the $I_{\text{Ca,L}}$ density was decreased in I/E cells, the amount of Ca^{2+} charge (current integral) remained unchanged (Figure 3.23C).

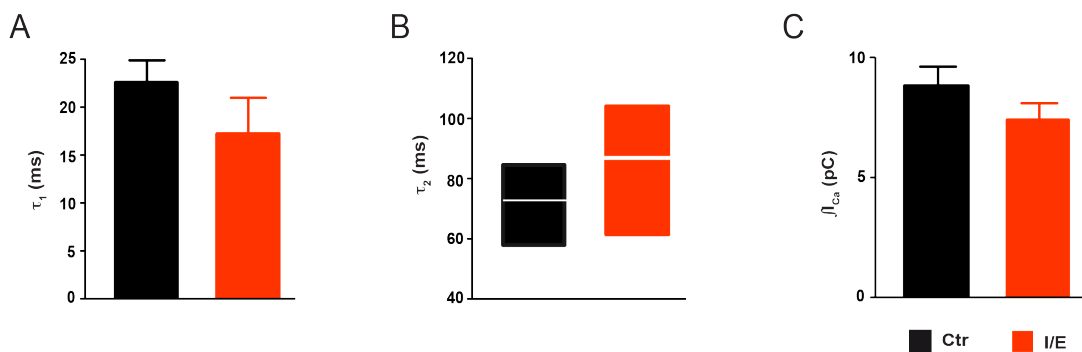


Figure 3.23: The effects of I/E mutation on $I_{\text{Ca,L}}$ inactivation. Time constant of Ca^{2+} -dependent inactivation (τ_1) (A), time constant of voltage-dependent inactivation (τ_2) (B), and the amount of charge entry ($\int I_{\text{Ca,L}}$) (C) at 0 mV. Number of animals and cells are shown in Supplementary table 3. Error bars represent mean \pm SEM.

In summary,

1. I/E mutation resulted in enhanced EC coupling gain.
2. I/E mutation caused the Ca^{2+} channel to be permanently locked in CDI.

3.4. $I_{Ca,L}$ and EC coupling gain in the ventricular myocytes expressing RacET

Rac is a small GTPase of the Rho-family and contributes to various cellular functions such as transcriptional regulation and cytoskeleton organization in nonmuscle cells¹⁹⁸. Increases in Rac expression and activity have been associated with human cardiac pathologies such as dilated and ischemic cardiomyopathies¹¹⁹ as well as atrial fibrillation⁴. Using an animal model with cardiac specific increases in Rac activity, the RacET mouse¹⁸⁴, my group recently described impaired ventricular function¹⁵⁷ (Oberhoffer, 2012 submitted paper). I thus investigated the relationship between $I_{Ca,L}$ and Ca^{2+} release by analyzing the EC coupling gain.

Since SR Ca^{2+} release is triggered by Ca^{2+} influx through LVDCCs, Changes in $I_{Ca,L}$ might be a substrate for subsequent alterations of Ca^{2+} handling. $I_{Ca,L}$ was measured in ventricular myocytes of RacET mice according to the protocol for $I_{Ca,L}$ activation described in 2.7.4. $I_{Ca,L}$ was unchanged in the cells from RacET mice (Figure 3.24Aa & Ab), as reflected in the overlapping IV relationships (Figure 3.24B).

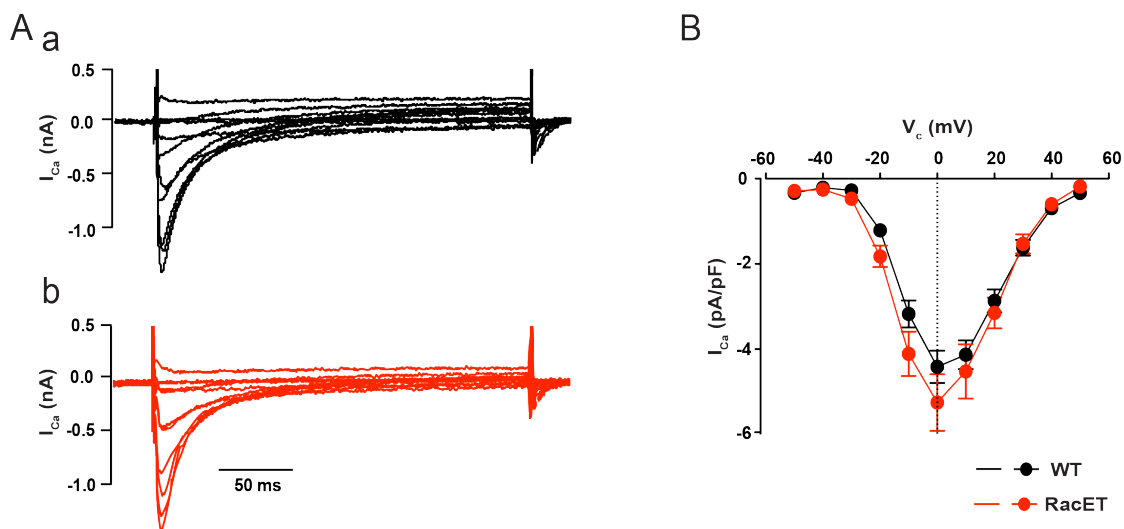


Figure 3.24: The effect of expression of a constitutively active Rac1 on the L-type Ca^{2+} current ($I_{Ca,L}$) in ventricular myocytes. Typical $I_{Ca,L}$ traces in control (Ctr) (Aa) and I/E (Ab), and corresponding current-voltage (IV) relationships (B). Number of animals and cells are shown in Supplementary table 4. Error bars represent mean \pm SEM.

To study EC coupling gain, I performed simultaneous $I_{Ca,L}$ and Ca^{2+} transients measurements (see 2.9). Interestingly, the peak steady-state $I_{Ca,L}$ was substantially reduced in myocytes from RacET mice compared to WT (Figure 3.25 Aa). Despite this decrease, the Ca^{2+} transient amplitude was enhanced by 2.5-fold (Figure 3.25Aa). Consequently, the EC coupling gain was significantly enhanced in the ventricular myocytes from RacET mice (Figure 3.25B).

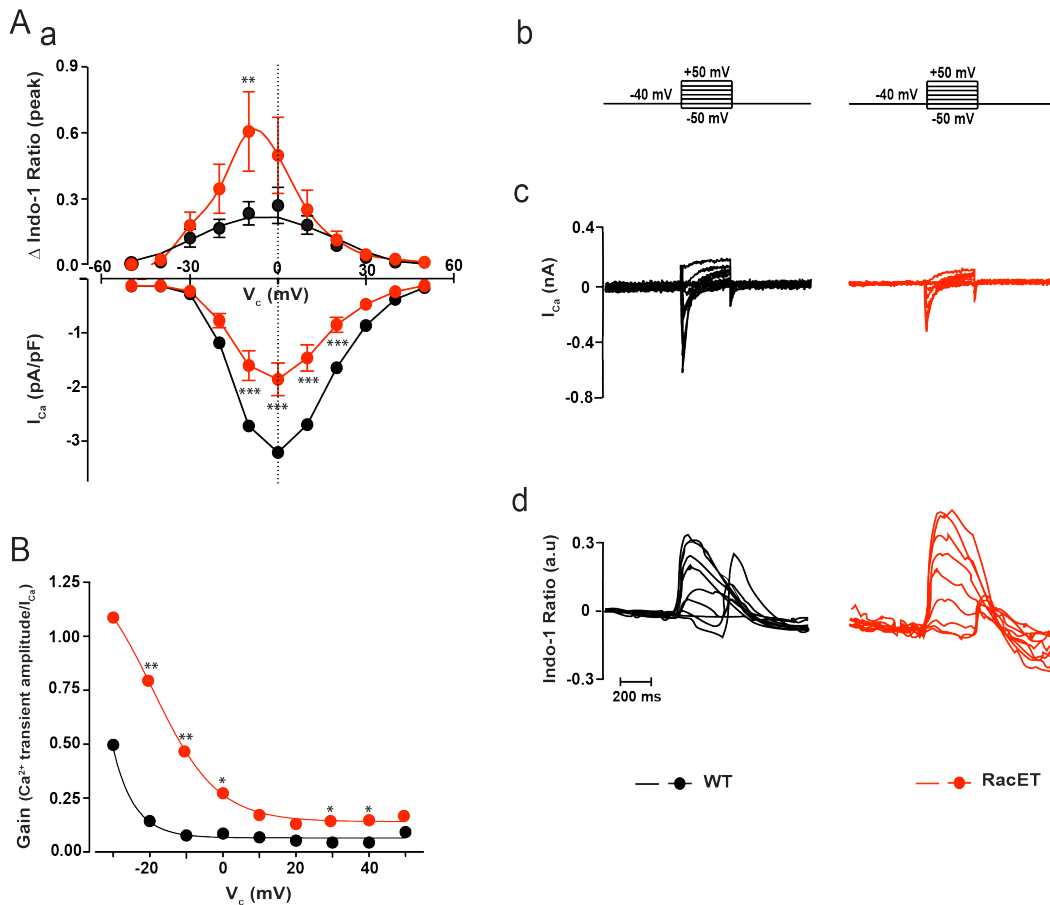


Figure 3.25: The effect of expression of a constitutively active Rac1 on EC coupling. V_m -dependencies of $I_{Ca,L}$ and global Ca^{2+} transients (Aa), schematic illustration of the protocol used for the measurements (Ab), representative examples for $I_{Ca,L}$ (Ac), and Ca^{2+} transients (Ad) in ventricular myocytes from WT and RacET mice. V_m -dependence of EC coupling gain calculated from the data in Aa (B). Number of animals and cells are shown in Supplementary table 4. Error bars represent mean \pm SEM.

The inactivation properties of $I_{Ca,L}$ were also investigated. τ_1 was ~ 1.5 times larger in RacET (Figure 3.26A) at 0 mV test pulse, indicating an altered CDI. Since CDI is believed to be a local process, one could speculate that the local control of CDI might have been altered in RacET myocytes, possibly brought about by an altered Ca^{2+} channel \leftrightarrow RyR interaction. Despite a significant larger τ_1 , the time constant of VDI (τ_2) appeared to be similar in both genotypes (Figure 3.26B). As expected, the amount of charge entering the cell by Ca^{2+} influx at 0 mV test pulse, was significantly reduced in RacET (Figure 3.26C).

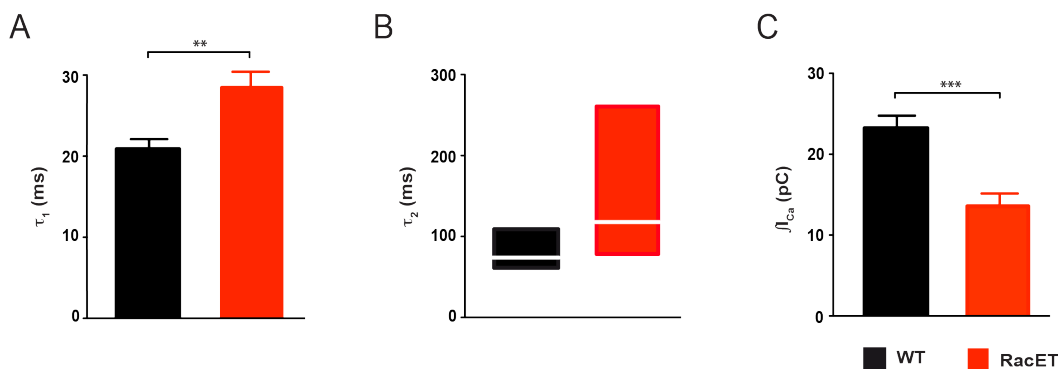


Figure 3.26: The effects of expression of a constitutively active Rac1 on $I_{Ca,L}$ inactivation. Time constant of Ca^{2+} -dependent inactivation (τ_1) (A), time constant of voltage-dependent inactivation (τ_2) (B), and the amount of charge entry ($\int I_{Ca,L}$) (C) at 0 mV. Number of animals and cells are shown in Supplementary table 4. Error bars represent mean \pm SEM.

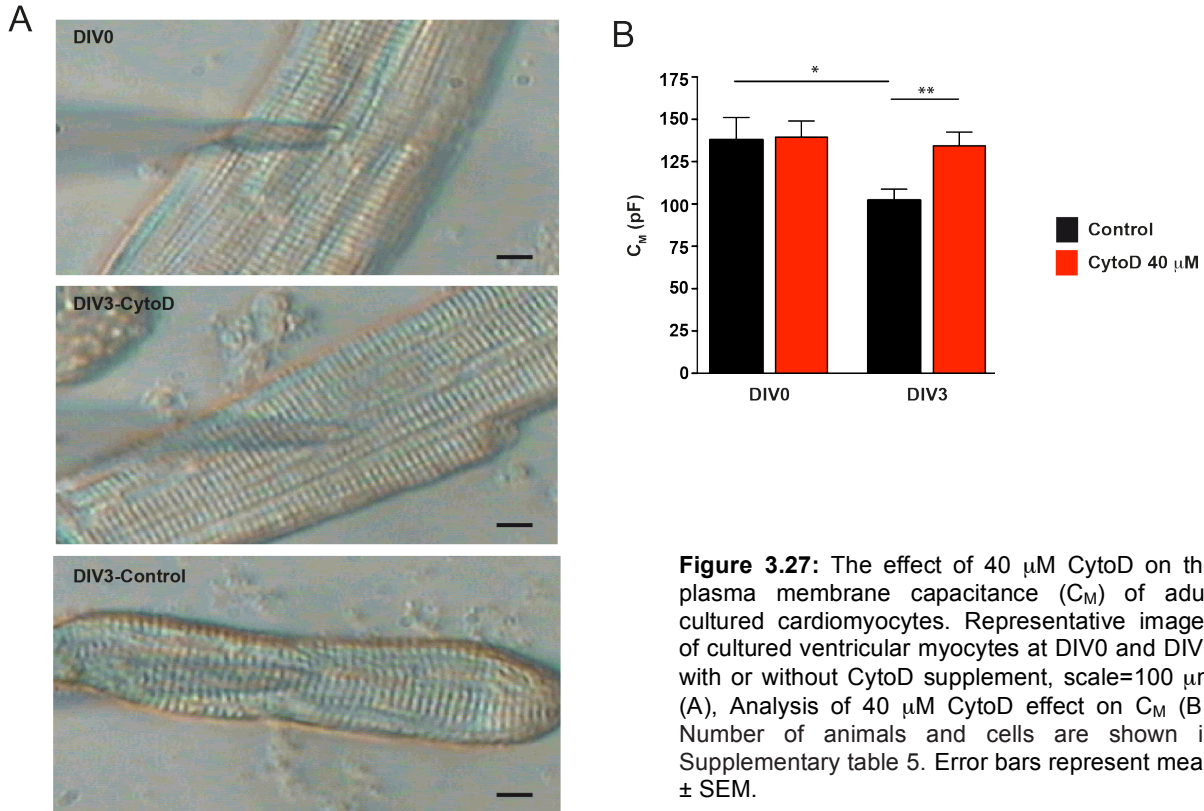
In summary,

1. Expression of a constitutively active Rac1 resulted in the reduction of steady-state $I_{Ca,L}$ in ventricular myocytes.
2. Expression of a constitutively active Rac1 caused higher EC coupling gains.
3. Expression of a constitutively active Rac1 resulted in CDI prolongation.

3.5. The effect of CytoD supplement on AP characteristics of cultured cardiomyocytes

Cytochalasin D (CytoD) is a fungal metabolite that inhibits cytokinesis. Cytoskeletal microfilaments are the targets of CytoD function. In cardiomyocytes, CytoD is supposed to function as a F-actin disruptor^{26,35}. However, some studies suggested a role for CytoD in stabilizing the actin filaments^{41,106}. These studies showed that CytoD could preserve the morphology of cardiomyocytes when used as a culture supplement at 40 μM . T-tubular disarray/loss accompanies short-term culture of adult ventricular myocytes, possibly mediated by cytoskeletal rearrangement⁷⁸ and CytoD could blunt this process. Since t-tubular disarray is a concomitant process to many cardiac diseases such as the development of heart failure, investigations toward the relation between cytoskeleton and t-tubular system would be of particular interest. The aim of this study was to investigate whether CytoD affects the morphology and function of adult cardiomyocytes in culture and whether and how it can be used as a routine supplement in primary culture of cardiomyocytes.

As reported previously⁴¹, we also applied CytoD at the suggested concentration of 40 μM to our optimized primary culture^{78,201} and evaluated its effects on the morphology and function of cultured adult rat ventricular myocytes. Recently our group reported that a 3-day culturing period was associated with significant t-tubular loss in cardiomyocytes⁷⁸. This was also reflected in a significant reduction of C_M (~26%) in control cells at DIV3 compared to DIV0 (Figure 3.27, black). As stated before, C_M is a measure of membrane area. When 40 μM CytoD was used as the culture supplement, C_M was preserved at DIV3 (Figure 3.27B, red). This finding was in agreement with morphological studies of the t-tubular system¹⁹¹ and indicated that a t-tubular loss was absent in the cultures supplemented with 40 μM CytoD. Nevertheless, a detailed study of the cells' plasma membrane system using confocal microscopy revealed significant rearrangements of the t-tubules, referred to as "t-tubular crowding"¹⁹¹.



When analyzing the AP characteristics in naïve cells, I found a significant depolarization of V_R at DIV3 compared to DIV0 (Figure 3.28A, black). In contrast, application of 40 μM CytoD induced V_R hyperpolarization during culturing (Figure 3.28A, red). Three days culturing did not result in significant changes of the AP amplitude regardless of the presence or absence of 40 μM CytoD (Figure 3.28B).

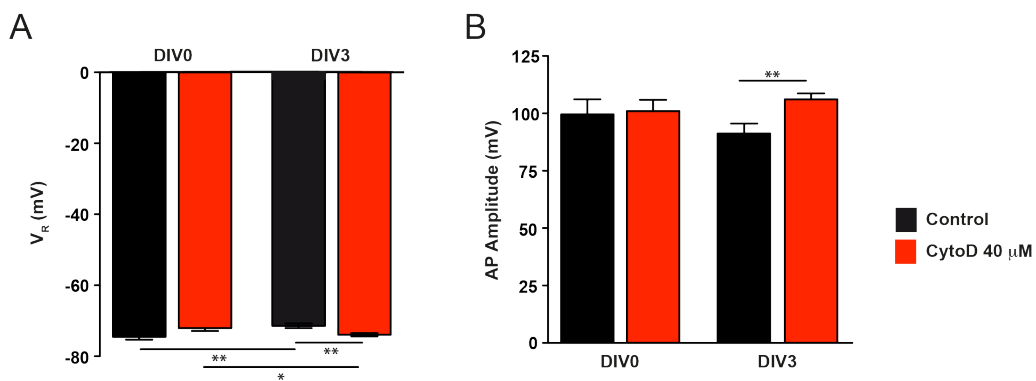


Figure 3.28: The effects of 40 μM CytoD on the electrophysiological characteristics of cultured adult ventricular myocytes. Resting membrane potential (V_R), and action potential amplitude (AP amplitude) (A–B) in cultured cells with or without 40 μM CytoD supplement. Number of animals and cells are shown in Supplementary table 5. Error bars represent mean ± SEM.

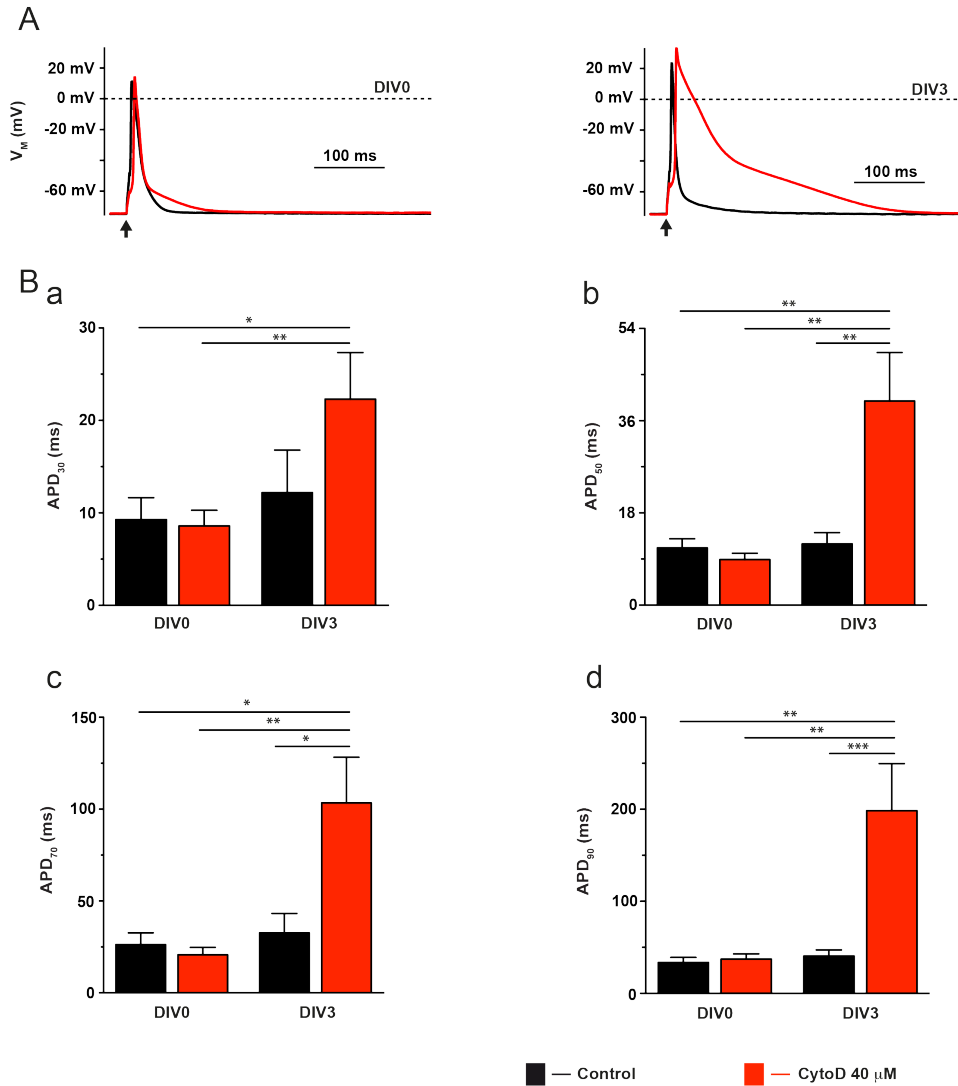


Figure 3.29: The effects of 40 μM CytoD on AP duration of cultured adult ventricular myocytes. AP durations after 30, 50, 70 and 90% repolarization, APD₃₀ (A), APD₅₀ (B), APD₇₀ (C), and APD₉₀ (D), respectively. Number of animals and cells are shown in Supplementary table 5. Error bars represent mean \pm SEM.

Chronic CytoD application at 40 μM , as a culture supplement, resulted in large alterations of the AP duration (Figure 3.29A). While at DIV3 AP duration was not altered in the absence of CytoD (Figure 3.29A, black), CytoD supplement evoked an AP prolongation (Figure 3.29A & B, red). CytoD had a considerable effect on the both early and late repolarization, however the impact on the late phase was more prominent. While at DIV3, APD₃₀ was prolonged \sim 2-fold, a 5-fold increase in APD₉₀ was observed with 40 μM CytoD in the culture medium (Figure 3.29Ba & Bd, red). Therefore, CytoD appeared to have unfavorable effects on the AP properties at this concentration.

We therefore searched for an optimal concentration at which CytoD would preserve both, the morphology and function. We performed dose-response experiments and investigated the amplitude of electrically induced Ca^{2+} transients as the readout of initial screening (dose-response experiment was performed by Dr. Tian). As a result, $0.5 \mu\text{M}$ CytoD appeared to be the optimal CytoD concentration which best preserved DIV0 properties at DIV3¹⁹¹.

Thereafter, we investigated whether additional important functional characteristics of cultured cells were also preserved at this CytoD concentration.

$0.5 \mu\text{M}$ CytoD had beneficial effect on the morphological properties of the cultured cardiomyocytes as indicated by the C_M measurements. While C_M was significantly altered at DIV3 compared to DIV0 (Figure 3.30B, black), $0.5 \mu\text{M}$ CytoD could diminish such changes (Figure 3.30B, white).

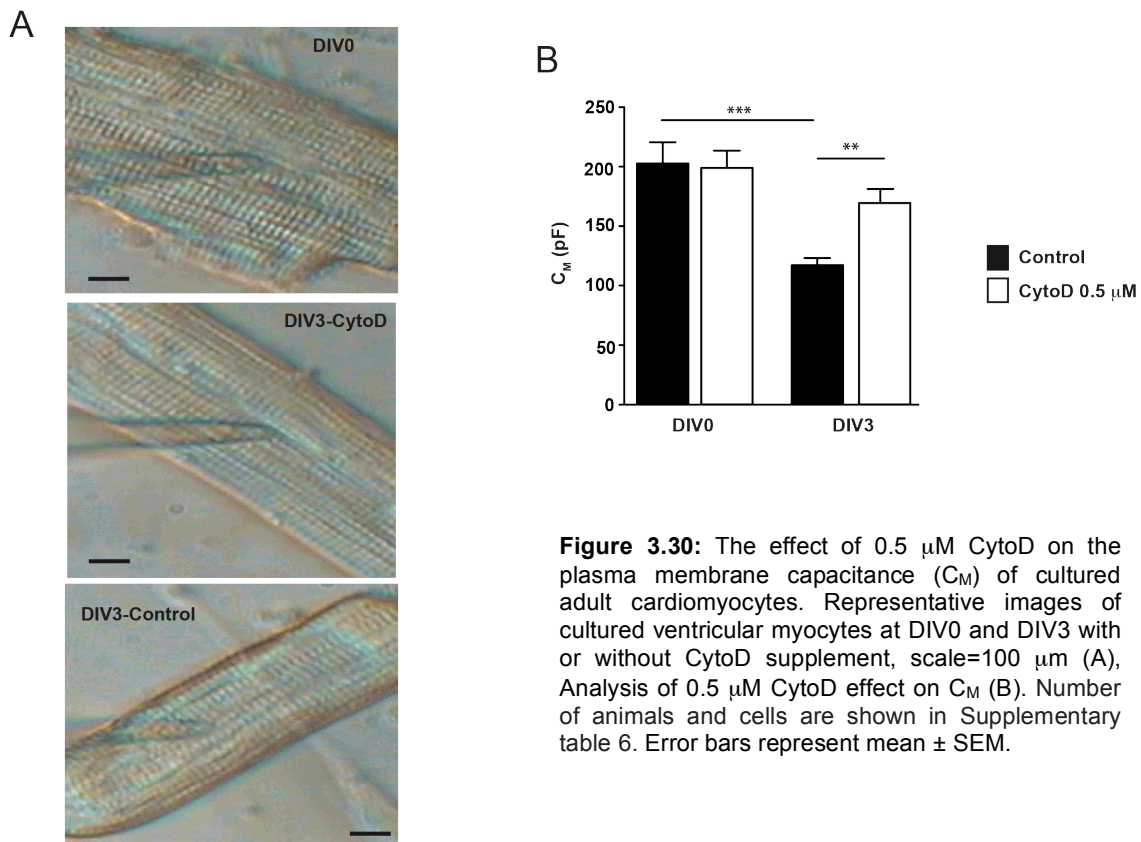


Figure 3.30: The effect of $0.5 \mu\text{M}$ CytoD on the plasma membrane capacitance (C_M) of cultured adult cardiomyocytes. Representative images of cultured ventricular myocytes at DIV0 and DIV3 with or without CytoD supplement, scale= $100 \mu\text{m}$ (A), Analysis of $0.5 \mu\text{M}$ CytoD effect on C_M (B). Number of animals and cells are shown in Supplementary table 6. Error bars represent mean \pm SEM.

0.5 μM CytoD did not display unfavorable effects on V_R (Figure 3.31A). Furthermore, the AP amplitude was well preserved by application of 0.5 μM CytoD supplement (Figure 3.31B). While the AP amplitude showed a 20% decrease at DIV3 in the absence of CytoD, 0.5 μM CytoD in the culture medium suppressed this alteration.

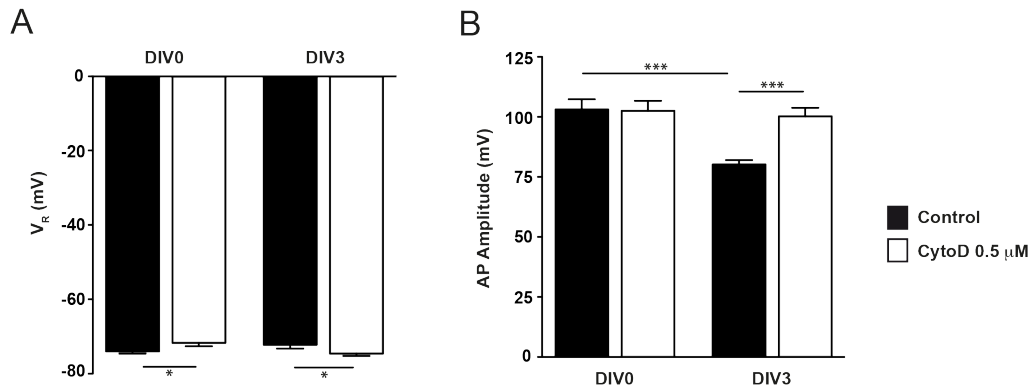


Figure 3.31: The effects of 0.5 μM CytoD on the electrophysiological characteristics of cultured adult ventricular myocytes. Resting membrane potential (V_R) (A), and action potential amplitude (AP amplitude) (B) in cultured cells with or without 0.5 μM CytoD supplement. Number of animals and cells are shown in Supplementary table 6. Error bars represent mean \pm SEM.

In addition to beneficial effects on the morphology, this CytoD concentration did not alter AP durations (Figure 3.32A & B).

In summary,

1. Application of 40 μM CytoD in culture medium resulted in the preservation of C_M at DIV3, but alteration of electrophysiological properties such as more hyperpolarized V_R and AP prolongation.
2. Application of 0.5 μM CytoD in culture medium resulted in the preservation of both C_M and electrophysiological properties including V_R and AP characteristics.

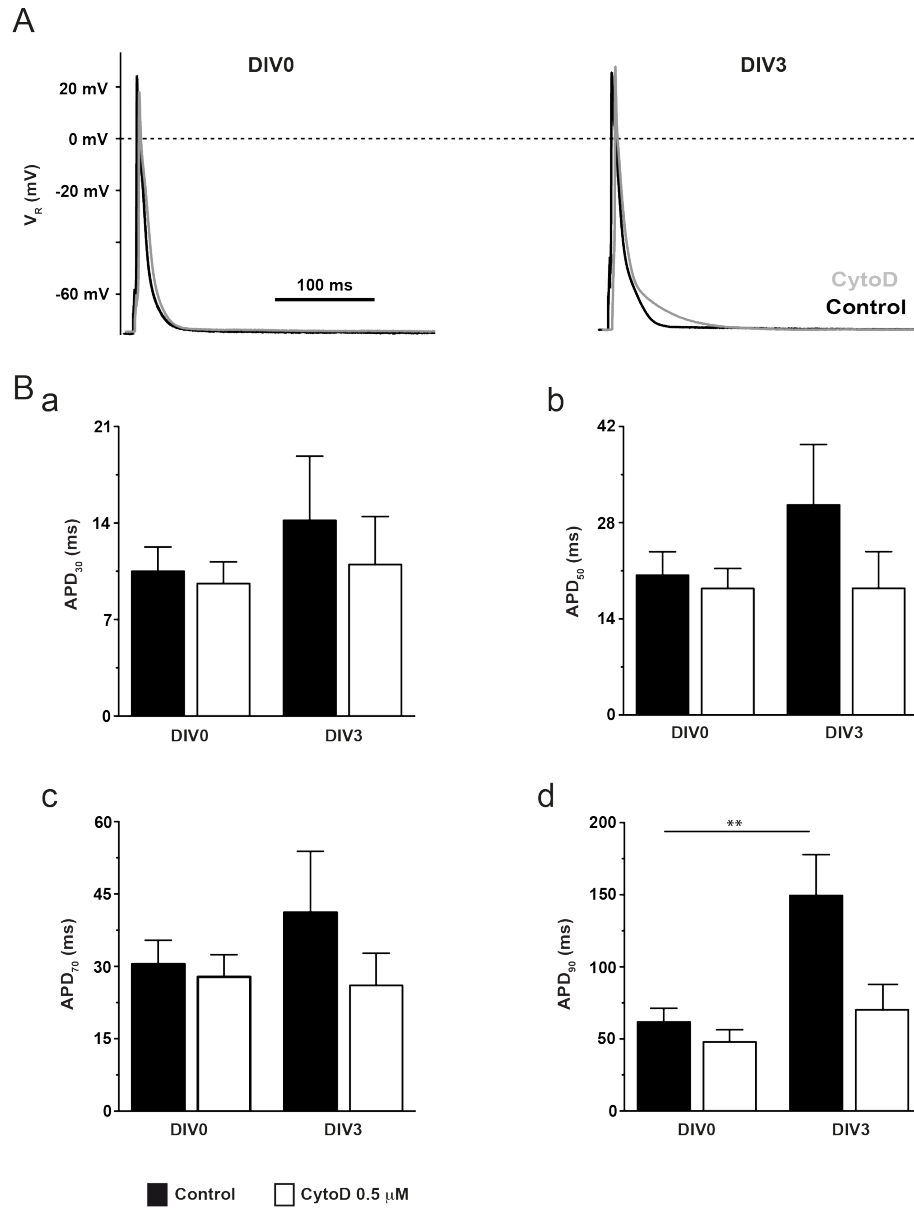


Figure 3.32: The effects of 0.5 μ M CytoD on AP duration of cultured adult ventricular myocytes. AP durations at 30, 50, 70 and 90% repolarization, APD₃₀ (A), APD₅₀ (B), APD₇₀ (C), and APD₉₀ (D), respectively. Number of animals and cells are shown in Supplementary table 6. Error bars represent mean \pm SEM.

4. Discussion

4.1. Heart-specific inducible $G\alpha_q/G\alpha_{11}$ knockout

Different hormones and neurotransmitters regulate cardiomyocyte's function by activation of intracellular signaling cascades ⁹⁸. These signaling molecules mainly function to maintain or to modulate cellular homeostasis ⁹⁸. However, chronic unbalanced stimulation leads to pathological responses. In the first chapter of my thesis, I aimed to investigate the possible contribution of $G\alpha_{q/11}$ signaling to the physiology of cardiac myocytes. To study the function of a protein in cardiac cells, different experimental tools can be employed. In earlier studies, primary culture of cardiac myocytes or "myocyte like" cell lines were the most common approaches to accomplish this aim ¹³⁴. However many physiological aspects such as paracrine interactions and cellular growth as a chronic response could not be investigated in these two-dimensional environments (*in vitro*). Inhibition of a protein was the classical approach but often accomplished by blockers lacking proper sensitivity and specificity. Thus, protein down-regulation by gene knockout or siRNA have also been employed on the cellular level. The generation of transgenic animals was a major step forward since it enabled such investigations including cellular signaling. To generate transgenic animals, different techniques have been developed and employed over the last decades. In the cardiac research field, the power to target gene manipulations to the heart was always a desire. The creation of transgenic mice expressing Cre recombinase under the control of the α -MHC promoter fulfilled this request ⁷. The further improvements of the Cre/LoxP system using Cre-ER, allowed defined genetic alterations in a temporal and tissue-specific manner (Figure 4.1). The most common Cre mice (MerCreMer) in cardiac research field was introduced by Sohal and co-workers ¹⁸². However these Cre mice showed cardiac dysfunction such as a decreased fractional shortening and increased end diastolic diameter ^{104,134}. Thus, recent publications emphasized the necessity for proper controls when using the Cre/LoxP technology due to these system-inherent deficiencies ^{104,134,172}.

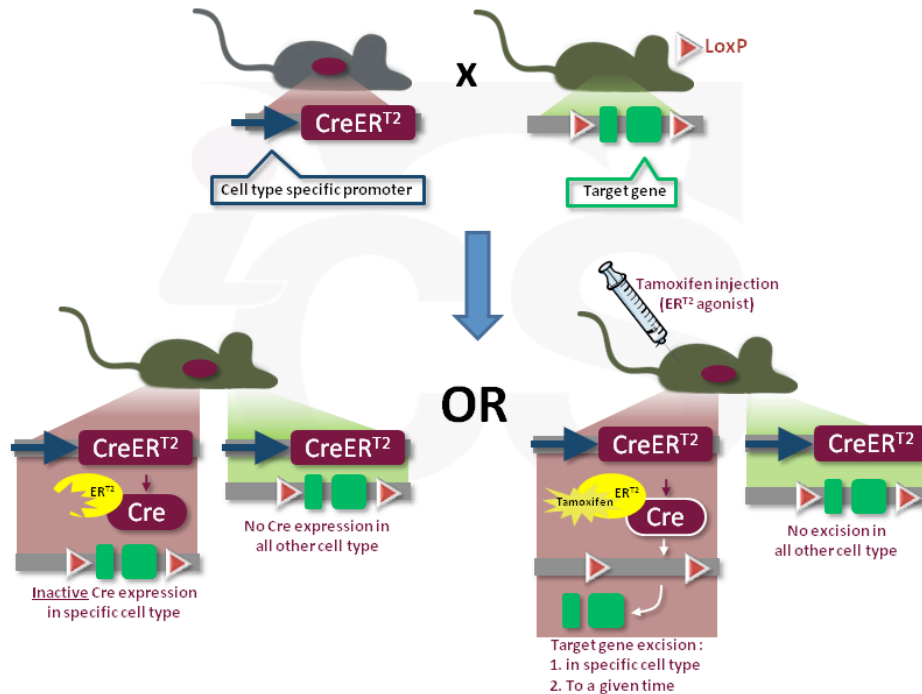


Figure 4.1: Cre-ER/LoxP system. Cre-ER is under the control of a cell type-specific promoter. The Cre mouse is crossbred to a mouse carrying the LoxP flanked-target gene. The resulting offspring contains both, the tissue-specific promoter-Cre-ER and LoxP flanked-target gene. Cre is only expressed in those cell types in which the promoter is active. However Cre is inactive unless tamoxifen (ER agonist) is injected to the mice. Tamoxifen injection activates Cre recombinase which leads to the excision of the target gene (i) in a specific cell type and (ii) to a given time. Taken from www.ics-mci.fr

In this study, we used a novel Cre mouse¹⁸⁷ to accomplish the heart-specific $G\alpha_q$ KO. For temporal control of Cre recombinase activation, we employed tamoxifen injection (50 mg/kg body weight, 5 consecutive days). Western blot analysis confirmed the functionality of the Cre/LoxP system as the expression of the $G\alpha_q$ protein diminished over the time course of 25 days following the 1st tamoxifen injection¹⁴³. The literature describes a variety of tamoxifen concentrations for Cre activation. Clearly, the lower the concentration, the lesser unwanted side effects of tamoxifen are to be expected. Sohal and co-workers typically used low tamoxifen doses (20 mg/kg body weight) for long time periods¹⁸² and revealed this to be insufficient for gene knockout later¹⁰⁴. Considering the fact that 50% of the initial tamoxifen concentration is expelled from the blood within around 5 days ($t_{1/2}$ =5 days) (Figure 3.4)¹¹⁶ we assume that at the end of our waiting period of at least 28 days, the tamoxifen concentration is too low to cause any effects. Nevertheless, this was addressed in a thorough experimental series.

4.1.1. The impact of tamoxifen treatment and Cre recombinase expression

As stated before, a novel Cre mouse was used to knock-down $G\alpha_q$ KO. $G\alpha_q$ KO effects have been evaluated on the whole heart as well as on the cellular level. On the cellular level, we decided to study two largely integrative cellular phenomena for isolated ventricular myocytes i.e. APs and electrically induced global Ca^{2+} transients. The results of the electrophysiological experiments will be discussed here.

Analysis of the AP parameters revealed significant alterations of the AP amplitude and the AP duration in cardiomyocytes from $G\alpha_q$ KO mice (Fig. 3.1). For my experiments I initially followed the classic approach, i.e. I compared tamoxifen-injected animals with those not injected with tamoxifen. However, when we carefully considered such an approach we wondered how valid this might have been. The KO group was different from control in two aspects; (i) the desired cardiomyocyte-specific $G\alpha_q$ KO and (ii) the unavoidable tamoxifen treatment. Furthermore since we were the first group employing this novel Cre mouse line, inherent genomic effects of such a system had to be evaluated. Thus, we were wondering whether these two factors i.e. (i) tamoxifen and (ii) Cre expression had any inherent effects and whether these could interfere with $G\alpha_q$ -KO results.

Unexpectedly, in those studies I found substantial alterations of the AP characteristics (Figure 3.5 and 3.6). In cardiomyocytes, the acute effects of tamoxifen are quite well known^{57,82}. Following acute tamoxifen (3 μ M) application, He and co-workers found an AP prolongation and significant reduction of K^+ currents (I_{to} , I_{sus} , I_{K1}) in rat ventricular myocytes. In addition to the repolarization phase of AP, acute tamoxifen application also decreased the maximal rate of depolarization and V_R . Moreover, the fast Na^+ current was depressed in ventricular myocytes exposed to 3 μ M tamoxifen⁸². In contrast, in rabbit ventricular myocytes Liu and colleagues reported unaltered AP, I_{to} and I_{K1} following acute application of tamoxifen (3.3 μ M). However, they observed a significant reduction of I_{Ca} at tamoxifen concentrations greater than 1 μ M and almost complete inhibition at 10 μ M¹¹³. Moreover, the major tamoxifen metabolite i.e. 4-

hydroxytamoxifen (1 μM) diminished the density of I_{to} , I_{Kur} and I_{K1} when applied acutely to mouse ventricular myocytes⁵⁶. In my experiments when injected into $G\alpha_{11}$ KO mice, tamoxifen caused AP prolongation and a substantial reduction of I_{toc} (Figure 3.5 and 3.6). Chronic tamoxifen treatment was also reported to modulate various K^+ currents in mouse ventricular myocytes⁵⁷. K^+ currents contributing to both the early and the late repolarization of the AP (I_{to} , I_{Kur} , I_{ss} , I_{K1}), were increased following 60 days constant tamoxifen administration. This effect was genomic and resulted from the alterations of K^+ channels' gene expression i.e. higher Kv4.3 (I_{to}), Kv1.5 (I_{Kur}), Kv2.1 (I_{ss}) and Kir2.1 (I_{K1})⁵⁷. However 60 days tamoxifen treatment does not reflect the usual tamoxifen injection regime for inducible KO systems, including our own. The AP alterations depicted here resulted from a brief period of tamoxifen administration (5-day injection) followed by more than 4 weeks without tamoxifen before recording started. Thus, we assume that the tamoxifen concentration was already very low after this time period (see Figure 3.4). Moreover, the tamoxifen treatment also caused opposite effects depending on the particular genetic background (e.g. APDs in Figure 3.5). When it was injected to wildtype mice ($Gq^{\text{wt}}G11^{\text{wt}}\text{Cre}^-$), the AP and I_{toc} density remained unchanged (Figure 3.5, brown vs. grey). In $G\alpha_{11}$ KO it caused alterations that were similar to the reported effects of an acute tamoxifen application rather than a chronic one, i.e. AP prolongation (Figure 3.5, violet vs. green) and I_{toc} reduction (Figure 3.6, violet vs. green).

Although tamoxifen treatment altered the electrophysiological properties of cardiac cells, its application is mandatory to induce $G\alpha_q$ KO when using the Cre/LoxP system. However other methods including primary culture of cardiomyocytes have been majorly advanced^{78,201}. Nevertheless, transgenic animals enable us to study protein functions in the context of the whole animal. Especially, research on the cardiac pathology benefitted from these improvements since they can often not be modeled in culture¹³⁴. Raloxifen was also proposed as an alternative for tamoxifen in inducible Cre/LoxP systems, however raloxifen had to be applied three times longer than tamoxifen to achieve similar Cre activity¹⁰⁴. Thus we decided to use tamoxifen for the activation of the Cre recombinase. Tamoxifen was administered to every group including our controls. Instead we used another determinant for gene KO.

Today, the Cre/LoxP system has been extended to perform tissue-, sometimes even cell type-specific gene excision. To generate a cardiac-specific gene knockout, the Cre expression was restricted under the control of a cardiomyocyte-specific promoter, α -MHC. However, high levels of α -MHC mediated Cre expression have been reported to cause a lethal cardiomyopathy between 8 and 12 months of age¹³⁴. Moreover, Koitabashi and co-workers found a severe transient dilated cardiomyopathy in the tamoxifen-inducible MerCreMer* mouse line even without loxP transgenes¹⁰⁴. Despite the great alterations of cardiac function in the MerCreMer mice, in our novel Cre mouse line the cardiomyocyte characteristics including electrophysiology were not altered greatly (Figure 3.11 and 3.12), thus eliminating the need for additional controls.

4.1.2. The optimized genetic combinations to study $G\alpha_q$ knockout

In studies using tamoxifen inducible Cre/LoxP system, controls are normally chosen from the same genetic backgrounds but not injected with tamoxifen (Figure 3.1 and 3.3). However, we believe that it is necessary to include tamoxifen injection in control groups as well for any possible genomic interventions. Therefore, we decided not to follow the conventional approach of comparing animals in which KO was primarily induced by tamoxifen injection (Tamoxifen vs. miglyol/-). But instead we employed a different molecular determinant (Cre recombinase) for the induction of KO while maintaining the tamoxifen injections in all genotypes. We suggested two sets of genetic combinations that could provide us with the required transgenic animals for investigating $G\alpha_q$ and $G\alpha_{11}$ function (Table 3.2 and 3.3).

Both approaches followed different strategies to knockout $G\alpha_q$. The gene excision could either be dependent on the presence of Cre recombinase (Table 3.3) or on the presence of the LoxP sites in the *gnaq* gene (Table 3.2), while always maintaining the tamoxifen injections. We chose the genetic combinations introduced in table 3.3 in which Cre expression is the molecular determinant for $G\alpha_q$ KO. While generation of

* Cre flanked by two mutant estrogen receptor ligand-binding domains

animals described in table 3.2 would have required breeding of 4 separate mouse lines, using Cre expression as the determinant for the KO required only breeding of 2 separate mouse lines and most importantly allowed us to utilize litter-mates (black vs. blue and red vs. green, Table 3.3). Moreover, breeding of 4 separate mouse lines would increase the genetic distance which might result in unfavorable genetic differences.

Using the genetic combinations shown in table 3.3, we generated 4 optimized genotypes to address our initial question about the physiological importance of basic $G_{\alpha_q/11}$ signaling (Figure 3.13 and 3.14).

4.1.3. Physiological relevance of G_{α_q} in ventricular myocytes

The pathological role of $G_{\alpha_q/11}$ signaling has been extensively studied in the heart. These studies benefitted from various kinds of G_{α_q} gene knock-out and knock-in^{10,44,163,211}. To date, there is a general agreement about the contribution of $G_{\alpha_q/11}$ signaling to the development of hypertrophy; $G_{\alpha_q}/G_{\alpha_{11}}$ KO can decrease a hypertrophic response^{10,211}. In general, the hypertrophic responses are accompanied not only by structural and electrophysiological remodeling of the cardiac tissue but also by structural remodeling of individual myocytes. In electrophysiological experiments, the plasma membrane structure of the myocytes can be assessed by determining the plasma membrane capacitance. In $G_{\alpha_q}/G_{\alpha_{11}}$ KO, the substantial reduction of C_M (Figure 3.13A, red) might suggest alterations of gene expression and/or the t-tubular disarray. Although we did not investigate this further, $G_{\alpha_q/11}$ signaling pathway is known to be involved in cell growth responses⁸³.

Another finding was unexpected increase of C_M in G_{α_q} KO (Figure 3.13A, blue). While deletion of both G_{α_q} and $G_{\alpha_{11}}$ caused substantial reduction of membrane capacitance, G_{α_q} single KO showed opposite effect. These results suggest that the relationship between G_{α_q} and $G_{\alpha_{11}}$ is not only compensatory behavior but they might have much more complex interrelations.

Different intracellular signaling cascades modulate the expression and regulation of cardiac ion channels. $I_{K(ATP)}$ and $I_{Ca,L}$ for instance are known to be regulated by G-protein-coupled signaling cascades¹⁸⁵. The PKA-mediated phosphorylation of Cav1.2 downstream of $G\alpha_s$ activation regulates the channel function. Since the AP is the product of multiple ionic currents, its properties are modulated by many intracellular signaling cascades. The effect of $G\alpha_q$ signaling on the cardiac AP is not very well studied. While $G\alpha_q$ overexpression resulted in markedly prolonged APs¹³¹, the knockout of this protein diminished this effect (Figure 3.13Db, blue). Thus, $G\alpha_q$ signaling might be important in the regulation of the AP properties and more precisely its underlying repolarizing currents such as different I_K . Wagner and his co-workers showed that $G\alpha_{11}$ signaling has a tonic inhibitory effect on I_{to} which results from alterations in the expression of the Kv4.2 protein²⁰². Moreover, calcineurin/NFAT signaling which is an important regulator of I_{to} , is activated downstream to $G\alpha_{q/11}$ signaling^{83,146,153}.

The membrane potential results from different concentrations and conductances of ions across the plasma membrane. In cardiac cells I_{K1} contributes to the physiological resting potential¹⁸⁸. The changes of V_R seen in cardiomyocytes from $G\alpha_q$ KO mice might be due to alterations of the inwardly rectifying K^+ current (I_{K1}) either by changing its expression or function. Regulation of I_{K1} by $G\alpha_q$ was suggested previously^{131,193}.

In addition to $G\alpha_q$, my experiments (Figure 3.5 and 3.6) strongly suggest a role of $G\alpha_{11}$ in regulating K^+ currents. In $G\alpha_{11}$ KO animals, I observed a large reduction of the AP duration and a concomitant augmentation of I_{toc} .

How do $G\alpha_q$ and $G\alpha_{11}$ proteins mediate changes in gene expression resulting in the alterations of electrophysiological characteristics? We believe that the changes were not induced by the proteins *per se*, but instead, our results strongly indicate the importance of a constant, possibly low-level stimulation of the upstream G-protein coupled receptors with agonists such as endothelin-1 or angiotensin-II²⁷⁰. When stimulated chronically at high levels, G-proteins contribute to the development of cardiac diseases and associated changes in gene expression^{52,74}. In contrast, with sustained stimulation

at a much lower hormone level, $G\alpha_q$ and $G\alpha_{11}$ -coupled signaling pathways appear to be important in the maintenance of the myocyte's homeostasis.

We thus conclude that both $G\alpha_q$ and $G\alpha_{11}$ are instrumental to the physiological properties of cardiac myocytes by mediating the continuance of a basic rate of gene expression.

Further studies on the effects of $G\alpha_{q/11}$ signaling in gene expression and regulation of K^+ channels that contribute to the cardiac AP would answer a lot of remaining questions. Particularly, the regulatory function of $G\alpha_q$ and/or $G\alpha_{11}$ on I_{to} would help to understand the alterations of early repolarization. Moreover, detailed studies on the downstream molecules of $G\alpha_{q/11}$ signaling such as PLC_β , PIP_2 , DAG and IP_3 are necessary to better understand the physiological function of this signaling pathway.

4.2. The relationship between aldosterone and $G\alpha_{q/11}$ signaling in cardiac pathology

The renin-angiotensin-aldosterone system's (RAAS) primary function is to maintain homeostasis in response to stress such as a drop in blood pressure⁷². Activation of RAAS results in retention of the intravascular volume and thus blood pressure. In contrast to its protective effects in acute stress responses, chronic stimulation of RAAS leads to deleterious effects on the cardiovascular system such as sustained hypertension. Hypertension in turn increases the cardiac workload which leads to the development of hypertrophy and heart failure⁸⁷. The role of aldosterone in hypertension-induced cardiac injury is well established. However, recent findings showed that aldosterone increases the risk of cardiac diseases independent of hypertension²¹². Various experimental approaches were employed to investigate the direct effect of aldosterone on the heart as well as single cardiomyocytes^{63,147,155}. On the cellular level, one of the major goals was to find the second messengers mediating the aldosterone function. In cardiomyocytes, $G\alpha_{q/11}$ signaling is one of the intracellular cascades that mediates the effects of many hormonal agonists. The genomic effects of $G\alpha_{q/11}$ signaling are known to be involved to the development of cardiac diseases such as hypertrophy and heart failure⁸³. While both, aldosterone excess and high chronic stimulation of $G\alpha_{q/11}$ signaling, result in pathological responses of the heart, we were wondering whether they are somehow connected. Therefore, we induced hyperaldosteronism (see 2.4) in our 4 optimized genotypes (Table 3.3) and studied the possible contribution of the $G\alpha_{q/11}$ signaling in the aldosterone-mediated cardiac effects. In vivo studies showed significantly larger LVID* in aldosterone-treated $G\alpha_q/G\alpha_{11}$ DKO at both systole and diastole. Moreover, the LV mass† and volume appeared to be significantly higher in these animals (studies on the heart were done by Ms. Kathrina Wiesen). Single cell measurements showed substantial alterations of AP characteristics and Ca^{2+} handling in both wildtype and $G\alpha_q/G\alpha_{11}$ DKO mice following HA. In particular,

* Left ventricular inner diameter

† left ventricular mass

HA caused significant reduction of the AP duration in wildtype mice, while the AP duration was unexpectedly increased when both, $G\alpha_q$ and $G\alpha_{11}$ were knocked out (Figure 3.17). In the following I will discuss the results of my electrophysiological measurements in ventricular myocytes from wildtype and transgenic mice following HA.

4.2.1. The effect of hyperaldosteronism on C_M and V_R

Patients with primary hyperaldosteronism, a condition caused by overproduction of aldosterone in the adrenal gland, develop left ventricular hypertrophy²¹². As explained before, the hypertrophic response can also be studied by evaluating the structural remodeling of cardiac cells. I observed a significant C_M reduction in $G\alpha_{11}$ - and $G\alpha_q/G\alpha_{11}$ KO following HA, which might suggest an interference of $G\alpha_{q/11}$ signaling with HA-mediated genomic effects (Fig. 3.15A).

V_R was decreased in wildtype mice following HA (Figure 3.15B, black). Dartsch and co-workers found a significant down-regulation of mRNA levels for Kir2.1 and Kir2.3 following a 4-week aldosterone administration using osmotic mini-pumps (1 $\mu\text{g/h}$)⁴⁶. Thus, the more hyperpolarized V_R in wildtype mice following HA (Figure 3.15B black) might have resulted from the altered expression and/or current properties of K_1 channels. Interestingly, the knockout of $G\alpha_q$ and/or $G\alpha_{11}$ diminished the aldosterone effect on V_R (Figure 3.15B, black). This result might be another evidence for the contribution of $G\alpha_{q/11}$ signaling to HA-mediated genomic effects.

4.2.2. The role of $G\alpha_{q/11}$ signaling in HA-induced AP alterations

HA-mediated cellular electrophysiological remodeling has been reported in atria¹⁵⁸ and ventricles¹⁴² of small rodents. I also observed HA-mediated alterations of AP characteristics in mouse ventricular myocytes (Figure 3.15 and 3.17, black). In HA, AP amplitudes were markedly increased in ventricular myocytes from wildtype mice (Figure 3.15C, black). Boixel and co-workers found a substantial increase of I_{Na} in mouse

ventricular myocytes incubated with 1 μ M aldosterone for 24 h. However, they did not find any alterations in the protein level of Nav1.5 ²⁹. We suggest that the larger AP amplitudes in wildtype mice following HA, are due to alterations in gene expression or function of the Na⁺ channels. Interestingly, G α_{11} KO or G α_q /G α_{11} DKO diminished the HA evoked changes of the AP amplitude (Figure 3.15C, green & red).

While Benitah and co-workers showed AP prolongation in aldosterone-treated ventricular myocytes ¹⁸, I found a substantial reduction of AP duration in the ventricular cells from wildtype mice (Figure 3.17, black). However, this controversy might be to a large extent due to different experimental settings. While in the former study they incubated rat ventricular myocytes with aldosterone for 48 h ¹⁸, we used chronic (42 days) HA in mice (see 2.4). We believe that 42 days are long enough for proliferating (genomic) effects of aldosterone. In another study by Ouvrard-Pascaud and co-workers, HA was mimicked in a mouse model by overexpression of the hMR* in the heart. They observed substantial prolongation of the repolarization phase of the AP in ventricular myocytes overexpressing hMR ¹⁴². Although our results were not in agreement with this AP prolongation, they might suggest different genomic effects induced through other intracellular signaling pathways.

Aldosterone has been shown to modulate the expression and function of various cardiac ion channels ^{18,19,46,147}, which might contribute to the AP alterations. Two important repolarizing currents, I_{to} and I_{Ca,L}, were shown to be altered by aldosterone ^{18,19,147}. I_{Ca,L} up-regulation and AP prolongation were found in ventricular myocytes from transgenic mice with renal salt loss resulting in HA ¹⁴⁷. I_{to} down-regulation has been attributed to the genomic effects of aldosterone in cardiac cells ¹⁸. However, my results of I_{toC} measurements did not reproduce those findings; they were in good agreement with alterations of the early phase of AP repolarization (Figure 3.18).

Unexpectedly, deletion of G α_q and G α_{11} proteins in the heart resulted in AP prolongation and I_{toC} down-regulation following HA (Figure 3.16 and 3.17, red). Both effects were opposite to the aldosterone-mediated effects on AP and I_{toC} seen in

* human mineralocorticoid receptor

wildtype mice. Considering these results, we suggest that $G_{\alpha_{q/11}}$ signaling might contribute to HA-mediated genomic effects in cardiomyocytes.

There is a growing body of evidence showing that the pathological effects of aldosterone on the heart are indeed independent of changes in blood pressure ²¹². Although, MR and 11 β -hydroxysteroid dehydrogenase have been characterized in cardiomyocytes ^{100,114,179}, the cellular mediators of the aldosterone effects remained unexplored. In the present study, the aldosterone-induced alterations of AP and I_{toc} were described. However, further experiments are crucial to resolve the underlying reasons for this AP alterations such as I_{Na} , $I_{Ca,L}$ and I_K measurements. Moreover, additional analysis of gene expression of ion channels would help to better interpret the results. Furthermore, the intracellular second messengers mediating these aldosterone effects should be explored. Our findings support the likelihood for contribution of $G_{\alpha_{q/11}}$ signaling in the aldosterone-induced electrophysiological remodeling of cardiomyocytes.

4.3. Mutation in the IQ motif of Cav1.2 and the impact on EC coupling gain

The contraction of cardiomyocytes is majorly dependent on Ca^{2+} influx through voltage-gated Ca^{2+} channels²³. These channels are regulated by different mechanisms among which CDI and VDI are well studied^{75,97,109}. These regulatory mechanisms require the contribution of several molecules that are mainly associated with Cav1.2^{15,45}. Among these molecules, Calmodulin (CaM) is permanently bound to Cav1.2 and functions as a Ca^{2+} sensor^{135,149}. Ca^{2+} -saturated CaM contributes to the fast CDI⁷⁷. It has been shown that the IQ sequence in the C-terminal cytoplasmic tail of Cav1.2 (amino acids 1624-1635) is the major binding site for CaM^{77,148}. Mutations in the IQ motif inhibited CaM binding to the Cav1.2, thus diminished CDI²²⁸. Amino acid exchange in the IQ motif (Ile-1624 with Glu; I/E mutation) resulted in 100-fold reduction of the CaM binding affinity and subsequent alteration of CDI in the *Xenopus* oocyte expression system²²⁸. However, the impact of mutations of the IQ motif on the Cav1.2 function in *in vivo* situations remained to be explored.

4.3.1. Generation of the murine cardiac Cav1.2^{I1624E}

To study the relationship between CaM and IQ motif and the possible role in the regulation of Cav1.2, the I/E mutation was primarily generated in a heterologous expression system (*Xenopus* oocyte) and resulted in the alteration of CDI²²⁸. But what happens if this mutation is in the cardiac cells and the *in vivo* situation?

To address this question, Ile-1624 was exchanged with Glu in the murine cardiac Cav1.2¹⁵². Homozygous mice (Cav1.2^{I1624E/I1624E}) were not viable. Therefore, Heterozygous Cav1.2^{+/I1624E} mice were crossbred with Cav1.2^{flox/flox} and MerCreMer^{176,182} to generate the basic genotype (Cav1.2^{flox/I1624E} x MerCreMer) to study the I/E mutation (see 2.3.2). The excision of the floxed gene (Cav1.2^{-/I1624E}) was induced by daily injections of tamoxifen at 4 consecutive days. Although this approach was successful, the I/E mice had a reduced life span and died within 3 weeks after the first tamoxifen injection (Figure 4.2).

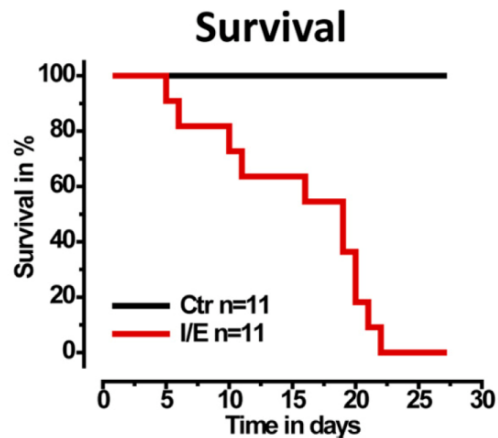


Figure 4.2: Survival curve of I/E and Ctr mice. T=0 reflects the start of tamoxifen injection. The survival rate of I/E mice reduced to 0% within 3 weeks after tamoxifen injection. Taken from Poomvanicha et al, 2011¹³⁴

Different morphological and functional properties of the whole heart as well as single cardiomyocytes were assessed. The hearts from I/E mice showed markedly reduced fractional shortening and developed a phenotype similar to dilated cardiomyopathy¹⁵². Single cell measurements displayed a significant reduction of $I_{Ca,L}$ in I/E mice (Figure 3.20). Despite $I_{Ca,L}$ attenuation, global Ca^{2+} transients and cellular contractility remained unchanged²⁷. To find out the reasons for this contradiction, I studied the coupling efficiency of $I_{Ca,L}$ and Ca^{2+} release in single cardiomyocytes and revealed an enhanced EC coupling gain in I/E mice (Figure 3.22C).

4.3.2. The impact of I/E mutation on the $I_{Ca,L}$

The IQ motif is supposed to contribute in Cav1.2 inactivation, but also resulted in a significant reduced $I_{Ca,L}$ density (Figure 3.20). Since CaM binding to Cav1.2 is disrupted by the I/E mutation, we assume that this interference might reduce trafficking of the channel to the membrane during biosynthesis and thus diminishes $I_{Ca,L}$, as shown for cultured neurons²⁰³. Western blot analysis showed significantly lower Cav1.2 protein in the hearts of I/E mice²⁷. Thus I_{Ca} down-regulation was not only caused by a change in channel kinetic *per se*, but also by reduced expression of the Cav1.2^{I1624E}.

Cardiac dysfunction results in various adaptive responses such as the stimulation of the sympathetic or the renin-angiotensin system leading to the activation of several different intracellular signaling molecules including CaMK-II⁸³. A recent publication suggested a suppressive role for CaMK-II on cardiac Cav1.2 gene transcription¹⁶⁴. CaMK-II phosphorylation was increased in the myocytes carrying I/E mutation²⁷, which might itself regulate the transcription of Cav1.2 gene, leading to $I_{Ca,L}$ down-regulation.

4.3.3. The impact of the I/E mutation on global Ca^{2+} transients

Although $I_{Ca,L}$ is the primary trigger for SR Ca^{2+} release, it is not the only determinant of the EC Coupling gain. In line with this, the *I1624E* mutation enhanced the gain of Ca^{2+} release despite a $I_{Ca,L}$ reduction. This finding strongly suggests an altered EC coupling (Figure 3.22C). EC coupling is mainly dependent on the amplitude and kinetics of the Ca^{2+} signal in the dyadic space¹⁰⁷. Besides the Cav1.2 channel, the RyR2 and the NCX all contribute to the Ca^{2+} signal in this microdomain. While there is no direct data on the $[Ca^{2+}]_i$ in these domains, a recent paper by Assai and colleagues estimated that during EC coupling, Ca^{2+} in the dyadic space might increase to 10-15 μ M within milliseconds³. Nevertheless, our results from simultaneous $I_{Ca,L}$ and Ca^{2+} transient measurements suggested significant alterations of signaling in this coupling space (Figure 3.22A).

My results showed significantly higher EC coupling gain in I/E mice (Figure 3.22C). What could be the reason for such a high gain in these cardiomyocytes? Presumably the inadequate cardiac performance in I/E mice stimulates the neuroendocrine system. β -AR stimulation is one of the major mechanisms to initially compensate such cardiac dysfunctions. However, high-level chronic stimulation causes cardiac insults and results in cardiac diseases. Activation of PKA downstream to β -AR initiates a wave of phosphorylation including the RyR2. PKA was shown to phosphorylate Ser2809^{214,215} which augments the RyR2 function via two mechanisms; (i) increase in the open probability of the channel and (ii) decrease in the binding affinity of a channel inhibitor, calstabin2. Furthermore, Marks and co-workers showed that phosphorylation of RYR2 by PKA results in the dissociation of FKBP12.6 from the channel¹²⁴. This uncoupling in

turn enhances the single-channel open probability. Valdivia et al. showed that PKA phosphorylation increases the RyR2 sensitivity to Ca^{2+} ¹⁹⁷. Thus, the phosphorylation enhances Ca^{2+} release activity of the channel in response to a rapid increase of local Ca^{2+} , as may be expected near L-type Ca^{2+} channels ²⁰⁶. Therefore, neurohormonal stimulation increases the RyR2 activity resulting in an enhanced EC coupling gain.

CaMK-II is another regulatory protein of RyR2. CaMK-II phosphorylation modulates the channel gating in a way that a given Ca^{2+} transient can be induced by smaller $I_{\text{Ca,L}}$ influx ^{111,224}. CaMK-II can be activated downstream to angiotensin/ $\text{G}\alpha_q$ signaling, which in turn results in the phosphorylation of RyR2 and the sensitization of EC coupling ²⁰⁶. CaMK-II phosphorylation increased in the myocytes carrying I/E mutation ²⁷.

Moreover, Blaich and co-workers showed a substantial reduction of NCX activity in cardiomyocytes from I/E mice ²⁷, which might in turn increase dyadic Ca^{2+} signals and EC coupling gain.

In conclusion, we suggest that the I/E mutation leads to cardiac dysfunction by reducing $I_{\text{Ca,L}}$ and subsequent intracellular Ca^{2+} transients. This cardiac dysfunction initiates a series of compensatory responses including neurohormonal stimulation to maintain cardiac function. Neurohormonal stimulation increases the EC coupling efficiency by modulating the RyR2 phosphorylation, which helps to preserve the myocyte contractility. The chronic high-level neurohormonal stimulation as well as sustained $[\text{Ca}^{2+}]_i$ increase stimulates signaling molecules which contribute to genomic responses. These genomic effects include cell growth and apoptotic responses that push the cardiac cell in a vicious cycle and quickly resulted in dilated cardiomyopathy and death (Figure 4.3).

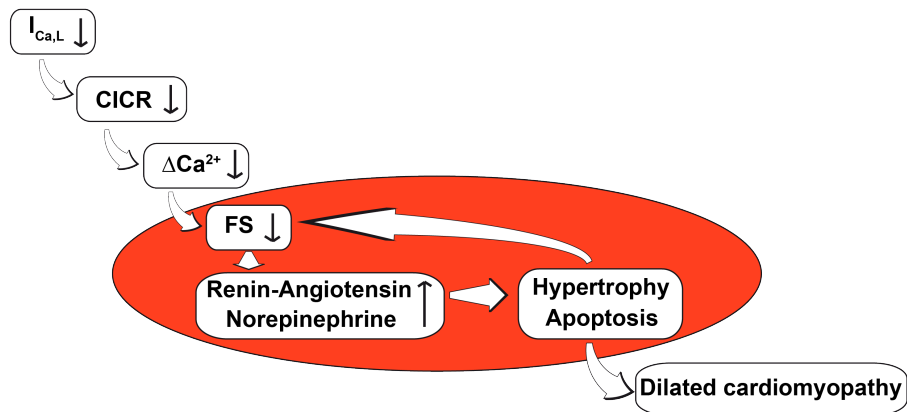


Figure 4.3: Schematic illustration of I/E mutation effects in the heart. For detailed explanation see 4.3.3.

Further studies on the stimulatory hormones such as norepinephrine or angiotensin-II would help to better understand the development of cardiac dysfunction in the I/E mice. One necessary step would be the evaluation of plasma level of these hormones. Moreover, further investigations on the expression and/or regulation of SR Ca²⁺ release channels (including RyR and IP₃-R), on the expression of actin and myosin, on the Ca²⁺ sensitivity of troponinC would answer a lot of remaining questions.

4.4. EC coupling gain in cardiomyocytes expressing RacET

Rac1 has been proposed to play an important role in the cardiac pathological responses by increasing ROS production^{119,171}. Cardiomyocytes from DCM* patients showed higher levels of ROS production associated with increased Rac1 activity¹¹⁹. Transgenic mice expressing cardiac-specific constitutively active Rac1 (RacET) developed transient hypertrophy in the early postnatal stage, which diminished a few weeks after birth¹⁸⁴. Atrial arrhythmias have been also reported in RacET mice¹⁵⁸. Previously, our group studied the hearts of RacET mice and showed a markedly reduced fractional shortening. Accordingly, a decrease in cellular contractility along with alterations of cellular Ca²⁺ handling was found in ventricular myocytes expressing RacET (Oberhofer et al., submitted manuscript). Because there appeared to be no effect of Rac1 on the functional properties of different molecules contributing to Ca²⁺ handling such as SERCA and NCX (Oberhofer et al., submitted manuscript), we were wondering whether EC coupling was altered. Therefore, EC coupling gain was assessed and showed substantially higher gains in RacET mice (Figure 3.25C).

RyR2 is one of the well-known redox-sensitive ion channels in the heart. ROS modulates the RyR2 sensitivity to Ca²⁺, thus influencing SR Ca²⁺ release²²⁵. Moreover, ROS has been shown to activate CaMK-II in cardiac myocytes⁸⁶, which in turn phosphorylates RyR2 and enhances SR Ca²⁺ release. Therefore Rac1 might increase SR Ca²⁺ release by activating ROS production.

The pore-forming subunit (α_{1c}) of the cardiac L-type Ca²⁺ channel contains more than 10 cystein residues¹²⁹, which can be potentially subjected to redox modification. I found a significant decrease in steady-state Ca²⁺ current of RacET mice (Figure 3.25A), which was in agreement with a previous report by Goldhaber showing ROS-mediated I_{Ca,L} down-regulation⁷¹.

In addition to ROS production, Rac1 mediates the cytoskeletal reorganization at focal adhesion sites¹⁸⁴. Our group showed t-tubular loss in the ventricular myocytes expressing RacET (Oberhofer et al., submitted manuscript) that could be linked to the

* Dilated cardiomyopathy

alterations of cytoskeletal organization. The t-tubular disarray might lead to the impairment of EC coupling and subsequent reduction of cardiomyocyte's contractility. The resulting cardiac dysfunction initiates a series of compensatory responses including neurohormonal stimulation to maintain cardiac function. As stated in 4.3.3, activation of cellular signaling cascades in response to neurohormonal stimulation leads to an increase in SR Ca^{2+} release and thus higher EC coupling gains.

Moreover, CDI of $I_{\text{Ca,L}}$ was prolonged in ventricular myocytes expressing RacET (Figure 3.26). Since CDI is believed to be a local process, we speculate that the local control of CDI might have been altered possibly by an altered Ca^{2+} channel-RyR interaction. This impaired coupling most probably resulted from the effects of Rac1 on the cytoskeletal reorganization and t-tubular loss.

Further studies on the expression and regulation of Cav1.2 and RyR are necessary to better explain the EC coupling alterations in RacET mice.

4.5. Cytochalasin D as a culture supplement

The potential to culture cardiac cells is extremely important since the process of remodeling starts within a few hours in isolated adult cardiomyocytes. However, various biological studies such as expression of exogenous proteins by adenoviral gene transfer are critically dependent on maintaining cardiomyocytes in culture for days^{102,171}.

Cardiomyocytes undergo profound alterations during long-term culture. Such alterations resulted in 50-70% reduction of cell density during the first week of culture^{54,175}. Among morphological and functional changes identified; internalization of intercalated discs⁹¹, decreased t-tubular density¹³², altered calcium handling¹⁵⁰ and reduced contractility as well as decreased V_R and $I_{Ca,L}$ ^{58,106}, were reported in the cultured adult rat cardiomyocytes. Therefore, several groups tried to design culture conditions in which cardiomyocyte's phenotype and function are preserved^{78,201}. To improve culture conditions, we took the advantage of a substance called CytoD, which was reported to be useful for long-term culture of adult cardiac myocytes^{41,106}. To verify the efficiency of this substance, we performed a general screening of cardiomyocyte's morphology and functional properties over long-term culture. As a part of the functional studies, I investigated the electrophysiological properties of cardiomyocytes over 3-day culture. Application of 40 μ M CytoD supplement in culture medium resulted in preservation of the morphology, whereas AP characteristics were greatly altered during the culturing period. In contrast 0.5 μ M CytoD could preserve both structure and function including AP characteristics.

4.5.1. C_M was reduced in long-term culture

Several studies showed that cardiomyocytes undergo t-tubular loss over long-term culture^{106,118,132,201}. We also assessed the cardiomyocyte's morphology using different approaches. In one approach the plasma membrane was stained using di-8-ANNEPS, which allowed visualizing t-tubular loss after 3 days culture¹⁹¹. Furthermore, C_M was also evaluated as a part of these studies since it provides information about plasma membrane area including both surface membrane and t-tubular system. The results of

C_M reduction were in great agreement with the membrane staining and provided additional independent support for t-tubular loss (Figure 3.27 and 3.30, black).

Cardiac t-tubules are regulated by different mechanisms: (i) special proteins such as Bin1⁸⁴ have been suggested to mediate t-tubular formation and ion channel organization in these membrane invaginations (ii) biomechanically sensitive regulatory proteins (e.g. JP-1/2) induce appropriate t-tubule/SR interaction¹⁹⁹.

All kinds of these regulatory molecules might be influenced by long-term culture resulting in observed t-tubular loss and C_M reduction.

4.5.2. Preservation of AP shape in long-term culture

The idea to use CytoD came from studies indicating beneficial effects of this substance in preserving cardiomyocytes' morphology^{41,106}. The reported concentration of 40 μM appeared to diminish t-tubular loss in cultured cells that was also reflected in the C_M measurements (Figure 3.27B).

While previous studies focused on the t-tubular preservation, in the present study different functional properties of the cultured cells were also investigated. Besides improvements in the morphological properties, APs were significantly prolonged after 3 days culture with 40 μM CytoD supplement (Figure 3.29). Moreover, further investigation of t-tubular structure showed alterations of the t-tubular arrangement after 3 days culturing with 40 μM CytoD supplement, a phenomena called "t-tubular crowding"¹⁹¹. Therefore, we decided to explore the potential of CytoD as a culture supplement by performing a dose-response assay. We employed an important physiological parameter i.e. the amplitude of electrically evoked Ca^{2+} transients, as the readout in these experiments. We found that with respect to global Ca^{2+} transients CytoD at sub-micromolar concentrations (0.5 μM) preserve DIV0 conditions at DIV3 extremely well¹⁹¹.

To further investigate the beneficial effect of the 0.5 μM CytoD supplement on functional properties of myocytes, APs were recorded in cultured cardiomyocytes. The AP shape

remained unchanged after 3 days in culture with 0.5 μM CytoD (Figure 3.32) together with morphological preservation (Figure 3.30, white). Therefore, AP recordings provided additional support for 0.5 μM CytoD as an appropriate culture supplement.

The effects of CytoD on cardiac AP and ion currents are rather unexplored. There are a few reports studying the acute effects of CytoD on cardiac ion currents ^{126,196}. Undrovinas et al. showed a significant reduction of I_{Na} after acute application of 20-40 μM CytoD ¹⁹⁶. CytoD (10 μM) was shown to influence the gating of inwardly rectifying K^+ channels ¹²⁶. Alterations in both Na^+ and K^+ currents would induce changes in the amplitude and shape of APs. However we did not find any changes in the shape of APs in the presence of 0.5 μM CytoD, but our results can not be compared with previous reports of acute CytoD application. Since in our experiments CytoD was only present in the culture medium and washed out prior to the experiments. If there had been changes of the AP in the presence of CytoD, this effect would have been diminished immediately after washout. Furthermore, the discrepancy between our results and previous findings can be explained by different concentrations of CytoD used for each study. While previous studies mainly used 10 to 80 μM CytoD ^{126,196} our primary culture benefitted from 0.5 μM CytoD supplement.

Taken together, we conclude that 0.5 μM is the optimal concentration to maximally preserve cellular electrophysiology over a culture period of 3 days. This time is sufficient for the expression of fusion proteins and genetically encoded biosensors ^{78,93,201}. Therefore primary culture of cardiomyocytes with 0.5 μM CytoD supplement can be used as an advanced cellular model for genetic as well as pharmacological manipulations *in vitro*.

5. References

- 1) Abbott GW, Sesti F, Splawski I, Buck ME, Lehmann MH, Timothy KW, Keating MT, Goldstein SA. MiRP1 forms IKr potassium channels with HERG and is associated with cardiac arrhythmia. *Cell* 1999 April 16;97(2):175-87.
- 2) Abernethy DR, Soldatov NM. Structure-functional diversity of human L-type Ca²⁺ channel: perspectives for new pharmacological targets. *J Pharmacol Exp Ther* 2002 March;300(3):724-8.
- 3) Acsai K, Antoons G, Livshitz L, Rudy Y, Sipido KR. Microdomain [Ca²⁺(+)] near ryanodine receptors as reported by L-type Ca²⁺(+) and Na⁺/Ca²⁺(+) exchange currents. *J Physiol* 2011 May 15;589(Pt 10):2569-83.
- 4) Adam O, Frost G, Custodis F, Sussman MA, Schafers HJ, Bohm M, Laufs U. Role of Rac1 GTPase activation in atrial fibrillation. *J Am Coll Cardiol* 2007 July 24;50(4):359-67.
- 5) Adams JW, Brown JH. G-proteins in growth and apoptosis: lessons from the heart. *Oncogene* 2001 March 26;20(13):1626-34.
- 6) Adams JW, Sakata Y, Davis MG, Sah VP, Wang Y, Liggett SB, Chien KR, Brown JH, Dorn GW. Enhanced Gα_q signaling: a common pathway mediates cardiac hypertrophy and apoptotic heart failure. *Proc Natl Acad Sci U S A* 1998 August 18;95(17):10140-5.
- 7) Agah R, Frenkel PA, French BA, Michael LH, Overbeek PA, Schneider MD. Gene recombination in postmitotic cells. Targeted expression of Cre recombinase provokes cardiac-restricted, site-specific rearrangement in adult ventricular muscle in vivo. *J Clin Invest* 1997 July 1;100(1):169-79.
- 8) Ahmed CM, Ware DH, Lee SC, Patten CD, Ferrer-Montiel AV, Schinder AF, McPherson JD, Wagner-McPherson CB, Wasmuth JJ, Evans GA, . Primary structure, chromosomal localization, and functional expression of a voltage-gated sodium channel from human brain. *Proc Natl Acad Sci U S A* 1992 September 1;89(17):8220-4.
- 9) Aikawa R, Komuro I, Yamazaki T, Zou Y, Kudoh S, Zhu W, Kadowaki T, Yazaki Y. Rho family small G proteins play critical roles in mechanical stress-induced hypertrophic responses in cardiac myocytes. *Circ Res* 1999 March 5;84(4):458-66.

- 10) Akhter SA, Luttrell LM, Rockman HA, Iaccarino G, Lefkowitz RJ, Koch WJ. Targeting the receptor-Gq interface to inhibit in vivo pressure overload myocardial hypertrophy. *Science* 1998 April 24;280(5363):574-7.
- 11) Alden KJ, Goldspink PH, Ruch SW, Buttrick PM, Garcia J. Enhancement of L-type Ca(2+) current from neonatal mouse ventricular myocytes by constitutively active PKC-beta1. *Am J Physiol Cell Physiol* 2002 April;282(4):C768-C774.
- 12) Apkon M, Nerbonne JM. Alpha 1-adrenergic agonists selectively suppress voltage-dependent K+ current in rat ventricular myocytes. *Proc Natl Acad Sci U S A* 1988 November;85(22):8756-60.
- 13) Apkon M, Nerbonne JM. Characterization of two distinct depolarization-activated K+ currents in isolated adult rat ventricular myocytes. *J Gen Physiol* 1991 May;97(5):973-1011.
- 14) Backx PH, Yue DT, Lawrence JH, Marban E, Tomaselli GF. Molecular localization of an ion-binding site within the pore of mammalian sodium channels. *Science* 1992 July 10;257(5067):248-51.
- 15) Balijepalli RC, Foell JD, Hall DD, Hell JW, Kamp TJ. Localization of cardiac L-type Ca(2+) channels to a caveolar macromolecular signaling complex is required for beta(2)-adrenergic regulation. *Proc Natl Acad Sci U S A* 2006 May 9;103(19):7500-5.
- 16) Balser JR. Structure and function of the cardiac sodium channels. *Cardiovasc Res* 1999 May;42(2):327-38.
- 17) Barry DM, Nerbonne JM. Myocardial potassium channels: electrophysiological and molecular diversity. *Annu Rev Physiol* 1996;58:363-94.
- 18) Benitah JP, Perrier E, Gomez AM, Vassort G. Effects of aldosterone on transient outward K+ current density in rat ventricular myocytes. *J Physiol* 2001 November 15;537(Pt 1):151-60.
- 19) Benitah JP, Vassort G. Aldosterone upregulates Ca(2+) current in adult rat cardiomyocytes. *Circ Res* 1999 December 3;85(12):1139-45.
- 20) Benndorf K, Markwardt F, Nilius B. Two types of transient outward currents in cardiac ventricular cells of mice. *Pflugers Arch* 1987 August;409(6):641-3.
- 21) Benndorf K. Three types of single K channels contribute to the transient outward current in myocardial mouse cells. *Biomed Biochim Acta* 1988;47(4-5):401-16.
- 22) Bers DM. Cardiac excitation-contraction coupling. *Nature* 2002 January 10;415(6868):198-205.

- 23) Bers DM. *Excitation-contraction coupling and cardiac contractile force*. 2nd ed. KLUWER ACADEMIC PUBLISHERS; 2002.
- 24) Bian J, Cui J, McDonald TV. HERG K(+) channel activity is regulated by changes in phosphatidyl inositol 4,5-bisphosphate. *Circ Res* 2001 December 7;89(12):1168-76.
- 25) Bian JS, McDonald TV. Phosphatidylinositol 4,5-bisphosphate interactions with the HERG K(+) channel. *Pflugers Arch* 2007 October;455(1):105-13.
- 26) Biermann M, Rubart M, Moreno A, Wu J, Josiah-Durant A, Zipes DP. Differential effects of cytochalasin D and 2,3 butanedione monoxime on isometric twitch force and transmembrane action potential in isolated ventricular muscle: implications for optical measurements of cardiac repolarization. *J Cardiovasc Electrophysiol* 1998 December;9(12):1348-57.
- 27) Blaich A, Pahlavan S, Tian Q, Oberhofer M, Poomvanicha M, Lenhardt P, Domes K, Wegener JW, Moosmang S, Ruppenthal S, Scholz A, Lipp P, Hofmann F. Mutation of the Calmodulin Binding Motif IQ of the L-type Cav1.2 Ca²⁺ Channel to EQ Induces Dilated Cardiomyopathy and Death. *J Biol Chem* 2012 June 29;287(27):22616-25.
- 28) Bodi I, Mikala G, Koch SE, Akhter SA, Schwartz A. The L-type calcium channel in the heart: the beat goes on. *J Clin Invest* 2005 December;115(12):3306-17.
- 29) Boixel C, Gavillet B, Rougier JS, Abriel H. Aldosterone increases voltage-gated sodium current in ventricular myocytes. *Am J Physiol Heart Circ Physiol* 2006 June;290(6):H2257-H2266.
- 30) Boyle WA, Nerbonne JM. A novel type of depolarization-activated K⁺ current in isolated adult rat atrial myocytes. *Am J Physiol* 1991 April;260(4 Pt 2):H1236-H1247.
- 31) Brette F, Orchard C. T-tubule function in mammalian cardiac myocytes. *Circ Res* 2003 June 13;92(11):1182-92.
- 32) Brette F, Salle L, Orchard CH. Differential modulation of L-type Ca²⁺ current by SR Ca²⁺ release at the T-tubules and surface membrane of rat ventricular myocytes. *Circ Res* 2004 July 9;95(1):e1-e7.
- 33) Brilla CG, Pick R, Tan LB, Janicki JS, Weber KT. Remodeling of the rat right and left ventricles in experimental hypertension. *Circ Res* 1990 December;67(6):1355-64.

- 34) Bunemann M, Gerhardstein BL, Gao T, Hosey MM. Functional regulation of L-type calcium channels via protein kinase A-mediated phosphorylation of the beta(2) subunit. *J Biol Chem* 1999 November 26;274(48):33851-4.
- 35) Calaghan SC, White E, Bedut S, Le Guennec JY. Cytochalasin D reduces Ca²⁺ sensitivity and maximum tension via interactions with myofilaments in skinned rat cardiac myocytes. *J Physiol* 2000 December 1;529 Pt 2:405-11.
- 36) Cannell MB, Cheng H, Lederer WJ. The control of calcium release in heart muscle. *Science* 1995 May 19;268(5213):1045-9.
- 37) Carlson HJ, Campbell RE. Genetically encoded FRET-based biosensors for multiparameter fluorescence imaging. *Curr Opin Biotechnol* 2009 February;20(1):19-27.
- 38) Catterall WA. Structure and regulation of voltage-gated Ca²⁺ channels. *Annu Rev Cell Dev Biol* 2000;16:521-55.
- 39) Chen H, Kim LA, Rajan S, Xu S, Goldstein SA. Charybdotoxin binding in the I(Ks) pore demonstrates two MinK subunits in each channel complex. *Neuron* 2003 September 25;40(1):15-23.
- 40) Cheng H, Lederer WJ, Cannell MB. Calcium sparks: elementary events underlying excitation-contraction coupling in heart muscle. *Science* 1993 October 29;262(5134):740-4.
- 41) Chung KY, Kang M, Walker JW. Contractile regulation by overexpressed ETA requires intact T tubules in adult rat ventricular myocytes. *Am J Physiol Heart Circ Physiol* 2008 May;294(5):H2391-H2399.
- 42) Clapham DE, Neer EJ. New roles for G-protein beta gamma-dimers in transmembrane signalling. *Nature* 1993 September 30;365(6445):403-6.
- 43) Cutler MJ, Jeyaraj D, Rosenbaum DS. Cardiac electrical remodeling in health and disease. *Trends Pharmacol Sci* 2011 March;32(3):174-80.
- 44) D'Angelo DD, Sakata Y, Lorenz JN, Boivin GP, Walsh RA, Liggett SB, Dorn GW. Transgenic Galphaq overexpression induces cardiac contractile failure in mice. *Proc Natl Acad Sci U S A* 1997 July 22;94(15):8121-6.
- 45) Dai S, Hall DD, Hell JW. Supramolecular assemblies and localized regulation of voltage-gated ion channels. *Physiol Rev* 2009 April;89(2):411-52.
- 46) Dartsch T, Fischer R, Gapelyuk A, Weiergraeber M, Ladage D, Schneider T, Schirdewan A, Reuter H, Mueller-Ehmsen J, Zobel C. Aldosterone induces electrical remodeling independent of hypertension. *Int J Cardiol* 2011 July 14.

- 47)De Jongh KS, Murphy BJ, Colvin AA, Hell JW, Takahashi M, Catterall WA. Specific phosphorylation of a site in the full-length form of the alpha 1 subunit of the cardiac L-type calcium channel by adenosine 3',5'-cyclic monophosphate-dependent protein kinase. *Biochemistry* 1996 August 13;35(32):10392-402.
- 48)De Jongh KS, Warner C, Catterall WA. Subunits of purified calcium channels. Alpha 2 and delta are encoded by the same gene. *J Biol Chem* 1990 September 5;265(25):14738-41.
- 49)Delgado C, Artiles A, Gomez AM, Vassort G. Frequency-dependent increase in cardiac Ca²⁺ current is due to reduced Ca²⁺ release by the sarcoplasmic reticulum. *J Mol Cell Cardiol* 1999 October;31(10):1783-93.
- 50)Dipla K, Mattiello JA, Margulies KB, Jeevanandam V, Houser SR. The sarcoplasmic reticulum and the Na⁺/Ca²⁺ exchanger both contribute to the Ca²⁺ transient of failing human ventricular myocytes. *Circ Res* 1999 March 5;84(4):435-44.
- 51)Dixon JE, McKinnon D. Quantitative analysis of potassium channel mRNA expression in atrial and ventricular muscle of rats. *Circ Res* 1994 August;75(2):252-60.
- 52)Domenighetti AA, Wang Q, Egger M, Richards SM, Pedrazzini T, Delbridge LM. Angiotensin II-mediated phenotypic cardiomyocyte remodeling leads to age-dependent cardiac dysfunction and failure. *Hypertension* 2005 August;46(2):426-32.
- 53)Dorn GW, Force T. Protein kinase cascades in the regulation of cardiac hypertrophy. *J Clin Invest* 2005 March;115(3):527-37.
- 54)Dubus I, Samuel JL, Marotte F, Delcayre C, Rappaport L. Beta-adrenergic agonists stimulate the synthesis of noncontractile but not contractile proteins in cultured myocytes isolated from adult rat heart. *Circ Res* 1990 March;66(3):867-74.
- 55)Egger M, Niggli E. Paradoxical block of the Na⁺-Ca²⁺ exchanger by extracellular protons in guinea-pig ventricular myocytes. *J Physiol* 2000 March 1;523 Pt 2:353-66.
- 56)El Gebeily G, Fiset C. 4-Hydroxytamoxifen inhibits K(+) currents in mouse ventricular myocytes. *Eur J Pharmacol* 2010 March 10;629(1-3):96-103.
- 57)El Gebeily G, Fiset C. Upregulation of ventricular potassium channels by chronic tamoxifen treatment. *Cardiovasc Res* 2011 April 1;90(1):68-76.

- 58) Ellingsen O, Davidoff AJ, Prasad SK, Berger HJ, Springhorn JP, Marsh JD, Kelly RA, Smith TW. Adult rat ventricular myocytes cultured in defined medium: phenotype and electromechanical function. *Am J Physiol* 1993 August;265(2 Pt 2):H747-H754.
- 59) Felix R. Voltage-dependent Ca²⁺ channel $\alpha_2\delta$ auxiliary subunit: structure, function and regulation. *Receptors Channels* 1999;6(5):351-62.
- 60) Feng J, Wible B, Li GR, Wang Z, Nattel S. Antisense oligodeoxynucleotides directed against Kv1.5 mRNA specifically inhibit ultrarapid delayed rectifier K⁺ current in cultured adult human atrial myocytes. *Circ Res* 1997 April;80(4):572-9.
- 61) Fisher B, Brown A, Wolmark N, Redmond C, Wickerham DL, Wittliff J, Dimitrov N, Legault-Poisson S, Schipper H, Prager D. Prolonging tamoxifen therapy for primary breast cancer. Findings from the National Surgical Adjuvant Breast and Bowel Project clinical trial. *Ann Intern Med* 1987 May;106(5):649-54.
- 62) Fozzard HA. Cardiac sodium and calcium channels: a history of excitatory currents. *Cardiovasc Res* 2002 July;55(1):1-8.
- 63) Fraccarollo D, Berger S, Galuppo P, Kneitz S, Hein L, Schutz G, Frantz S, Ertl G, Bauersachs J. Deletion of cardiomyocyte mineralocorticoid receptor ameliorates adverse remodeling after myocardial infarction. *Circulation* 2011 February 1;123(4):400-8.
- 64) Fruen BR, Bardy JM, Byrem TM, Strasburg GM, Louis CF. Differential Ca(2+) sensitivity of skeletal and cardiac muscle ryanodine receptors in the presence of calmodulin. *Am J Physiol Cell Physiol* 2000 September;279(3):C724-C733.
- 65) Ganong WF. *Review of medical physiology*. 21 ed. The McGraw-Hill companies; 2003.
- 66) Gellens ME, George AL, Jr., Chen LQ, Chahine M, Horn R, Barchi RL, Kallen RG. Primary structure and functional expression of the human cardiac tetrodotoxin-insensitive voltage-dependent sodium channel. *Proc Natl Acad Sci U S A* 1992 January 15;89(2):554-8.
- 67) George AL, Jr., Komisarof J, Kallen RG, Barchi RL. Primary structure of the adult human skeletal muscle voltage-dependent sodium channel. *Ann Neurol* 1992 February;31(2):131-7.
- 68) Gerhardstein BL, Puri TS, Chien AJ, Hosey MM. Identification of the sites phosphorylated by cyclic AMP-dependent protein kinase on the beta 2 subunit of L-type voltage-dependent calcium channels. *Biochemistry* 1999 August 10;38(32):10361-70.

- 69)Giancotti FG. Integrin signaling: specificity and control of cell survival and cell cycle progression. *Curr Opin Cell Biol* 1997 October;9(5):691-700.
- 70)Giles WR. Ca-independent transient outward current in mammalian heart. Clark RB BA, editor. 1995. in Molecular physiology and pharmacology of cardiac ion channels and transporters.
- 71)Goldhaber JI, Ji S, Lamp ST, Weiss JN. Effects of exogenous free radicals on electromechanical function and metabolism in isolated rabbit and guinea pig ventricle. Implications for ischemia and reperfusion injury. *J Clin Invest* 1989 June;83(6):1800-9.
- 72)Gradman AH. Evolving understanding of the renin-angiotensin-aldosterone system: pathophysiology and targets for therapeutic intervention. *Am Heart J* 2009 June;157(6 Suppl):S1-S6.
- 73)Grover GJ, Garlid KD. ATP-Sensitive potassium channels: a review of their cardioprotective pharmacology. *J Mol Cell Cardiol* 2000 April;32(4):677-95.
- 74)Gusev K, Domenighetti AA, Delbridge LM, Pedrazzini T, Niggli E, Egger M. Angiotensin II-mediated adaptive and maladaptive remodeling of cardiomyocyte excitation-contraction coupling. *Circ Res* 2009 July 2;105(1):42-50.
- 75)Hadley RW, Hume JR. An intrinsic potential-dependent inactivation mechanism associated with calcium channels in guinea-pig myocytes. *J Physiol* 1987 August;389:205-22.
- 76)Hagiwara N, Irisawa H, Kameyama M. Contribution of two types of calcium currents to the pacemaker potentials of rabbit sino-atrial node cells. *J Physiol* 1988 January;395:233-53.
- 77)Halling DB, Aracena-Parks P, Hamilton SL. Regulation of voltage-gated Ca²⁺ channels by calmodulin. *Sci STKE* 2006 January 17;2006(318):er1.
- 78)Hammer K, Ruppenthal S, Viero C, Scholz A, Edelmann L, Kaestner L, Lipp P. Remodelling of Ca²⁺ handling organelles in adult rat ventricular myocytes during long term culture. *J Mol Cell Cardiol* 2010 September;49(3):427-37.
- 79)Hanlon MR, Wallace BA. Structure and function of voltage-dependent ion channel regulatory beta subunits. *Biochemistry* 2002 March 5;41(9):2886-94.
- 80)Hartmann HA, Tiedeman AA, Chen SF, Brown AM, Kirsch GE. Effects of III-IV linker mutations on human heart Na⁺ channel inactivation gating. *Circ Res* 1994 July;75(1):114-22.

- 81)Hayashi S, McMahon AP. Efficient recombination in diverse tissues by a tamoxifen-inducible form of Cre: a tool for temporally regulated gene activation/inactivation in the mouse. *Dev Biol* 2002 April 15;244(2):305-18.
- 82)He J, Kargacin ME, Kargacin GJ, Ward CA. Tamoxifen inhibits Na⁺ and K⁺ currents in rat ventricular myocytes. *Am J Physiol Heart Circ Physiol* 2003 August;285(2):H661-H668.
- 83)Heineke J, Molkenin JD. Regulation of cardiac hypertrophy by intracellular signalling pathways. *Nat Rev Mol Cell Biol* 2006 August;7(8):589-600.
- 84)Hong TT, Smyth JW, Gao D, Chu KY, Vogan JM, Fong TS, Jensen BC, Colecraft HM, Shaw RM. BIN1 localizes the L-type calcium channel to cardiac T-tubules. *PLoS Biol* 2010 February;8(2):e1000312.
- 85)Hordijk PL. Regulation of NADPH oxidases: the role of Rac proteins. *Circ Res* 2006 March 3;98(4):453-62.
- 86)Howe CJ, Lahair MM, McCubrey JA, Franklin RA. Redox regulation of the calcium/calmodulin-dependent protein kinases. *J Biol Chem* 2004 October 22;279(43):44573-81.
- 87)Iravanian S, Dudley SC, Jr. The renin-angiotensin-aldosterone system (RAAS) and cardiac arrhythmias. *Heart Rhythm* 2008 June;5(6 Suppl):S12-S17.
- 88)Isom LL, Ragsdale DS, De Jongh KS, Westenbroek RE, Reber BF, Scheuer T, Catterall WA. Structure and function of the beta 2 subunit of brain sodium channels, a transmembrane glycoprotein with a CAM motif. *Cell* 1995 November 3;83(3):433-42.
- 89)Isom LL, Scheuer T, Brownstein AB, Ragsdale DS, Murphy BJ, Catterall WA. Functional co-expression of the beta 1 and type IIA alpha subunits of sodium channels in a mammalian cell line. *J Biol Chem* 1995 February 17;270(7):3306-12.
- 90)Iwamoto T, Watano T, Shigekawa M. A novel isothioureia derivative selectively inhibits the reverse mode of Na⁺/Ca²⁺ exchange in cells expressing NCX1. *J Biol Chem* 1996 September 13;271(37):22391-7.
- 91)Jacobson SL, Piper HM. Cell cultures of adult cardiomyocytes as models of the myocardium. *J Mol Cell Cardiol* 1986 July;18(7):661-78.
- 92)Kaab S, Dixon J, Duc J, Ashen D, Nabauer M, Beuckelmann DJ, Steinbeck G, McKinnon D, Tomaselli GF. Molecular basis of transient outward potassium current downregulation in human heart failure: a decrease in Kv4.3 mRNA

correlates with a reduction in current density. *Circulation* 1998 October 6;98(14):1383-93.

- 93)Kaestner L, Scholz A, Hammer K, Vecerdea A, Ruppenthal S, Lipp P. Isolation and genetic manipulation of adult cardiac myocytes for confocal imaging. *J Vis Exp* 2009;(31).
- 94)Kamp TJ, Hell JW. Regulation of cardiac L-type calcium channels by protein kinase A and protein kinase C. *Circ Res* 2000 December 8;87(12):1095-102.
- 95)Kannel WB. Vital epidemiologic clues in heart failure. *J Clin Epidemiol* 2000 March 1;53(3):229-35.
- 96)Kass RS, Moss AJ. Long QT syndrome: novel insights into the mechanisms of cardiac arrhythmias. *J Clin Invest* 2003 September;112(6):810-5.
- 97)Kass RS, Sanguinetti MC. Inactivation of calcium channel current in the calf cardiac Purkinje fiber. Evidence for voltage- and calcium-mediated mechanisms. *J Gen Physiol* 1984 November;84(5):705-26.
- 98)Katz AM. *Physiology of the heart*. 4th ed. Lippincott Williams & Wilkins; 2012.
- 99)Kawai M, Hussain M, Orchard CH. Excitation-contraction coupling in rat ventricular myocytes after formamide-induced detubulation. *Am J Physiol* 1999 August;277(2 Pt 2):H603-H609.
- 100) Kayes-Wandover KM, White PC. Steroidogenic enzyme gene expression in the human heart. *J Clin Endocrinol Metab* 2000 July;85(7):2519-25.
- 101) Keef KD, Hume JR, Zhong J. Regulation of cardiac and smooth muscle Ca(2+) channels (Ca(V)1.2a,b) by protein kinases. *Am J Physiol Cell Physiol* 2001 December;281(6):C1743-C1756.
- 102) Kirshenbaum LA, MacLellan WR, Mazur W, French BA, Schneider MD. Highly efficient gene transfer into adult ventricular myocytes by recombinant adenovirus. *J Clin Invest* 1993 July;92(1):381-7.
- 103) Klabunde RE. *cardiovascular physiology concepts*. 2nd ed. Lippincott Williams and Wilkins; 2011.
- 104) Koitabashi N, Bedja D, Zaiman AL, Pinto YM, Zhang M, Gabrielson KL, Takimoto E, Kass DA. Avoidance of transient cardiomyopathy in cardiomyocyte-targeted tamoxifen-induced MerCreMer gene deletion models. *Circ Res* 2009 July 2;105(1):12-5.

- 105) Lafrenie RM, Wahl LM, Epstein JS, Yamada KM, Dhawan S. Activation of monocytes by HIV-Tat treatment is mediated by cytokine expression. *J Immunol* 1997 October 15;159(8):4077-83.
- 106) Leach RN, Desai JC, Orchard CH. Effect of cytoskeleton disruptors on L-type Ca channel distribution in rat ventricular myocytes. *Cell Calcium* 2005 November;38(5):515-26.
- 107) Lederer WJ, Niggli E, Hadley RW. Sodium-calcium exchange in excitable cells: fuzzy space. *Science* 1990 April 20;248(4953):283.
- 108) Lee E, Marcucci M, Daniell L, Pypaert M, Weisz OA, Ochoa GC, Farsad K, Wenk MR, De CP. Amphiphysin 2 (Bin1) and T-tubule biogenesis in muscle. *Science* 2002 August 16;297(5584):1193-6.
- 109) Lee KS, Marban E, Tsien RW. Inactivation of calcium channels in mammalian heart cells: joint dependence on membrane potential and intracellular calcium. *J Physiol* 1985 July;364:395-411.
- 110) Letts VA, Felix R, Biddlecome GH, Arikath J, Mahaffey CL, Valenzuela A, Bartlett FS, Mori Y, Campbell KP, Frankel WN. The mouse stargazer gene encodes a neuronal Ca²⁺-channel gamma subunit. *Nat Genet* 1998 August;19(4):340-7.
- 111) Li L, Satoh H, Ginsburg KS, Bers DM. The effect of Ca(2+)-calmodulin-dependent protein kinase II on cardiac excitation-contraction coupling in ferret ventricular myocytes. *J Physiol* 1997 May 15;501 (Pt 1):17-31.
- 112) Li X, Zima AV, Sheikh F, Blatter LA, Chen J. Endothelin-1-induced arrhythmogenic Ca²⁺ signaling is abolished in atrial myocytes of inositol-1,4,5-trisphosphate(IP3)-receptor type 2-deficient mice. *Circ Res* 2005 June 24;96(12):1274-81.
- 113) Liu XK, Katchman A, Ebert SN, Woosley RL. The antiestrogen tamoxifen blocks the delayed rectifier potassium current, I_{Kr}, in rabbit ventricular myocytes. *J Pharmacol Exp Ther* 1998 December;287(3):877-83.
- 114) Lombes M, Alfaidy N, Eugene E, Lessana A, Farman N, Bonvalet JP. Prerequisite for cardiac aldosterone action. Mineralocorticoid receptor and 11 beta-hydroxysteroid dehydrogenase in the human heart. *Circulation* 1995 July 15;92(2):175-82.
- 115) Lonning PE, Hall K, Aakvaag A, Lien EA. Influence of tamoxifen on plasma levels of insulin-like growth factor I and insulin-like growth factor binding protein I in breast cancer patients. *Cancer Res* 1992 September 1;52(17):4719-23.

- 116) Lonning PE, Lien EA, Lundgren S, Kvinnsland S. Clinical pharmacokinetics of endocrine agents used in advanced breast cancer. *Clin Pharmacokinet* 1992 May;22(5):327-58.
- 117) Lopatin AN, Nichols CG. Inward rectifiers in the heart: an update on I(K1). *J Mol Cell Cardiol* 2001 April;33(4):625-38.
- 118) Louch WE, Bito V, Heinzel FR, Macianskiene R, Vanhaecke J, Flameng W, Mubagwa K, Sipido KR. Reduced synchrony of Ca²⁺ release with loss of T-tubules—a comparison to Ca²⁺ release in human failing cardiomyocytes. *Cardiovasc Res* 2004 April 1;62(1):63-73.
- 119) Maack C, Kartes T, Kilter H, Schafers HJ, Nickenig G, Bohm M, Laufs U. Oxygen free radical release in human failing myocardium is associated with increased activity of rac1-GTPase and represents a target for statin treatment. *Circulation* 2003 September 30;108(13):1567-74.
- 120) Mackenzie L, Bootman MD, Laine M, Berridge MJ, Thuring J, Holmes A, Li WH, Lipp P. The role of inositol 1,4,5-trisphosphate receptors in Ca(2+) signalling and the generation of arrhythmias in rat atrial myocytes. *J Physiol* 2002 June 1;541(Pt 2):395-409.
- 121) Manser E, Leung T, Salihuddin H, Zhao ZS, Lim L. A brain serine/threonine protein kinase activated by Cdc42 and Rac1. *Nature* 1994 January 6;367(6458):40-6.
- 122) Mark MD, Herlitz S. G-protein mediated gating of inward-rectifier K⁺ channels. *Eur J Biochem* 2000 October;267(19):5830-6.
- 123) Martens JR, Kwak YG, Tamkun MM. Modulation of Kv channel alpha/beta subunit interactions. *Trends Cardiovasc Med* 1999 November;9(8):253-8.
- 124) Marx SO, Reiken S, Hisamatsu Y, Jayaraman T, Burkhoff D, Rosemblit N, Marks AR. PKA phosphorylation dissociates FKBP12.6 from the calcium release channel (ryanodine receptor): defective regulation in failing hearts. *Cell* 2000 May 12;101(4):365-76.
- 125) Matsumura K, Fujii K, Oniki H, Oka M, Iida M. Role of aldosterone in left ventricular hypertrophy in hypertension. *Am J Hypertens* 2006 January;19(1):13-8.
- 126) Mazzanti M, Assandri R, Ferroni A, DiFrancesco D. Cytoskeletal control of rectification and expression of four substates in cardiac inward rectifier K⁺ channels. *FASEB J* 1996 February;10(2):357-61.

- 127) McPhee JC, Ragsdale DS, Scheuer T, Catterall WA. A critical role for transmembrane segment IVS6 of the sodium channel alpha subunit in fast inactivation. *J Biol Chem* 1995 May 19;270(20):12025-34.
- 128) Mende U, Kagen A, Cohen A, Aramburu J, Schoen FJ, Neer EJ. Transient cardiac expression of constitutively active G α q leads to hypertrophy and dilated cardiomyopathy by calcineurin-dependent and independent pathways. *Proc Natl Acad Sci U S A* 1998 November 10;95(23):13893-8.
- 129) Mikami A, Imoto K, Tanabe T, Niidome T, Mori Y, Takeshima H, Narumiya S, Numa S. Primary structure and functional expression of the cardiac dihydropyridine-sensitive calcium channel. *Nature* 1989 July 20;340(6230):230-3.
- 130) Mishra S, Ling H, Grimm M, Zhang T, Bers DM, Brown JH. Cardiac hypertrophy and heart failure development through Gq and CaM kinase II signaling. *J Cardiovasc Pharmacol* 2010 December;56(6):598-603.
- 131) Mitarai S, Reed TD, Yatani A. Changes in ionic currents and beta-adrenergic receptor signaling in hypertrophied myocytes overexpressing G α (q). *Am J Physiol Heart Circ Physiol* 2000 July;279(1):H139-H148.
- 132) Mitcheson JS, Hancox JC, Levi AJ. Cultured adult cardiac myocytes: future applications, culture methods, morphological and electrophysiological properties. *Cardiovasc Res* 1998 August;39(2):280-300.
- 133) Mitterdorfer J, Froschmayr M, Grabner M, Striessnig J, Glossmann H. Calcium channels: the beta-subunit increases the affinity of dihydropyridine and Ca $^{2+}$ binding sites of the alpha 1-subunit. *FEBS Lett* 1994 September 26;352(2):141-5.
- 134) Molkenin JD, Robbins J. With great power comes great responsibility: using mouse genetics to study cardiac hypertrophy and failure. *J Mol Cell Cardiol* 2009 February;46(2):130-6.
- 135) Mori MX, Erickson MG, Yue DT. Functional stoichiometry and local enrichment of calmodulin interacting with Ca $^{2+}$ channels. *Science* 2004 April 16;304(5669):432-5.
- 136) Nerbonne JM. Molecular basis of functional voltage-gated K channel diversity in the mammalian myocardium. [525], 285-298. 2012. *J Physiol*.
- 137) Nichols CG. Adenosine triphosphate-sensitive potassium channel in the cardiovascular system. Lederer JW, editor. [261], H1675-1686. 1991. *Am J Physiol*.

- 138) Nicoletti A, Heudes D, Hinglais N, Appay MD, Philippe M, Sassy-Prigent C, Bariety J, Michel JB. Left ventricular fibrosis in renovascular hypertensive rats. Effect of losartan and spironolactone. *Hypertension* 1995 July;26(1):101-11.
- 139) Nicoll DA, Ottolia M, Lu L, Lu Y, Philipson KD. A new topological model of the cardiac sarcolemmal Na⁺-Ca²⁺ exchanger. *J Biol Chem* 1999 January 8;274(2):910-7.
- 140) Noda M, Shimizu S, Tanabe T, Takai T, Kayano T, Ikeda T, Takahashi H, Nakayama H, Kanaoka Y, Minamino N, . Primary structure of Electrophorus electricus sodium channel deduced from cDNA sequence. *Nature* 1984 November 8;312(5990):121-7.
- 141) Oudit GY, Kassiri Z, Sah R, Ramirez RJ, Zobel C, Backx PH. The molecular physiology of the cardiac transient outward potassium current (I_{to}) in normal and diseased myocardium. *J Mol Cell Cardiol* 2001 May;33(5):851-72.
- 142) Ouvrard-Pascaud A, Sainte-Marie Y, Benitah JP, Perrier R, Soukaseum C, Nguyen Dinh CA, Royer A, Le QK, Charpentier F, Demolombe S, Mechta-Grigoriou F, Beggah AT, Maison-Blanche P, Oblin ME, Delcayre C, Fishman GI, Farman N, Escoubet B, Jaisser F. Conditional mineralocorticoid receptor expression in the heart leads to life-threatening arrhythmias. *Circulation* 2005 June 14;111(23):3025-33.
- 143) Pahlavan S, Oberhofer M, Sauer B, Ruppenthal S, Tian Q, Scholz A, Kaestner L, Lipp P. Galphaq and Galpha11 contribute to the maintenance of cellular electrophysiology and Ca²⁺ handling in ventricular cardiomyocytes. *Cardiovasc Res* 2012 Jul;95(1):48-58.
- 144) Patel SP, Campbell DL. Transient outward potassium current, 'I_{to}', phenotypes in the mammalian left ventricle: underlying molecular, cellular and biophysical mechanisms. *J Physiol* 2005 November 15;569(Pt 1):7-39.
- 145) Perez-Garcia MT, Chiamvimonvat N, Ranjan R, Balsler JR, Tomaselli GF, Marban E. Mechanisms of sodium/calcium selectivity in sodium channels probed by cysteine mutagenesis and sulfhydryl modification. *Biophys J* 1997 March;72(3):989-96.
- 146) Perrier E, Perrier R, Richard S, Benitah JP. Ca²⁺ controls functional expression of the cardiac K⁺ transient outward current via the calcineurin pathway. *J Biol Chem* 2004 September 24;279(39):40634-9.
- 147) Perrier R, Richard S, Sainte-Marie Y, Rossier BC, Jaisser F, Hummler E, Benitah JP. A direct relationship between plasma aldosterone and cardiac L-type Ca²⁺ current in mice. *J Physiol* 2005 November 15;569(Pt 1):153-62.

- 148) Peterson BZ, DeMaria CD, Adelman JP, Yue DT. Calmodulin is the Ca²⁺ sensor for Ca²⁺-dependent inactivation of L-type calcium channels. *Neuron* 1999 March;22(3):549-58.
- 149) Pitt GS, Zuhlke RD, Hudmon A, Schulman H, Reuter H, Tsien RW. Molecular basis of calmodulin tethering and Ca²⁺-dependent inactivation of L-type Ca²⁺ channels. *J Biol Chem* 2001 August 17;276(33):30794-802.
- 150) Poindexter BJ, Smith JR, Buja LM, Bick RJ. Calcium signaling mechanisms in dedifferentiated cardiac myocytes: comparison with neonatal and adult cardiomyocytes. *Cell Calcium* 2001 December;30(6):373-82.
- 151) Pond AL, Scheve BK, Benedict AT, Petrecca K, Van Wagoner DR, Shrier A, Nerbonne JM. Expression of distinct ERG proteins in rat, mouse, and human heart. Relation to functional I(Kr) channels. *J Biol Chem* 2000 February 25;275(8):5997-6006.
- 152) Poomvanicha M, Wegener JW, Blaich A, Fischer S, Domes K, Moosmang S, Hofmann F. Facilitation and Ca²⁺-dependent inactivation are modified by mutation of the Ca(v)1.2 channel IQ motif. *J Biol Chem* 2011 July 29;286(30):26702-7.
- 153) Pourrier M, Schram G, Nattel S. Properties, expression and potential roles of cardiac K⁺ channel accessory subunits: MinK, MiRPs, KChIP, and KChAP. *J Membr Biol* 2003 August 1;194(3):141-52.
- 154) Pragnell M, De WM, Mori Y, Tanabe T, Snutch TP, Campbell KP. Calcium channel beta-subunit binds to a conserved motif in the I-II cytoplasmic linker of the alpha 1-subunit. *Nature* 1994 March 3;368(6466):67-70.
- 155) Qin W, Rudolph AE, Bond BR, Rocha R, Blomme EA, Goellner JJ, Funder JW, McMahon EG. Transgenic model of aldosterone-driven cardiac hypertrophy and heart failure. *Circ Res* 2003 July 11;93(1):69-76.
- 156) Radermacher M, Rao V, Grassucci R, Frank J, Timerman AP, Fleischer S, Wagenknecht T. Cryo-electron microscopy and three-dimensional reconstruction of the calcium release channel/ryanodine receptor from skeletal muscle. *J Cell Biol* 1994 October;127(2):411-23.
- 157) Reil JC, Hohl M, Oberhofer M, Kazakov A, Kaestner L, Mueller P, Adam O, Maack C, Lipp P, Mewis C, Allessie M, Laufs U, Bohm M, Neuberg HR. Cardiac Rac1 overexpression in mice creates a substrate for atrial arrhythmias characterized by structural remodelling. *Cardiovasc Res* 2010 August 1;87(3):485-93.

- 158) Reil JC, Hohl M, Selejan S, Lipp P, Drautz F, Kazakow A, Munz BM, Muller P, Steendijk P, Reil GH, Allessie MA, Bohm M, Neuberger HR. Aldosterone promotes atrial fibrillation. *Eur Heart J* 2011 August 4.
- 159) Richard S, Perrier E, Fauconnier J, Perrier R, Pereira L, Gomez AM, Benitah JP. 'Ca(2+)-induced Ca(2+) entry' or how the L-type Ca(2+) channel remodels its own signalling pathway in cardiac cells. *Prog Biophys Mol Biol* 2006 January;90(1-3):118-35.
- 160) Roden DM, Balsler JR, George AL, Jr., Anderson ME. Cardiac ion channels. *Annu Rev Physiol* 2002;64:431-75.
- 161) Roden DM, George AL, Jr. Structure and function of cardiac sodium and potassium channels. *Am J Physiol* 1997 August;273(2 Pt 2):H511-H525.
- 162) Roderick HL, Bootman MD. Pacemaking, arrhythmias, inotropy and hypertrophy: the many possible facets of IP₃ signalling in cardiac myocytes. *J Physiol* 2007 June 15;581(Pt 3):883-4.
- 163) Rogers JH, Tamirisa P, Kovacs A, Weinheimer C, Courtois M, Blumer KJ, Kelly DP, Muslin AJ. RGS4 causes increased mortality and reduced cardiac hypertrophy in response to pressure overload. *J Clin Invest* 1999 September;104(5):567-76.
- 164) Ronkainen JJ, Hanninen SL, Korhonen T, Koivumaki JT, Skoumal R, Rautio S, Ronkainen VP, Tavi P. Ca²⁺-calmodulin-dependent protein kinase II represses cardiac transcription of the L-type calcium channel alpha(1C)-subunit gene (*Cacna1c*) by DREAM translocation. *J Physiol* 2011 June 1;589(Pt 11):2669-86.
- 165) Sakmann B, Neher E. *Single-channel recording*. Second ed. Springer; 2009.
- 166) Salazar NC, Chen J, Rockman HA. Cardiac GPCRs: GPCR signaling in healthy and failing hearts. *Biochim Biophys Acta* 2007 April;1768(4):1006-18.
- 167) Sanguinetti MC, Jurkiewicz NK, Scott A, Siegl PK. Isoproterenol antagonizes prolongation of refractory period by the class III antiarrhythmic agent E-4031 in guinea pig myocytes. Mechanism of action. *Circ Res* 1991 January;68(1):77-84.
- 168) Sanguinetti MC, Jurkiewicz NK. Two components of cardiac delayed rectifier K⁺ current. Differential sensitivity to block by class III antiarrhythmic agents. *J Gen Physiol* 1990 July;96(1):195-215.
- 169) Santana LF, Cheng H, Gomez AM, Cannell MB, Lederer WJ. Relation between the sarcolemmal Ca²⁺ current and Ca²⁺ sparks and local control theories for cardiac excitation-contraction coupling. *Circ Res* 1996 January;78(1):166-71.

- 170) Sato R, Koumi S, Singer DH, Hisatome I, Jia H, Eager S, Wasserstrom JA. Amiodarone blocks the inward rectifier potassium channel in isolated guinea pig ventricular cells. *J Pharmacol Exp Ther* 1994 June;269(3):1213-9.
- 171) Satoh M, Ogita H, Takeshita K, Mukai Y, Kwiatkowski DJ, Liao JK. Requirement of Rac1 in the development of cardiac hypertrophy. *Proc Natl Acad Sci U S A* 2006 May 9;103(19):7432-7.
- 172) Schmidt-Supprian M, Rajewsky K. Vagaries of conditional gene targeting. *Nat Immunol* 2007 July;8(7):665-8.
- 173) Schreibmayer W. Isoform diversity and modulation of sodium channels by protein kinases. *Cell Physiol Biochem* 1999;9(4-5):187-200.
- 174) Schroeter A, Walzik S, Blechschmidt S, Haufe V, Benndorf K, Zimmer T. Structure and function of splice variants of the cardiac voltage-gated sodium channel Na(v)1.5. *J Mol Cell Cardiol* 2010 July;49(1):16-24.
- 175) Schwarzfeld TA, Jacobson SL. Isolation and development in cell culture of myocardial cells of the adult rat. *J Mol Cell Cardiol* 1981 June;13(6):563-75.
- 176) Seisenberger C, Specht V, Welling A, Platzer J, Pfeifer A, Kuhbandner S, Striessnig J, Klugbauer N, Feil R, Hofmann F. Functional embryonic cardiomyocytes after disruption of the L-type alpha1C (Cav1.2) calcium channel gene in the mouse. *J Biol Chem* 2000 December 15;275(50):39193-9.
- 177) Shubeita HE, Martinson EA, van BM, Chien KR, Brown JH. Transcriptional activation of the cardiac myosin light chain 2 and atrial natriuretic factor genes by protein kinase C in neonatal rat ventricular myocytes. *Proc Natl Acad Sci U S A* 1992 February 15;89(4):1305-9.
- 178) Singer D, Biel M, Lotan I, Flockerzi V, Hofmann F, Dascal N. The roles of the subunits in the function of the calcium channel. *Science* 1991 September 27;253(5027):1553-7.
- 179) Slight SH, Ganjam VK, Gomez-Sanchez CE, Zhou MY, Weber KT. High affinity NAD(+)-dependent 11 beta-hydroxysteroid dehydrogenase in the human heart. *J Mol Cell Cardiol* 1996 April;28(4):781-7.
- 180) Smyth JW, Shaw RM. Forward trafficking of ion channels: what the clinician needs to know. *Heart Rhythm* 2010 August;7(8):1135-40.
- 181) Snyders DJ. Structure and function of cardiac potassium channels. *Cardiovasc Res* 1999 May;42(2):377-90.

- 182) Sohal DS, Nghiem M, Crackower MA, Witt SA, Kimball TR, Tymitz KM, Penninger JM, Molkentin JD. Temporally regulated and tissue-specific gene manipulations in the adult and embryonic heart using a tamoxifen-inducible Cre protein. *Circ Res* 2001 July 6;89(1):20-5.
- 183) Splawski I, Timothy KW, Sharpe LM, Decher N, Kumar P, Bloise R, Napolitano C, Schwartz PJ, Joseph RM, Condouris K, Tager-Flusberg H, Priori SG, Sanguinetti MC, Keating MT. Ca(V)1.2 calcium channel dysfunction causes a multisystem disorder including arrhythmia and autism. *Cell* 2004 October 1;119(1):19-31.
- 184) Sussman MA, Welch S, Walker A, Klevitsky R, Hewett TE, Price RL, Schaefer E, Yager K. Altered focal adhesion regulation correlates with cardiomyopathy in mice expressing constitutively active rac1. *J Clin Invest* 2000 April;105(7):875-86.
- 185) Szabo G, Otero AS. G protein mediated regulation of K⁺ channels in heart. *Annu Rev Physiol* 1990;52:293-305.
- 186) Takeda Y, Yoneda T, Demura M, Usukura M, Mabuchi H. Calcineurin inhibition attenuates mineralocorticoid-induced cardiac hypertrophy. *Circulation* 2002 February 12;105(6):677-9.
- 187) Takefuji M, Wirth A, Lukasova M, Takefuji S, Boettger T, Braun T, Althoff T, Offermanns S, Wettschurek N. A G13-Mediated Signaling Pathway is Required for Pressure Overload-Induced Cardiac Remodeling and Heart Failure. *Circulation* 2012 September 17.
- 188) Tamargo J, Caballero R, Gomez R, Valenzuela C, Delpon E. Pharmacology of cardiac potassium channels. *Cardiovasc Res* 2004 April 1;62(1):9-33.
- 189) Tang L, Kallen RG, Horn R. Role of an S4-S5 linker in sodium channel inactivation probed by mutagenesis and a peptide blocker. *J Gen Physiol* 1996 August;108(2):89-104.
- 190) Tareilus E, Roux M, Qin N, Olcese R, Zhou J, Stefani E, Birnbaumer L. A Xenopus oocyte beta subunit: evidence for a role in the assembly/expression of voltage-gated calcium channels that is separate from its role as a regulatory subunit. *Proc Natl Acad Sci U S A* 1997 March 4;94(5):1703-8.
- 191) Tian Q, Pahlavan S, Oleinikow K, Jung J, Ruppenthal S, Scholz A, Schumann C, Kraegeloh A, Oberhofer M, Lipp P, Kaestner L. Functional and morphological preservation of adult ventricular myocytes in culture by sub-micromolar cytochalasin D supplement. *J Mol Cell Cardiol* 2012 January;52(1):113-24.

- 192) Tilley DG. G protein-dependent and G protein-independent signaling pathways and their impact on cardiac function. *Circ Res* 2011 July 8;109(2):217-30.
- 193) Timofeyev V, He Y, Tuteja D, Zhang Q, Roth DM, Hammond HK, Chiamvimonvat N. Cardiac-directed expression of adenylyl cyclase reverses electrical remodeling in cardiomyopathy. *J Mol Cell Cardiol* 2006 July;41(1):170-81.
- 194) Tohse N, Kameyama M, Irisawa H. Intracellular Ca²⁺ and protein kinase C modulate K⁺ current in guinea pig heart cells. *Am J Physiol* 1987 November;253(5 Pt 2):H1321-H1324.
- 195) Treinys R, Jurevicius J. L-type Ca²⁺ channels in the heart: structure and regulation. *Medicina (Kaunas)* 2008;44(7):491-9.
- 196) Undrovinas AI, Shander GS, Makielski JC. Cytoskeleton modulates gating of voltage-dependent sodium channel in heart. *Am J Physiol* 1995 July;269(1 Pt 2):H203-H214.
- 197) Valdivia HH, Kaplan JH, Ellis-Davies GC, Lederer WJ. Rapid adaptation of cardiac ryanodine receptors: modulation by Mg²⁺ and phosphorylation. *Science* 1995 March 31;267(5206):1997-2000.
- 198) Van AL, D'Souza-Schorey C. Rho GTPases and signaling networks. *Genes Dev* 1997 September 15;11(18):2295-322.
- 199) van Oort RJ, Garbino A, Wang W, Dixit SS, Landstrom AP, Gaur N, De Almeida AC, Skapura DG, Rudy Y, Burns AR, Ackerman MJ, Wehrens XH. Disrupted junctional membrane complexes and hyperactive ryanodine receptors after acute junctophilin knockdown in mice. *Circulation* 2011 March 8;123(9):979-88.
- 200) Varro A, Lathrop DA, Hester SB, Nanasi PP, Papp JG. Ionic currents and action potentials in rabbit, rat, and guinea pig ventricular myocytes. *Basic Res Cardiol* 1993 March;88(2):93-102.
- 201) Viero C, Kraushaar U, Ruppenthal S, Kaestner L, Lipp P. A primary culture system for sustained expression of a calcium sensor in preserved adult rat ventricular myocytes. *Cell Calcium* 2008 January;43(1):59-71.
- 202) Wagner M, Rudakova E, Schutz V, Frank M, Ehmke H, Volk T. Larger transient outward K(+) current and shorter action potential duration in Galpha(11) mutant mice. *Pflugers Arch* 2010 March;459(4):607-18.

- 203) Wang HG, George MS, Kim J, Wang C, Pitt GS. Ca²⁺/calmodulin regulates trafficking of Ca(V)_{1.2} Ca²⁺ channels in cultured hippocampal neurons. *J Neurosci* 2007 August 22;27(34):9086-93.
- 204) Wang Y, Su B, Sah VP, Brown JH, Han J, Chien KR. Cardiac hypertrophy induced by mitogen-activated protein kinase kinase 7, a specific activator for c-Jun NH₂-terminal kinase in ventricular muscle cells. *J Biol Chem* 1998 March 6;273(10):5423-6.
- 205) Weerapura M, Nattel S, Chartier D, Caballero R, Hebert TE. A comparison of currents carried by HERG, with and without coexpression of MiRP1, and the native rapid delayed rectifier current. Is MiRP1 the missing link? *J Physiol* 2002 April 1;540(Pt 1):15-27.
- 206) Wehrens XH, Lehnart SE, Marks AR. Intracellular calcium release and cardiac disease. *Annu Rev Physiol* 2005;67:69-98.
- 207) Wei S, Guo A, Chen B, Kutschke W, Xie YP, Zimmerman K, Weiss RM, Anderson ME, Cheng H, Song LS. T-tubule remodeling during transition from hypertrophy to heart failure. *Circ Res* 2010 August 20;107(4):520-31.
- 208) Wei X, Pan S, Lang W, Kim H, Schneider T, Perez-Reyes E, Birnbaumer L. Molecular determinants of cardiac Ca²⁺ channel pharmacology. Subunit requirement for the high affinity and allosteric regulation of dihydropyridine binding. *J Biol Chem* 1995 November 10;270(45):27106-11.
- 209) Westwick JK, Lambert QT, Clark GJ, Symons M, Van AL, Pestell RG, Der CJ. Rac regulation of transformation, gene expression, and actin organization by multiple, PAK-independent pathways. *Mol Cell Biol* 1997 March;17(3):1324-35.
- 210) Wettschureck N, Offermanns S. Mammalian G proteins and their cell type specific functions. *Physiol Rev* 2005 October;85(4):1159-204.
- 211) Wettschureck N, Rutten H, Zywiets A, Gehring D, Wilkie TM, Chen J, Chien KR, Offermanns S. Absence of pressure overload induced myocardial hypertrophy after conditional inactivation of Galphaq/Galpha11 in cardiomyocytes. *Nat Med* 2001 November;7(11):1236-40.
- 212) White PC. Aldosterone: direct effects on and production by the heart. *J Clin Endocrinol Metab* 2003 June;88(6):2376-83.
- 213) Wible BA, De BM, Majumder K, Taglialatela M, Brown AM. Cloning and functional expression of an inwardly rectifying K⁺ channel from human atrium. *Circ Res* 1995 March;76(3):343-50.

- 214) Witcher DR, Kovacs RJ, Schulman H, Cefali DC, Jones LR. Unique phosphorylation site on the cardiac ryanodine receptor regulates calcium channel activity. *J Biol Chem* 1991 June 15;266(17):11144-52.
- 215) Witcher DR, Striffler BA, Jones LR. Cardiac-specific phosphorylation site for multifunctional Ca²⁺/calmodulin-dependent protein kinase is conserved in the brain ryanodine receptor. *J Biol Chem* 1992 March 5;267(7):4963-7.
- 216) Woodcock EA, Kistler PM, Ju YK. Phosphoinositide signalling and cardiac arrhythmias. *Cardiovasc Res* 2009 May 1;82(2):286-95.
- 217) Yamaguchi H, Hara M, Strobeck M, Fukasawa K, Schwartz A, Varadi G. Multiple modulation pathways of calcium channel activity by a beta subunit. Direct evidence of beta subunit participation in membrane trafficking of the alpha1C subunit. *J Biol Chem* 1998 July 24;273(30):19348-56.
- 218) Yellen G. The voltage-gated potassium channels and their relatives. *Nature* 2002 September 5;419(6902):35-42.
- 219) Yokoshiki H, Sunagawa M, Seki T, Sperelakis N. ATP-sensitive K⁺ channels in pancreatic, cardiac, and vascular smooth muscle cells. *Am J Physiol* 1998 January;274(1 Pt 1):C25-C37.
- 220) Young M, Fullerton M, Dilley R, Funder J. Mineralocorticoids, hypertension, and cardiac fibrosis. *J Clin Invest* 1994 June;93(6):2578-83.
- 221) Yue Y, Qu Y, Boutjdir M. Beta- and alpha-adrenergic cross-signaling for L-type Ca current is impaired in transgenic mice with constitutive activation of epsilonPKC. *Biochem Biophys Res Commun* 2004 February 13;314(3):749-54.
- 222) Zechner D, Thuerauf DJ, Hanford DS, McDonough PM, Glembotski CC. A role for the p38 mitogen-activated protein kinase pathway in myocardial cell growth, sarcomeric organization, and cardiac-specific gene expression. *J Cell Biol* 1997 October 6;139(1):115-27.
- 223) Zhang L, Kelley J, Schmeisser G, Kobayashi YM, Jones LR. Complex formation between junctin, triadin, calsequestrin, and the ryanodine receptor. Proteins of the cardiac junctional sarcoplasmic reticulum membrane. *J Biol Chem* 1997 September 12;272(37):23389-97.
- 224) Zhang T, Maier LS, Dalton ND, Miyamoto S, Ross J, Jr., Bers DM, Brown JH. The deltaC isoform of CaMKII is activated in cardiac hypertrophy and induces dilated cardiomyopathy and heart failure. *Circ Res* 2003 May 2;92(8):912-9.
- 225) Zima AV, Blatter LA. Redox regulation of cardiac calcium channels and transporters. *Cardiovasc Res* 2006 July 15;71(2):310-21.

- 226) Zimmer T, Benndorf K. The intracellular domain of the beta 2 subunit modulates the gating of cardiac Na v 1.5 channels. *Biophys J* 2007 June 1;92(11):3885-92.
- 227) Zuhlke RD, Pitt GS, Deisseroth K, Tsien RW, Reuter H. Calmodulin supports both inactivation and facilitation of L-type calcium channels. *Nature* 1999 May 13;399(6732):159-62.
- 228) Zuhlke RD, Pitt GS, Tsien RW, Reuter H. Ca²⁺-sensitive inactivation and facilitation of L-type Ca²⁺ channels both depend on specific amino acid residues in a consensus calmodulin-binding motif in the(alpha)1C subunit. *J Biol Chem* 2000 July 14;275(28):21121-9.
- 229) Zuhlke RD, Reuter H. Ca²⁺-sensitive inactivation of L-type Ca²⁺ channels depends on multiple cytoplasmic amino acid sequences of the alpha1C subunit. *Proc Natl Acad Sci U S A* 1998 March 17;95(6):3287-94.
- 230) Zygmunt AC, Gibbons WR. Properties of the calcium-activated chloride current in heart. *J Gen Physiol* 1992 March;99(3):391-414.
- 231) Zygmunt AC. Intracellular calcium activates a chloride current in canine ventricular myocytes. *Am J Physiol* 1994 November;267(5 Pt 2):H1984-H1995.

Curriculum Vitae

Sara Pahlavan

Institut für Molekulare Zellbiologie, Medizinischen Fakultät, Universität des Saarlandes
Gebäude 61 / Anatomie, 66421 Homburg/Saar

PERSONAL INFORMATION

Gender: Female

Birthdate: 15th of July 1981

Birthplace: Damavand, Tehran, Iran

Present citizenship: Iranian

EDUCATION

1995-1999 High School Diploma in Experimental (Natural) Science, Tehran, Iran

1999-2003 B.Sc. In Biology, University of Agricultural Sciences of Gorgan, Golestan,
Iran

2003-2005 M.Sc. in Animal physiology, Shiraz University, Shiraz, Iran

2009-present PhD student, Saarland University, Homburg (Saar), Germany

SCHOOLS AND CONFERENCES

2009 Graduate research program 1326, calcium signaling and cellular nanodomains,
medical faculty, Saarland University Hospital, Saarland University, Homburg
(Saar), Germany

2011 90th Annual Meeting, Deutsche Physiologische Gesellschaft, Regensburg
University, Regensburg, Germany

2012 56th Annual Biophysical Society Meeting, San Diego, California, USA

2012 91th Annual Meeting, Deutsche Physiologische Gesellschaft, Dresden, Germany

CONFERENCE ABSTRACTS

- 2010 Hammer, K., Scholz, A., Tian, Q., **Pahlavan, S.**, Ruppenthal, S., Oberhofer, M., Kaestner, L., Lipp, P. Influence of Cytochalasin D on Morphology and Physiology of Rat Cardiac Myocytes. 2010, *Acta Physiologica*, Vol. 198, Supplement 677: P-SUN-87
- 2011 Kaestner, L., Tian, Q., **Pahlavan, S.**, Oleinikow, K., Ruppenthal, S., Scholz, A., Oberhofer, M., Schumann, C., Kraegeloh, A., Lipp, P. The Differential Action of Cytochalasin D in T-tubular Remodelling of Ventricular Myocytes. 2011 Biophysical Society Meeting Abstracts, *Biophys. J*, Vol. 100(3), Supplement, pp.292-3a
- 2011 Tian, Q., **Pahlavan, S.**, Ruppenthal, S., Scholz, A., Wiesen, K., Oberhofer, M., Kaestner, L., Lipp, P. Alterations of Membrane Currents, Contractility and Calcium Signaling in Gq/G11 Single and Double KO Mice. 2011 Biophysical Society Meeting Abstracts, *Biophys. J*, Vol. 100(3), Supplement, pp.517a
- 2011 **Pahlavan, S.**, Wiesen, K., Oberhofer, M., Kaestner, L., Lipp, P. The Electrophysiological Effects of Chronic Application of Aldosterone on Ventricular Myocytes of Gq/11 Knockout Mice. 2011, *Acta Physiologica*, Vol. 201, Supplement 682: P021
- 2012 **Pahlavan, S.**, Sauer, B., Wiesen, K., Oberhofer, M., Kaestner, L., Lipp, P. GaQ/Ga11 Modulate Aldosterone Mediated Electrical Remodeling and Ca²⁺ Handling Alterations in Ventricular Myocytes. 2012 Biophysical Society Meeting Abstracts, *Biophys. J*. Vol. 102(3), Supplement, pp.340a
- 2012 **Pahlavan, S.**, Oberhofer, M., Lipp, P. Excitation-Contraction Coupling Alterations in Ventricular Myocytes of RacET Mice. 2012, *Acta Physiologica*, Vol. 204, Supplement 689: P186

LANGUAGES

Persian, English

Publications

During PhD period

1. Blaich A, **Pahlavan S**, Tian Q, Oberhofer M, Poomvanicha M, Lenhardt P, Domes K, Wegener JW, Moosmang S, Ruppenthal S, Scholz A, Lipp P, Hofmann F. Mutation of the Calmodulin Binding Motif IQ of the L-type Cav1.2 Ca²⁺ Channel to EQ Induces Dilated Cardiomyopathy and Death. *J Biol Chem* 2012 June 29;287(27):22616-25.
2. **Pahlavan S**, Oberhofer M, Sauer B, Ruppenthal S, Tian Q, Scholz A, Kaestner L, Lipp P. Galphaq and Galpha11 contribute to the maintenance of cellular electrophysiology and Ca²⁺ handling in ventricular cardiomyocytes. *Cardiovasc Res* 2012 Jul 1;95(1):48-58.
3. Tian Q, **Pahlavan S**, Oleinikow K, Jung J, Ruppenthal S, Scholz A, Schumann C, Kraegeloh A, Oberhofer M, Lipp P, Kaestner L. Functional and morphological preservation of adult ventricular myocytes in culture by sub-micromolar cytochalasin D supplement. *J Mol Cell Cardiol* 2012 January;52(1):113-24.

During Master degree period

1. Monsefi M, **Pahlavan S**. Effects of Aqueous Extract of *Anethum graveolens* (L.) On Male Reproductive System of Rats. *Journal of Biological Sciences* 2007;7(5):815-8.

Acknowledgement

My PhD time is coming to the end with all its great memories. Here I would like to thank all people who were the lights in this long and meandering way:

My special thanks to Prof. Dr. Peter Lipp who offered me the opportunity to be a PhD student in the institute for molecular cell biology. He offered me his countless help in sophisticated design of electrophysiological experiments, interpretation of results and presenting them as scientific papers.

Many many thanks to Dr. Martin Oberhofer who taught me patch clamp technique and all necessary details for being a cardiac electrophysiologist. He always helped me in discussing my results and presenting them in a scientific manner. Special thanks to him that taught me how to be a good scientist.

I would like to thank Dr. Lars Kästner who offered me great support in hardware part of my experiments specially Ca^{2+} imaging and I enjoyed discussing with him physical aspects of my work.

Thanks to Dr. Sandra Ruppenthal and Dr. Anke Scholtz who provided all transgenic mice used in my work.

Thanks to Dr. Kathrina Wiesen who contributed to most of the projects presented in this thesis and was a close friend of me.

Thanks to Mrs. Anne Vecerdea for preparing cardiac cells and Mrs. Tanja Kuhn for organizing all chemicals.

Thanks to Mr. Jorg Sauerbaum for constructing all custom-made mechanical devices.

And many thanks to Mrs. Karin Schumacher for countless help in my paper works and daily life concerns.

And thanks to all colleagues in institute for molecular cell biology; Karin Hammer, Oliver Müller, Qinghai Tian, Silke Wagner, Jue Wang, Xin Hui, Benjamin Sauer, Cornelia Feß, Elisabeth Kaiser and Laura Schroeder whom I shared my scientific life.

Thanks to all my great friends in Saarland; Mahnaz, Haleh, Nouma, Eric, Meena, Keihan, Mohammad, Nina, Mahmud, Bijan, Fatemeh, Maryam and Hessam.

And many many thanks to my beloved parents and lovely sisters and brother who are my hope for life.

Attachments

A compact disc containing supplementary tables, Patchmaster protocols, personal publications and Signal Macro that were mentioned in this thesis, is attached.

List of supplementary tables:

Supplementary table 1: The electrophysiological results of transgenic mice used in 3.1

Supplementary table 2: The electrophysiological results of hyperaldosteronism described in 3.2

Supplementary table 3: The results of $I_{Ca,L}$ and gain measurements in I/E mice described in 3.3

Supplementary table 4: The results of $I_{Ca,L}$ and gain measurements in RacET mice described in 3.4

Supplementary table 5: The electrophysiological results of application of 40 μ M CytoD culture supplement described in 3.5

Supplementary table 6: The electrophysiological results of application of 0.5 μ M CytoD culture supplement described in 3.5

List of patchmaster protocols

Protocol 1: AP recording

Protocol 2: I_{toC} recording

Protocol 3: $I_{Ca,L}$ recording

Protocol 4: Simultaneous $I_{Ca,L}$ and Ca^{2+} transients recording-prepulse

Protocol 5: Simultaneous $I_{Ca,L}$ and Ca^{2+} transients recording

Protocol 6: Protocol editor for $G\alpha_q$ KO and hyperaldosteronism projects

Protocol 7: Protocol editor for I/E mutation and RacET projects

List of personal papers

Paper 1: Journal of Molecular and Cellular Cardiology (CytoD paper)

Paper 2: Cardiovascular Research ($G\alpha_q$ KO paper)

Paper 3: Journal of Biological Chemistry (I/E mutation paper)

List of Macros

Macro 1: Signal Macro for analysis of AP duration

Supplementary table 1: The electrophysiological results of transgenic mice used in 3.1. In the first row of each genotype either the results are shown as median with corresponding 25/75 percentiles or as mean \pm SEM. In the second row the first number shows the animal number, the second number shows the amount of cells.

| Genotype | C _M (pF) | V _R (mV) | AP Amplitude (mV) | APD ₃₀ (ms) | APD ₅₀ (ms) | APD ₇₀ (ms) | APD ₉₀ (ms) | I _{toC} (pA/pF) |
|---|------------------------|------------------------|-----------------------|------------------------|------------------------|------------------------|------------------------|--------------------------|
| Gq^{fl} G11⁻ Cre⁺ Tam⁻ | 145.4 (128.8/166.4) | -73.2 \pm 0.7 | 101.1 \pm 4.0 | 1.5 (1.2/1.9) | 2.4 (2.0/3.3) | 4.1 (3.3/5.6) | 7.9 (6.4/15.2) | 23.8 \pm 2.6 |
| | (3/22) | (3/16) | (3/16) | (3/16) | (3/16) | (3/16) | (3/16) | (3/20) |
| Gq^{fl} G11⁻ Cre⁺ Tam⁺ | 128.2 (96.9/155.1) | -73.4 \pm 0.5 | 114.5 \pm 1.6 | 2.0 (1.2/3.3) | 4.5 (2.1/7.7) | 8.1 (3.8/14.3) | 28.1 (8.8/53.6) | 16.6 \pm 2.2 |
| | (5/45) | (5/31) | (5/31) | (5/31) | (5/31) | (5/31) | (5/31) | (5/24) |
| Gq^{wt} G11^{wt} Cre⁻ Tam⁻ | 177.1 (149.6/219.5) | -73.0 \pm 0.5 | 115.2 \pm 1.7 | 1.9 (1.4/3.6) | 3.9 (2.7/9.3) | 7.2 (5.0/15.2) | 19.4 (12.9/43.1) | 19.3 \pm 2.0 |
| | (4/33) | (4/28) | (4/27) | (4/27) | (4/27) | (4/27) | (4/27) | (4/23) |
| Gq^{wt} G11^{wt} Cre⁻ Tam⁺ | 195.0 (166.5/297.4) | -73.7 \pm 0.7 | 115.0 \pm 1.3 | 1.7 (1.1/2.3) | 3.9 (2.02/5.6) | 6.8 (3.6/9.6) | 40.2 (10.2/58.5) | 25.0 \pm 3.5 |
| | (3/25) | (3/21) | (3/19) | (3/19) | (3/19) | (3/19) | (3/19) | (3/20) |
| Gq^{fl} G11⁻ Cre⁻ Tam⁻ | 128.3 (102.3/166.3) | -73.7 \pm 0.5 | 110.2 \pm 2.7 | 1.1 (1.0/1.2) | 1.8 (1.5/2.2) | 3.0 (2.6/3.5) | 6.0 (5.2/7.3) | 36.3 \pm 3.0 |
| | (3/27) | (3/22) | (3/21) | (3/20) | (3/20) | (3/20) | (3/20) | (3/21) |
| Gq^{fl} G11⁻ Cre⁻ Tam⁺ | 123.0 (110.1/195.8) | -72.8 \pm 0.6 | 110.4 \pm 2.5 | 1.8 (1.4/2.8) | 3.0 (2.4/7.3) | 5.5 (4.2/10.7) | 18.0 (8.7/33.6) | 23.2 \pm 3.5 |
| | (3/22) | (3/19) | (3/19) | (3/18) | (3/18) | (3/18) | (3/18) | (3/19) |
| Gq^{wt} G11^{wt} Cre⁺ Tam⁻ | 176.9 (138.7/192.4) | -71.8 \pm 0.4 | 111.2 \pm 1.9 | 2.1 (1.6/2.4) | 3.8 (3.0/5.2) | 6.8 (5.4/9.7) | 16.2 (11.3/25.6) | 16.5 \pm 1.8 |
| | (4/30) | (4/23) | (4/23) | (4/22) | (4/22) | (4/22) | (4/22) | (4/21) |
| Gq^{fl} G11^{wt} Cre⁻ Tam⁺ | 170.9 (140.7/215.6) | -72.0 \pm 0.5 | 103.4 \pm 2.3 | 2.4 (1.4/4.0) | 4.4 (2.6/7.7) | 7.0 (4.3/12.4) | 24.2 (9.9/64.4) | 16.7 \pm 2.0 |
| | (4/32) | (4/24) | (4/23) | (4/23) | (4/23) | (4/23) | (4/23) | (4/20) |
| Gq^{fl} G11^{wt} Cre⁺ Tam⁺ | 183.8 (168.5/239.8) | -75.6 \pm 0.5 | 118.1 \pm 2.5 | 2.6 (1.2/3.6) | 5 (2/6.8) | 9.7 (3.9/16.5) | 41.5 (21.1/85.8) | 20.8 \pm 3.5 |
| | (3/22) | (3/22) | (3/19) | (3/19) | (3/19) | (3/19) | (3/19) | (3/17) |
| Gq^{wt} G11^{wt} Cre⁻ Mig⁺ | 162.2 (143.3/184.7) | -72.6 \pm 1.4 | 117.2 (92.1/125.6) | 1.9 \pm 0.3 | 3.9 \pm 1 | 7.2 \pm 1.7 | 27.6 \pm 8.3 | 26.1 \pm 4 |
| | 17/2 | 9/2 | 8/2 | 8/2 | 8/2 | 8/2 | 8/2 | 11/2 |
| Gq^{fl} G11⁻ Cre⁺ Mig⁺ | 140.3 (123.7/164.3) | -72.3 (-74.5/-70.8) | 108.8 \pm 2.5 | 1.5 (1.2/1.9) | 2.9 (2.2/3.9) | 5.05 (3.7/6.9) | 11.8 (7.3/20.2) | 25.5 \pm 2.8 |
| | 42/4 | 33/4 | 33/4 | 34/4 | 34/4 | 34/4 | 34/4 | 17/4 |

Supplementary table 2: The electrophysiological results of hyperaldosteronism described in 3.2. In the first row of each genotype the results are shown either as median with corresponding 25/75 percentiles or as mean \pm SEM. In the second row the first number shows the animal number and the second number shows the cell number.

| Genotype | C_m | V_R | AP amplitude | TTP | APD30 | APD50 | APD70 | APD90 | I_{toc} |
|--|------------------------|------------------------|------------------------|-------------------|-------------------|-------------------|---------------------|-----------------------|----------------|
| Gq^{fl} G11^{wt} Cre⁻ Tam⁺ | 207.7 (164.9/252) | -74.5 (-75.5/-71.2) | 107.5 (96.1/121.9) | 7.2 (5.7/12.2) | 2. (1.2/7.6) | 5.7 (2.8/15.3) | 14 (8.1/80.7) | 116.1 (55.7/168.9) | 20.3 \pm 1.9 |
| | 41/4 | 36/4 | 16/4 | 29/4 | 15/4 | 15/4 | 15/4 | 15/4 | 29/4 |
| Gq^{fl} G11^{wt} Cre⁻ Tam⁺ (Aldo) | 192.7 (161.6/229.2) | -76.2 (-77.7/-74.7) | 123.3 (115.5/127.7) | 5.7 (5.1/6.2) | 0.9 (0.7/2.3) | 2.2 (1.5/7.2) | 5.1 (3.2/15.8) | 75.8 (44.8/110.4) | 30.4 \pm 2.9 |
| | 55/6 | 54/6 | 16/6 | 36/6 | 15/6 | 15/6 | 15/6 | 15/6 | 36/6 |
| Gq^{fl} G11^{wt} Cre⁺ Tam⁺ | 188.2 (155.1/227.3) | -75.9 (-77.7/-73.5) | 111 (107.9/124.5) | 6.1 (5.9/6.4) | 1.5 (1.2/3.9) | 5.8 (3.4/15.4) | 13.5 (7.6/42.3) | 100.5 (76.9/125.7) | 21.4 \pm 3 |
| | 38/4 | 41/4 | 15/4 | 22/4 | 22/4 | 22/4 | 22/4 | 22/4 | 22/4 |
| Gq^{fl} G11^{wt} Cre⁺ Tam⁺ (Aldo) | 192.1 (158.6/235) | -75.4 (-77.6/-73.2) | 101.3 (69.3/130.8) | 6.1 (5.2/8.1) | 2.6 (2.1/12.4) | 7.8 (4.9/22.8) | 23.1 (16.0/51.4) | 93 (64.8/151.8) | 25.7 \pm 2.1 |
| | 57/4 | 50/4 | 13/4 | 28/4 | 28/4 | 28/4 | 28/4 | 28/4 | 28/4 |
| Gq^{fl} G11⁻ Cre⁻ Tam⁺ | 205.9 (176.3/287) | -73.4 (-76.3/-71.1) | 105.7 (90.3/113.3) | 8.4 (6.7/9.2) | 1.0 (0.7/1.4) | 1.9 (1.4/3.6) | 3.6 (2.8/8.6) | 66.9 (33.5/103.8) | 42.8 \pm 3.6 |
| | 33/3 | 22/3 | 18/3 | 24/3 | 24/3 | 24/3 | 24/3 | 24/3 | 24/3 |
| Gq^{fl} G11⁻ Cre⁻ Tam⁺ (Aldo) | 172.8 (147.1/205.9) | -75.6 (-77.3/-73.8) | 103.7 (88.2/118.7) | 5.9 (4.9/6.9) | 1.1 (0.6/6.9) | 3.2 (1.3/17.4) | 9.7 (2.9/59.2) | 84.2 (39.3/137.9) | 33.6 \pm 4.3 |
| | 24/4 | 23/4 | 15/4 | 16/4 | 14/4 | 14/4 | 14/4 | 14/4 | 16/4 |
| Gq^{fl} G11⁻ Cre⁺ Tam⁺ | 190.3 (132.1/238) | -75.8 (-77.5/-73.7) | 109.8 (91.9/116.2) | 6.4 (5.5/7.3) | 0.7 (0.5/1) | 1.4 (1/1.9) | 2.7 (1.8/3.9) | 28.7 (16.0/94) | 46.5 \pm 5.2 |
| | 38/3 | 20/3 | 14/3 | 15/3 | 14/3 | 14/3 | 14/3 | 14/3 | 15/3 |
| Gq^{fl} G11⁻ Cre⁺ Tam⁺ (Aldo) | 134.5 (111.7/167.1) | -75.9 (-78.9/-73.3) | 115.1 (99/126.2) | 5.2 (4.8/6.3) | 1.4 (0.7/4.3) | 3.6 (1.5/10.7) | 8.2 (3.1/30.3) | 95 (32.8/146.4) | 28.4 \pm 5.1 |
| | 23/4 | 22/4 | 18/4 | 16/4 | 18/4 | 18/4 | 18/4 | 18/4 | 16/4 |

Supplementary table 3: The results of $I_{Ca,L}$ and gain measurements in I/E mice described in 3.3. In the first row of each parameter the results are shown either as mean \pm SEM or as median with corresponding 25/75 percentiles at 0 mV test potential. In the second row the first number shows the animal number and the second number shows the cell number.

| Parameter | Ctr | I/E |
|-----------------|---------------------|----------------------|
| $I_{Ca,L}$ | -2.73 | -1.84 |
| | 18/3 | 23/3 |
| C_M | 185.1 \pm 11.6 | 194.1 \pm 12.0 |
| | 20/3 | 24/3 |
| Gain | 0.10 \pm 0.02 | 0.43 \pm 0.11 |
| | 18/3 | 19/3 |
| τ_1 | 22.6 \pm 2.3 | 17.2 \pm 3.8 |
| | 17/3 | 14/3 |
| τ_2 | 72.8 (57.9/84.5) | 86.9 (61.5/104.1) |
| | 13/3 | 16/3 |
| $\int I_{Ca,L}$ | 0.088 \pm 0.008 | 0.073 \pm 0.007 |
| | 17/3 | 18/3 |

Supplementary table 4: The results of $I_{Ca,L}$ and gain measurements in RacET mice described in 3.4. In the first row of each parameter the results are shown either as mean \pm SEM or as median with corresponding 25/75 percentiles at 0 mV test potential. In the second row the first number shows the animal number and the second number shows the cell number.

| Parameter | WT | RacET |
|-----------------|----------------------|-----------------------|
| $I_{Ca,L}$ | -4.41 | -5.25 |
| | 13/3 | 8/3 |
| Gain | 0.08 ± 0.02 | 0.28 ± 0.1 |
| | 14/3 | 17/3 |
| τ_1 | 20.9 ± 1.2 | 28.4 ± 2 |
| | 14/3 | 21/3 |
| τ_2 | 73.9 (61.3/109.1) | 117.8 (78.3/260.7) |
| | 14/3 | 18/3 |
| $\int I_{Ca,L}$ | 23.2 ± 1.5 | 13.6 ± 1.6 |
| | 12/3 | 20/3 |

Supplementary table 5: The electrophysiological results of application of 40 μ M CytoD culture supplement described in 3.5. In the first row of each parameter the results are shown as mean \pm SEM. In the second row the first number shows the animal number and the second number shows the cell number.

| Parameter | DIV0 | DIV0 | DIV3 | DIV3 |
|-------------------|-----------------|-----------------|-----------------|------------------|
| C_m | 137.9 \pm 3.2 | 139.5 \pm 9.6 | 102.2 \pm 6.6 | 134.4 \pm 8.2 |
| | 9/3 | 17/3 | 14/3 | 21/3 |
| V_R | -74.5 \pm 0.8 | -72.0 \pm 0.8 | -71.4 \pm 0.6 | -73.9 \pm 0.5 |
| | 9/3 | 16/3 | 16/3 | 23/3 |
| AP amplitude | 99.6 \pm 6.5 | 101.0 \pm 4.9 | 91.3 \pm 4.3 | 106.1 \pm 2.5 |
| | 8/3 | 14/3 | 10/3 | 21/3 |
| APD ₃₀ | 9.3 \pm 2.3 | 8.6 \pm 1.7 | 12.2 \pm 4.6 | 22.3 \pm 5.0 |
| | 8/3 | 12/3 | 12/3 | 9/3 |
| APD ₅₀ | 11.2 \pm 1.8 | 8.9 \pm 1.2 | 12 \pm 2.2 | 39.8 \pm 9.4 |
| | 8/3 | 12/3 | 12/3 | 9/3 |
| APD ₇₀ | 26.3 \pm 6.4 | 20.7 \pm 4.0 | 32.7 \pm 10.5 | 103.4 \pm 24.9 |
| | 8/3 | 12/3 | 12/3 | 9/3 |
| APD ₉₀ | 33.4 \pm 5.5 | 37.1 \pm 5.7 | 40.6 \pm 6.7 | 198.6 \pm 51.1 |
| | 8/3 | 12/3 | 12/3 | 9/3 |

Supplementary table 6: The electrophysiological results of application of 0.5 μ M CytoD culture supplement described in 3.5. In the first row of each parameter the results are shown as mean \pm SEM. In the second row the first number shows the animal number and the second number shows the cell number.

| Parameter | DIV0 | DIV0 | DIV3 | DIV3 |
|-------------------|------------------|------------------|-----------------|------------------|
| C_m | 202.8 \pm 17.8 | 199.0 \pm 14.5 | 117.2 \pm 6.1 | 169.5 \pm 11.7 |
| | 10/3 | 10/3 | 11/3 | 25/3 |
| V_R | -74.0 \pm 0.6 | -71.7 \pm 0.9 | -72.2 \pm 1.0 | -74.6 \pm 0.6 |
| | 20/3 | 10/3 | 10/3 | 10/3 |
| AP amplitude | 103.1 \pm 4.2 | 102.6 \pm 4.1 | 80.2 \pm 1.8 | 100.3 \pm 3.5 |
| | 18/3 | 12/3 | 14/3 | 10/3 |
| APD ₃₀ | 10.5 \pm 1.8 | 9.6 \pm 1.6 | 14.2 \pm 4.6 | 11.0 \pm 3.5 |
| | 13/3 | 14/3 | 7/3 | 7/3 |
| APD ₅₀ | 20.4 \pm 3.4 | 30.6 \pm 8.8 | 18.4 \pm 2.9 | 18.5 \pm 5.3 |
| | 13/3 | 14/3 | 7/3 | 7/3 |
| APD ₇₀ | 30.5 \pm 4.9 | 27.8 \pm 4.6 | 41.2 \pm 12.7 | 26.1 \pm 6.7 |
| | 13/3 | 14/3 | 7/3 | 7/3 |
| APD ₉₀ | 61.8 \pm 9.5 | 149.6 \pm 28.2 | 47.9 \pm 8.3 | 70.2 \pm 18.3 |
| | 13/3 | 14/3 | 7/3 | 7/3 |